博士論文（要約）

Doctoral thesis (Abridged)

Development of secondary-side-only simultaneous power and efficiency control in wireless power transfer system

(ワイヤレス電力伝送システムにおける二次側のみ
の制御による電力と効率の同時制御法の開発研究)

ロビソン　ジョルジョ

Lovison Giorgio

博士論文

Doctoral thesis

Development of secondary-side-only simultaneous power and efficiency control in wireless power transfer system

(ワイヤレス電力伝送システムにおける二次側のみ
の制御による電力と効率の同時制御法の開発研究)

指導教員: 堀 洋一 教授

Supervisor: Yoichi HORI

平成 29 年 12 月

December, 2017

東京大学大学院 新領域創成科学研究科 先端エネルギー工学専攻

Department of Advanced Energy, Graduate School of Frontier Sciences, The University of Tokyo

ロビソン　ジョルジョ

Lovison Giorgio

Abstract

Wireless power transfer (WPT) via magnetic resonance coupling is a technology allowing the transmission of electric energy without the need of cables and with a high efficiency even over several tens of centimeters. As such, it is expected that many applications, ranging from medical field to domestic appliance to electric vehicles, will benefit greatly from this technology. In particular, current electric vehicle problems and issues such as potential dangers to the users during battery charging process, low cruising range, long battery charging time and the like can be solved or at least mitigated, thus making wireless power transfer one of the most suitable methods for spreading electrification of vehicles. In fact, wireless power transfer can be performed not only when the transmitting side and the receiving side are not moving (a static scenario), but also during their relative motion (a dynamic scenario).

As it is not a novel research theme, previous research about wireless power transfer has been abundant with respect to the hardware design of resonant network, compensation topology and converter structure. However, simultaneous efficiency and power regulation by means of power converter control only on a single side has not been given any consideration. In this dissertation, both the circuit topology and the control method are the focus of research. It is necessary to ascertain if power and efficiency control are performing as expected in both static and dynamic condition; in other words, it is necessary to understand the model and control the response of a wireless power transfer system by magnetic resonance coupling. In so doing, it becomes possible to include all the control in only one side of the system, which is a desirable feature in the future since it allows real time adaptation to the power transmission facility, intended as the primary side of the whole system. This means actively using all the power converters, refraining from adopting passive components such as diodes, especially on the secondary side of the system. Until now, the possibility of single-side control for both transmission efficiency and power flow has never been considered, preferring to rely on control for both sides with communication. In this sense, in most literature, communication availability between sides is regarded as a given feature of the circuit, and the communication speed is not taken into account. This can easily be an issue in dynamic scenarios, where the control objective has to maintain high efficiency and desired power while the system parameters are varying. In other words, the control must be robust against parameter variation and operate always in a stable zone even without communication. This is why, in this dissertation, communication between primary and secondary

side is not used.

Therefore, this thesis discusses the control methods for secondary-side-only power and efficiency control for WPT systems when many constraints such as lack of communication are included. This dissertation explores the following two main themes: secondary-side-only power and efficiency control with two converters in static scenario and secondary-side-only power and efficiency control with two converters in dynamic scenario. Thus, a part is devoted to the explanation about the necessity of field programmable gate array for use in converter control for WPT systems, as well as the guidelines for creating from scratch a digital controller for power converter at a machine logic level. Finally, by virtue of FPGA's superior characteristics, the concepts of secondary-side-only power control with one converter in case of constant power load are explained and evaluated. By the aforementioned points of investigation, the work of this thesis aims at providing the design process of robust controllers able to satisfy the requirements of power and efficiency by only the secondary side. The controllers do not need communication and offer great versatility at a slight trade-off, making them very application-oriented.

In Chapter 1, the research background regarding control methods for power converters in wireless power transfer systems by magnetic resonant coupling is introduced in order to establish the motivation and the position of the research described in this dissertation. In previous research, the regulation of the transmission efficiency and power has been designed without considering the circuit composition, such as the number of power converters or the type of load. Previous research strongly suggested that a coordinated control should be performed on both the transmitting (primary) side and the receiving (secondary) side, but in some scenarios the operating conditions may not allow it. Therefore, in this thesis, the power converters in the receiving side and their relative controllers are discussed. Then, the cases of static wireless power transfer and dynamic wireless power transfer are described.

In Chapter 2, the power control and efficiency control concepts presented in past research are reviewed. Thus, the applications for wireless power transfer by magnetic resonant coupling are discussed, with particular focus on electric vehicles. Wireless power transfer by magnetic resonance coupling encompasses different compensation methods leading to constant voltage or constant current output characteristics, thus making it appealing to many different applications. In particular, series-series (SS) compensation is found suitable for automotive.

In Chapter 3, the single-side control concept is introduced. Real time adaptation to primary side in constrained conditions is desirable, especially when considering a dynamic scenario. In this sense, it is necessary to use active converters on the secondary side. By using two converters, there are two degree of freedom, thus both load power and transmission efficiency can be controlled. In this chapter, a novel control strategy for the receiving side with a battery load is proposed, where the AC/DC converter regulates the average power and the DC/DC converter controls the equivalent AC resistance to match the optimal value. The primary side is not involved in the active control, merely working with a fixed operation point. The AC/DC converter uses a two-mode control, taking advantage of

the inverting characteristics of SS compensation topology and periodically shorting the receiving coil terminals. The proposed control theory and the controller design are explained, followed by verification by both simulations and experiments.

In Chapter 4, a discussion about the advantages of field programmable gate array (FPGA) in controlling the converters for wireless power transfer systems will be presented. In fact, FPGA is a necessary tool because of its superiority when compared to conventional DSP control board in terms of calculation time, diagnostics and flexibility in system integration. After explaining the netlist project design flow and logic block creation process inside of the FPGA, a case of study is presented. In order to provide an effective current limiter for use in case of vehicle detection failure in dynamic WPT environment, a customized logic block automatically acquiring the AC peak value of the current from the sensor and updating it to the highest value is created. At the same time, a simple current controller based on combined phase locked loop (PLL) algorithm and phase shifting is proposed for the secondary side. This is necessary in case the secondary side has only one AC/DC converter. The proposed approach is verified by experiments.

In Chapter 5, a discussion about the number of converters is presented. Reducing the number of converters generally implicates reducing losses and simplifying the circuit. However, also the degrees of freedom end up reduced, thus complicating the control. In this chapter, a control for the secondary side AC/DC converter is proposed. While performing synchronous rectification for minimizing the losses, the conversion ratio is manipulated by the shift coefficient, thus allowing voltage control for constant power load or current control for constant voltage load. Therefore, in this chapter, too, the proposed control theory, system analysis and controller design are explained, followed by verification by both simulations and experiments.

In Chapter 6, the vision of the future society derived from widespread exploitation of WPT both in public and private life is presented. It is deduced that society will benefit in terms of higher flexibility and safety, with increased quality of life. The secondary-side-only control concept presented in this thesis will help in the diffusion of WPT technology since it can be successfully applied to many different scenarios.

In Chapter 7, the results and the discussions presented in this thesis are collected and summarized, underlining the contribute to the scientific community, therefore concluding this thesis.

Table of contents

Figures

Tables

Chapter 1

Introduction

1.1 Research background

Wireless power transfer (WPT) dates back to Nikola Tesla experiments with AC current. However, the real interest for this technology and its potential clearly arose after a paper reported an experiment performed in 2007 at Massachusetts Institute of Technology [1]. The experimental results showed that 60W of electric power can be successfully transmitted through magnetic induction by having two copper coils, positioned at a distance of 2.5 meters, resonate at the same operating frequency. Consequently, having proved the capability of mid-range operation, the range of target applications is very broad: mobile phone charging pads [2][3], medical implants [4]–[7], servo stages[8], electric vehicles (EVs) [9]–[18], drones[19], nuclear waste storage monitoring supply [20] and more. The condition of resonance is critical for achieving several desirable characteristics, such as the extension of the gap between the transmitter coil and the receiver coil, the conservation of high transmission efficiency and the tolerance to mechanical misalignment conditions between the coils. The coil self-resonance is achieved by connecting a capacitive device to the coil, effectively creating an equivalent LCR circuit from the point of view of physical behaviour. If both the primary side and the secondary side coil have the same resonance frequency by means of compensation circuit, then the transmission efficiency and the transferred power become even higher than in the case of normal magnetic induction. There are four basic compensation topologies [21][22] for the resonant network: SS compensation, SP compensation, PP compensation and PS compensation. While the first letter is referred to the primary side and the second letter is referred to the secondary side, S means series connection of the coil with the capacitor and P denotes parallel connection of the coil with the capacitor. In particular, the design process in case of SS compensation is easy since the compensation capacitance value does not depend on the mutual inductance and effective load and therefore is suitable for many applications [23]. However, it is possible to devise a coil structure able to achieve resonance without using physical capacitors. In this case, by properly designing the coil wire pitch and the layer gap, it is possible to

exploit the stray capacitances between the wire and, even more, having multiple resonant frequencies in only one coil [24]. This opens up several scenarios and will be a popular topic for future research. The magnetic field between the coils determines the strength of the coupling between the transmitter coil and the receiver coil. In short, the whole WPT basic concept is similar to a transformer ' s one. Of course, there is a multitude of system configurations depending on the final application: it is the designer's job to decide how many transmitting coils and receiving coils should be used, to decide what resonant circuit topology is most suitable, to decide whether to add intermediate repeater coils [25] and so on and so forth. There is abundant literature concerning the resonant circuit modelling and transfer functions [26], and therefore it will not be the focus of this thesis.

In recent years, EVs have been the technology whose combination with WPT holds more expectations [11][15]. The electrification of vehicles is becoming an increasingly needed action to mitigate the pollution problem. Recently, not only vehicle makers but also entire governments are strongly pushing for complete renewal of the car park in the wake of the progress of EV technology. In this sense, using wireless power transfer increases their mobility and reliability. It is well known that EVs have several advantages such as fast response, high torque delivery to the wheels and easy torque measurement from the motor current; on the other hand, their relatively limited range and long battery charging time are known as well and are considered the brake on their widespread use. Methods for increasing the cruising distance based on the adopting of in-wheel motors have been proposed in past research [27]–[30] and the reported results are promising in terms of losses reduction. However, WPT offers a feasible solution to those disadvangates by allowing charging of the EV battery both while stopping and while moving. Currently, the allowed operating frequencies are between 75 and 90 kilohertz, as established by the Society of Automotive Engineers [31], although in past research different operating frequencies have also been used [17]. Various multi-coil configurations such as double-D (DD), double-D quadrature (DDQ) and bipolar BP [32] have been studied. Moreover, different coil configurations such as spaced loops [15], sectional loops [33], or long wire loops [34] have been explored. Long track distance leads to low coupling due to large leakage flux [33] and possibility of energizing and heating unwanted loads.

In the case of static WPT, the scenario is a parking lot or an intersection with traffic lights in which the primary side coil and related circuit should be buried 60-80 cm below the ground [35]. WPT then occurs from the primary side to the secondary side and consequently the energy storage system mounted on the stopped EV. Since the charging happens in a static scenario, the coupling coefficient does not change; moreover, since it is usually a one-transmitter/one-receiver condition, a communication signal (e.g. Bluetooth) for coordinated control between both sides can be adopted.

On the other hand, in case of dynamic WPT, the transmission occurs in the same method as in static WPT, but the scenario becomes a highway. The energy storage system is then composed by battery and eventually supercapacitors, which supply the EV motor. Giving the relative motion between the primary coil and the secondary coil, the coupling coefficient is subject to variation. Furthermore,

the primary side circuit must be prepared for a long distance in order to provide sufficient energy to the EV, thus, from the cost viewpoint, it is desirable that the primary side is as simple as possible. Consequently, it is natural to think that the primary should be operating at fixed condition while the secondary side must perform the dedicated control to adapt to the primary side. From these considerations, at the current state of the art it can be said that the most suitable composition is given by having a primary side composed by multiple coils equally spaced and embedded in the ground. In so doing, it is possible to usually have a one-transmitter/one receiver condition, which is the simplest in terms of control complexity and the most advantageous in terms of transmitting efficiency.

As mentioned before, in practical applications the load is almost always a constant voltage load (CVL). Past research about power control in WPT with CVL has been carried out extensively; in particular, using a full bridge diode rectifier with a cascoded DC/DC converter and controlling the DC link voltage to maximize the transmitting efficiency by an equivalent resistance model has been widely reported upon. However, little to no attention has been paid to the variation of coupling coefficient or transients or difficulty of communication. Other research has also considered bidirectionality, whose concept lies in the secondary side mirroring the primary side circuit and operating switching phase control in order to ensure synchronization between primary and secondary side. As it can be inferred, in most research many constraints are not even considered, using approximations and ideal conditions. It is not clear what is possible to control with multiple constraints at the same time, as it is the case real applications. In particular, control on the secondary side has never really been investigated apart from the conventional combination of full bridge diode rectifier and DC/DC converter. As the load is in the secondary side, it is desirable that the secondary side adapts itself to the condition of the primary side.

However, not all WPT systems have a CVL. The load may also be a motor or a constant power load (CPL). In [36], a in-wheel motor is powered wirelessly from the battery embedded in an EV. The main reason to choose a wireless supply to the three-phase inverter connected to the in-wheel motor is to eliminate the risk of disconnection of signal and power cables. As a CPL presents an unstable open loop plant, it was necessary to force a discontinuous operation with an ON/OFF mode (two-mode control), as described in [37]. Another stablization method consists in coordinated control between primary and secondary side to stabilize the load voltage [38]. Both methods are valid, but present some disadvantages: in the first one, the transients of two-mode control are big and may cause false triggering of the devices gate driver or surpass the reverse voltage of the device, actually destroying the converter; on the other hand, the second method requires the primary side to keep some voltage margin to deliver the power. Other research [39] proposed a capacitive power transfer in which the power is transmitted from a plate on the road to a metal band inside the EV tire and then delivered to the motor. In the CPL case, too, the aforementioned concept of adding constraints and letting the secondary side adapt to the primary side is valid. Hence, achieving load voltage stabilization while having smooth operation with only secondary side becomes a worthy research topic.

In order to perform these kinds of advanced control satisfying the requirements of WPT systems, a conventional digital signal processor is not powerful enough at hardware level. This is especially true as the frequency used in WPT is very high, up to ISM band (i.e. from 6.78 to 13.56 MHz), and the gate triggering signal generation is not fast enough. Conventional control boards are suitable for frequencies of some tens of kilohertz, otherwise it becomes necessary using higher performance hardware. Such hardware is the field programmable gate array (FPGA), a popular tool in software development field. In the future, it is expected that the frequency level will be even higher, therefore using a FPGA should be a standard in converter control and guidelines on its utilization as a digital converter controller should be given.

1.2 Research purpose

In this thesis, the objective is to analyze the composition of the power converter circuit and consequently propose novel controls for achieving the desired power and the maximum extractable transmitting efficiency in WPT system adopting magnetic resonance coupling. In those systems, there are four different manners of connection for the resonant capacitance; however, since this thesis is dealing mainly with WPT applied to EVs, then only the SS compensation is considered. While most of previous research only examined the state of the art and stated several assumptions making the system close to ideal, in this thesis the approach is based on a different point of view. In this dissertation, a system for WPT is designed according to the control viewpoint: if there are many constraints, such as the lack of communication or variation of coupling coefficient, it is necessary to understand how much controllability is possible to maintain. Considering the case of WPT performed while in-motion, it is stressed the fact that it is necessary to devise a system not relying on communication between sides because of the unacceptable delay in the current technology that may cause incorrent operation. Moreover, given that the reference application involves EVs, it is clear that secondary side must be controlled and adapt to primary side. Consequently, the focus of this research is on the secondary side because the proposed controls must perform well both in static and dynamic WPT systems. Similarly, since the load is in the secondary side, the type of the load will determine the characteristics of the transients, which is one more reason to study the case of control performed only in the secondary side. It is expected that implementing secondary-side-only control will allow for a reduction of system costs due to the adoption of active devices in the converters; in so doing, it is possible to perfom smarter controls, allowing to decrease the number of components and therefore reduce the overall costs.

Past research proposed several control methods for power flow and transmitting efficiency, such as power control on primary side [40][41], efficiency control on secondary side [42]–[44] or power and efficiency control by using both sides[45][46]. If efficiency control was performed on the secondary

side, the power had to be regulated on the primary side and vice versa, as until now it has been impossible to manipulate them both on the same side. This research however proposes a control method able to simultaneously regulate the power flow and the transmitting efficiency. It is achieved with two converters: the half active rectifier (HAR) and the cascoded DC/DC converter. The proposed control is performed at resonance and targets a CVL. The modelling and settings are described, and its results are compared to a conventional efficiency control with a full bridge diode rectifier and the cascoded DC/DC converter.

Also, past research about WPT to a CPL has provided different methods for load voltage stabilization. However, they could not achieve smooth operation by secondary side only, instead having to rely on discontinuous operation or primary side coordination. Therefore, in this thesis, stability analysis of CPL in WPT systems by magnetic resonant coupling is performed and, from that, the design of a simple voltage controller along with the closed loop model stability limit analysis is proposed.

On top of that, FPGA technology is introduced and it was found that it is a necessary tool for the development of more precise and efficient controllers to be adopted in WPT systems. The process of block creation and the necessary signal coordination in the logical project inside the board is clarified and recommended.

1.3 Thesis composition

The composition of this dissertation is shown in Fig. 1.

Chapter 2 reviews the fundamental concepts of power and efficiency control presented in past research in WPT systems with magnetic resonant coupling and relates them with the cases of static and dynamic wireless power transfer. The type of compensation determines critical characteristics of the system, therefore a little review of the compensation method is presented as well.

Chapter 3 introduces the research topic of simultaneous power and efficiency control. Previous research could achieve it only by exploiting both primary and secondary side, but the control strategy proposed in this chapter can achieve it with only the secondary side and without need of communication. The secondary side is equipped with a HAR followed by a DC/DC buck/boost converter, consequently there are two degrees of freedom. By setting a different switching frequency for each converter, the risk of conflict is avoided and it is possible to control the averaged transmitted power and the transmitting efficiency at the same time. In this case of study, the average transmitted power is controlled by the HAR with a two-mode operation and the transmitting efficiency is regulated by the DC/DC converter. Simulation and experimental results show the validity of the proposed control, whose target is CVLs, in both static and dynamic charging environment.

Chapter 4 is dedicated to the explanation of the process of netlist and creation of logic blocks to be

implemented in a field programmable gate array (FPGA). In fact, FPGA is remarkably superior in hardware performance with respect to normal digital signal processors (DSP), thus allowing very fast parallel calculation and thus implementation of more advanced digital control schemes apart from the usual pulse width modulation (PWM). Then, the design of a simple secondary-side-only current controller for constant power load and constant voltage load with only one converter is proposed. The concept used is symmetric phase shift, which is the only approach available in case of a secondary side with one converter. The other advantage is that the current transient response is smooth. The effectiveness is verified with experiments.

Chapter 5 pursues the concept of secondary-side-only control presented in the previous chapter and applies it to CPL. Furthermore, as an additional constraint, a single converter is considered. This means that all the devices in the converter must be active devices. Moreover, the analysis of CPL shows that the open loop function is unstable, therefore requiring stabilization in the closed loop. Taking into account the analysis of past research, the only method available in the case of study is the combination of synchronous rectification and symmetric phase shift control. By manipulation of the shift coefficient, the load voltage can be stabilized around an arbitrary equilibrium point by means of a high bandwith PI feedback controller. The stability of the closed loop function is analyzed and the limits of stability are described and verified by experiments. The same control concept can be adopted for current control and CVL.

Chapter 6 introduces a prediction of the future scenario in the case of widespread WPT. The benefits for the society will be obtained in many fields, from automotive to medical to industrial application. Consequently, the quality of life of the future wireless society will be improved, with better flexibility and safety in both public and private life. Secondary-side-only control concept can be easily implemented and contributes not only to WPT for electric vehicle but also to other application fields.

Chapter 7 finally concludes this dissertation about secondary-side-only control for WPT systems by magnetic resonant coupling by summarizing the results of all the previous chapters.

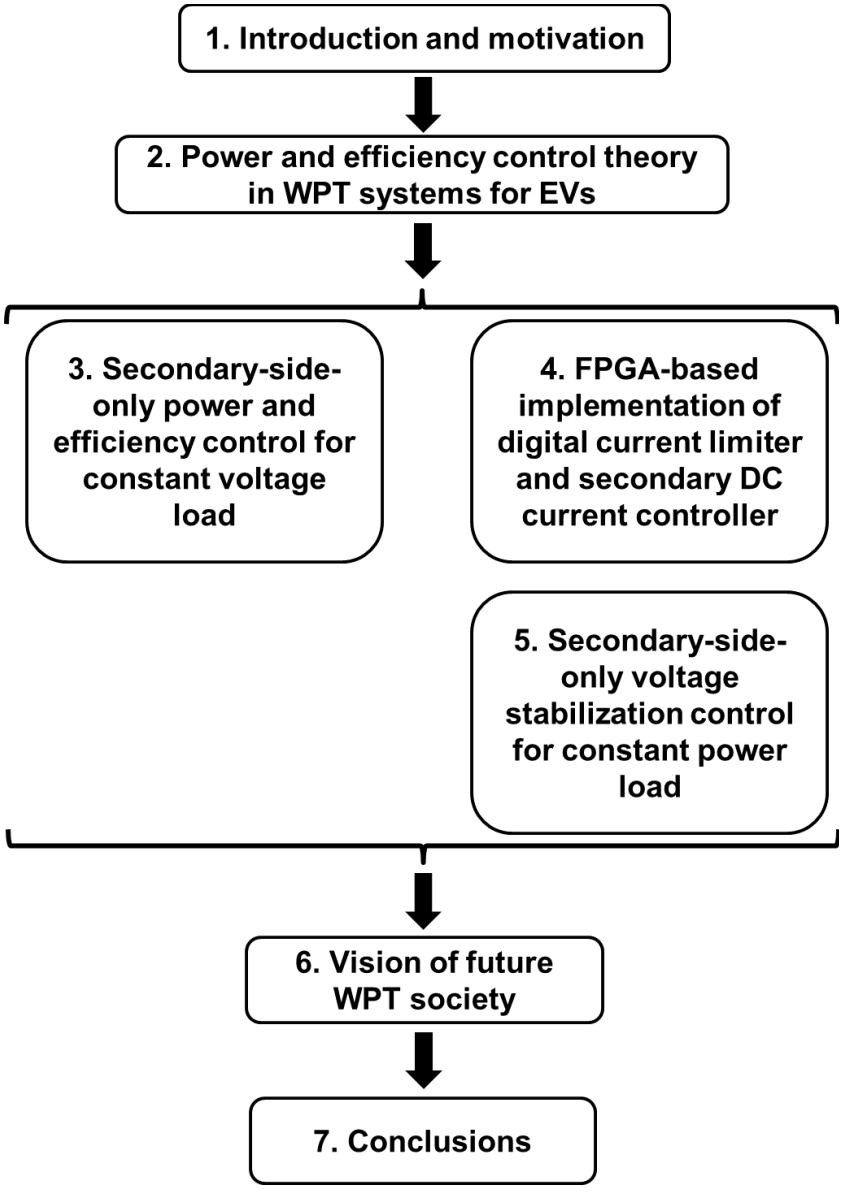

Fig. 1: Thesis organization.

Chapter 2

Power and efficiency control theory in WPT systems for EVs

In this chapter, brief review of the research topics and the particularities differentiating the static charging scenario and the dynamic charging scenario is conducted. A brief discussion about the most suitable compensation topology for electric vehicles (EVs) follows. Consequently, the mainstream theories about power and efficiency control for WPT systems by magnetic resonance coupling are reviewed.

2.1 Overview on EVs

EVs are an excellent alternative to internal combustion engines vehicles. As the problem of world pollution grows increasingly dire, a mitigation by cutting the CO_2 emissions of venicles is the readiest and most feasible among the countermeasures towards a definitive solution. The advantages of EVs, apart from low environmental impact, include high controllability due to the fast response to transients of the electric motor, high torque delivery to the wheels and easy measurement thereof from the electric motor current. The recent progress of renewable energy systems is a further incentive to use EVs; in fact, they can also be exploited for vehicle-to-grid (V2G) and can be excellently integrated into the grid. Further progress in these field is expected by making intelligent use of data through the Internet of Things (IoT), to tailor services for each user and provide optimal coordinated control. However, the bottleneck slowing down the widespread use of EVs is represented by the still long battery charging time and the limited range compared to conventional internal combustion engines. This results in the need of big built-in energy storage systems, which means increased weight and cost, and frequent recharges. Even though energy savings approaches such as the improvement of power train efficiency [28], optimal distribution of driving force in indipendent in-wheel motors of front or rear wheels [27] and optimization of speed profile [29] achieved results and effectively increase the

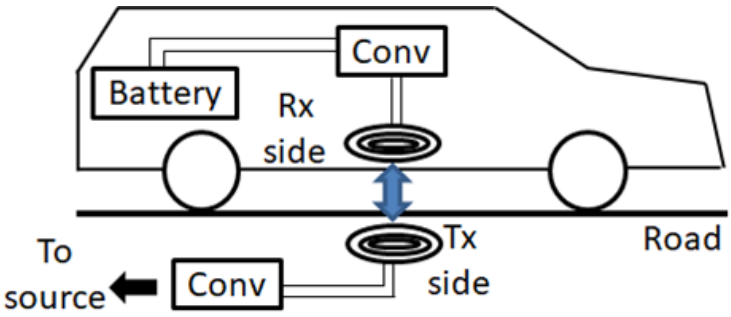

Fig. 2: Concept of static WPT.

cruising range, it is still insufficient to satisfy the requirements of users. Other practical issues also arise: the process of plug-in charging may be potentially dangerous in hands of a careless user, with risk of electrocution at high voltages.

Thus, the only way to promote and make EVs accepted by the public is to solve or at least mitigate their disadvantages. Although much attention is given to the improvement and progress of battery technology (for instance, the most recent EVs have installed a battery module capable of covering 400 kilometers with a single full charge [47]), it is worthwhile to think about merging with other technologies. Among the vast array of possible matching technologies, WPT is the one showing the most potential and feasibility. With WPT, cables and cords are eliminated, thus making the whole charging process safer and reliable, with less maintenance. Without cables, two main scenarios can be considered: using WPT to charge the EV battery or storage system while the EV is stopped, and using WPT to charge the EV battery while in motion. Moreover, the same concept of WPT can be applied to supply power to an in-wheel motor from the energy storage system [36], eliminating the risk of disconnection of power and signal cables as well as achieving a compact design with reduced vehicle weight.

2.2 Static WPT

Static WPT occurs when the relative position of the primary coil and the secondary coil is still, as shown in Fig. 2. The scenario is a parking lot or a charging station in a similar fashion of current electric vehicles. In this case, the system load is a CVL, there is no variation of coupling coefficient, the load voltage variation is slow; consequently, at the current stage it is a technology with high feasibility and implementation potential. As a matter of fact, the launch on the market of static WPT is imminent: many car makers (e.g. Nissan [47], Mercedes [48], Toyota [49]) are actively researching and hope to include it in their vehicle fleet starting from 2018. The theoretical design is already established and, as shown in Fig. 3, the proposed static WPT systems in Fig. 3a and Fig. 3b are very similar.

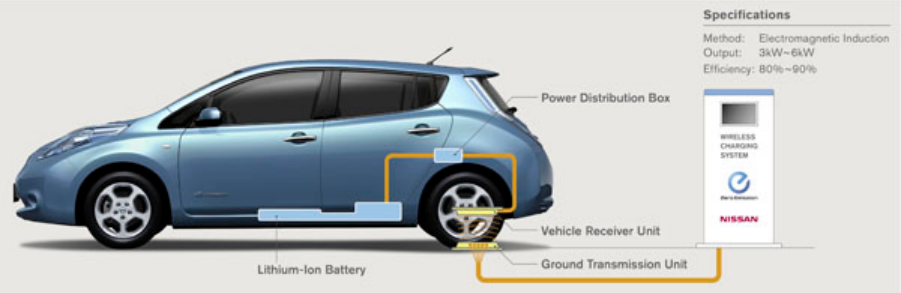

(a) Case of Nissan.

(b) Case of Toyota.

Fig. 3: Examples of static WPT.

In case of static WPT, its utility depends on the robustness to misalignment of the resonant network. The design of the coil couplers is critical for achieving high coupling coefficient and high quality factor and therefore high efficiency. In this sense, past research has been extensive [13] [14]. Another point is that, currently, static charging for EVs occurs on a one transmitter/one receiver base, making the overall control method effective and simple. Moreover, given that the load voltage is assumed slow to change (because it is a CVL), the communication between sides can be adopted without problems caused by time delay as the coils are not moving. The communication serves a moltitude of purposes, from control coordination to coil sensing and foreign object detection [50]. In particular, the latter task is frequently ignored, but is important nevertheless to prevent transmitting efficiency drop and risk of fire due to foreign metal object caught in the magnetic flux between the coils.

From the control point of view, the efficiency is generally optimized by proper design of the primary and secondary side coil; consequently, it is not necessary to perform any particular matching control. The only variable that needs regulation then becomes the power delivered to the load. In fact, in the simplest case of a completely passive secondary side circuit, power control in the primary side is a popular choice, made possible from the aforementioned situation of one-transmitter/one-receiver. However, this kind of control is not practical to implement in dynamic charging scenarios: two totally

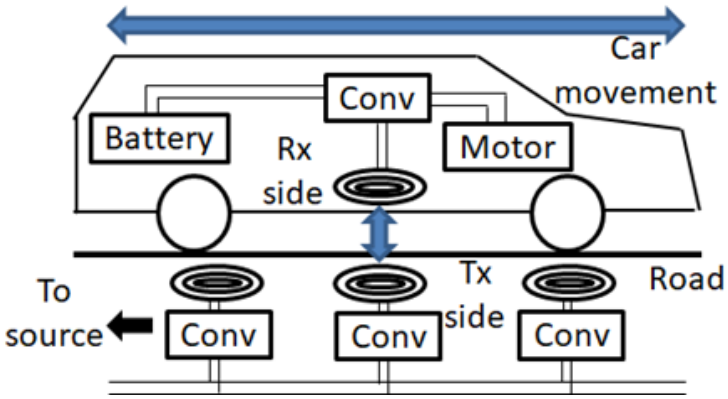

Fig. 4: Concept of dynamic WPT.

different controls would be needed. The need of a control that can be used successfully both in static and dynamic charging condition is then evident. This thesis proposes a control that can be used both in static and dynamic condition in chapter 3.

2.3 Dynamic WPT

As surmised before, a big problem of EVs is the short cruising range. Even though with recent progresses the maximum distance possible with a single full charge has increased to around 400 kilometers, it is still little more than half the maximum distance offered by conventional internal combustion engine vehicles. This value is further reduced if air conditioning or other features are activated. As a countermeasure, feasibility of WPT while EVs are in motion has been researched [51][17]. In this dynamic scenario, the power is transmitted from the primary coil buried in the ground to the secondary coil mounted in the vehicle. The power received from the on-board coil is then delivered to the energy storage system (which includes battery and eventually supercapacitors), which in turn supplies the electric motor, as shown in Fig. 4. In so doing, the driving range is extended indefinitely as long as the vehicle's coil is coupled with the ground side coil connected to the grid. This means that the energy storage system can be downsized, making the vehicle lighter. Concepts of dynamic WPT systems are shown in Fig. 5. The electric bus OLEV from Korea Advanced Institute of Technology (KAIST) [17][18] of Fig. 5a achieved good results, boasting 60 kW of power transferred at DC-to-DC efficiency of 0.7, with misaligment tolerance of 160 millimeters. It uses a segmented module structure using a ferrite core to maximize the magnetic flux density. On the other hand, the prototype of Oak Ridge National Laboratory (ORNL) [41][51] used circular pad coils placed at a distance of 1 meter from center to center, whose activation sequencing is controlled by vehicle passage using trackside photocell interruption. The DC-to-DC efficiency is nearly 0.9 for 3 kW power delivery, and power peaks caused by low coupling coefficient are smoothed by the installed LiC on the primary side. Notable is the fact that a battery-less vehicle whose motor is supplied directly by capacitive WPT has

(a) Case of KAIST. (b) Case of ORNL.

Fig. 5: Examples of dynamic WPT.

been reported [39].

Dynamic WPT shares with static WPT most of the research topics, from coil shape to primary side circuit and compensation topology [52][53], from human safety to reduction of leakage flux . However, there are some critical aspects that are different. First, the coupling coefficient changes accordingly to the misalignment between the coils. This poses some challenges from a control point of view. Second, communication between primary and secondary sides cannot be included in the design of the controller because either the delay may be too long for the control to be effective or the harsh environment may prevent the use of communication. Third, depending on the compensation topology, vehicle detection [54][56] by either wireless signal or by control derived from parameter analysis is necessary. Fourth, depending on the primary side composition, the WPT system will operate in a situation of one-transmitter/multiple-receiver. Fifth, it is necessary to maximize the time for powering while moving in order to lower the power requirements for the power converters and the electric grid. Other than designing the dimension of the coils, it is important to select also a suitable distance between the coils in terms of systems optimization.

Upon considering these characteristics, it is necessary to design a proper control for the system.

2.4 Discussion about compensation topologies

As mentioned in chapter 1, in WPT systems by magnetic resonance coupling there are four different types of compensation topologies, depending on the side and the type of connection of the resonant capacitor. They are series-series (SS), series-parallel (SP), parallel-series (PS) and parallel-parallel (PP) connection. They are shown in Fig. 6. If the primary is series compensated, a voltage source converter could be connected directly to the coil. If the primary is parallel compensated, usually an inductor is inserted to change the converter to a current source.When the primary side coil has a

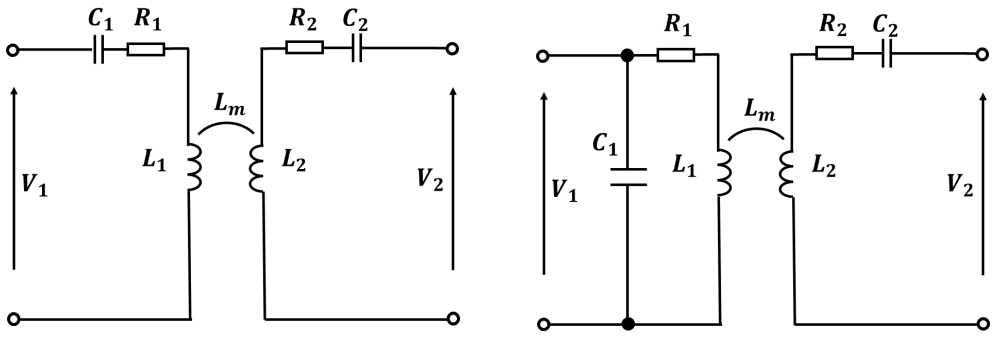

(a) Series-series (SS).

(b) Parallel-series (PS).

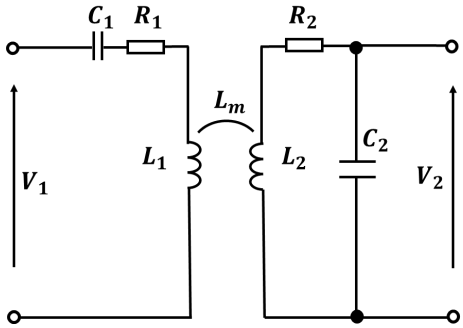

(c) Series-parallel (SP).

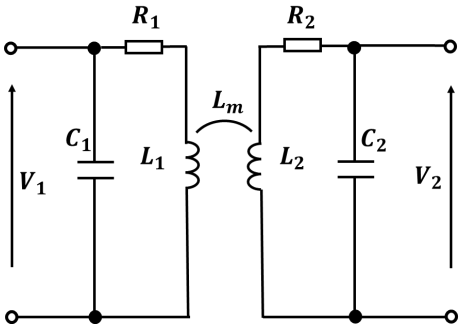

(d) Parallel-parallel (PP).

Fig. 6: Fundamental compensation topologies for WPT by magnetic resonant coupling.

constant current, a series compensation at the secondary side makes the output like a voltage source, while a parallel compensation makes the output like a current source. The primary compensation capacitance design changes according to the type: it is a constant value for SS compensation regardless of the coupling and load conditions. For SP compensation, the capacitance varies when the coupling changes. For PS and PP compensation, the capacitance is affected by both the coupling and load conditions. Another consideration can be done on the value of the equivalent load impdeance related to maximum transmitting efficiency condition: in SS and PS compensation its value is low, on the order of tens of ohm. On the other hand, in SP and PP compensation, its value is two orders for magnitude greater, a couple of thousands ohm. By simple calculation based on practical values of voltage and power for EVs currently on the market, it is possible to determine that the equivalent load impedance varies from a few ohms to some tens of ohms. Based on the previous characteristics, it can be said that, for EV application, the most suitable compensation method is SS. Therefore, this thesis focuses on the case of SS compensation.

2.5 Control in WPT

In this section, the main approaches in control theory for WPT systems are presented. In past research, it was reported that optimal coil design is fundamental to achieve high transmitting efficiency

in WPT systems and much literature has been produced about it. However, this is not a sufficient condition for ensure maximum transmitting efficiency. Furthermore, in case the load requires a determined control (e.g. a battery works in constant current or constant voltage mode), a control of the power flow is required. It so happens that combining efficiency and power is not a simple task. Consequently, control of the converters also plays an important part is securing fully functional WPT. Furthermore, it is important to distinguish the type of the load; in fact, each load has its own characteristics. The difference becomes apparent in dynamic WPT scenario: in fact, while in steady state it is applicable an approximation and substitute a CVL or a CPL with an equivalent resistance, this is not possible during transients. Therefore, a control should not work properly only in steady state, but also in transient conditions deriving from motion or the startup or turn-off.

2.5.1 Efficiency control theory

Since the objective of WPT is to maximize the transmission efficiency with which the desired power is delivered to the load, it requires approaches both from power electronics field and antenna field.
From the point of view of efficiency, the most natural method is reducing losses. Therefore, using a small source impedance, adopting air core couplers and low AC resistance wiring (Litz wire) for the coils contribute altogether to reduce the losses [22]. Apart from these hardware precautions, the factor that effectively determines the efficiency condition is control. For starters, considering the simplest circuit possibile without special converter topologies or additional components, introducing a slight phase shift between the secondary coil AC current and voltage it is possible to force a slight current lag and create an inductive load, augmenting the current loading on the primary side coil; in so doing, the controllability will benefit as it soft switching control by zero-voltage switching (ZVS) or zero-current-switching (ZCS) can be performed. It is in fact worth noting that in case of no phase displacement between AC current and AC voltage (i.e. unity power factor), it is not necessarily guaranteed that the losses of power converters in primary and secondary side are minimum. It is true, however, that if the power factor gets too low the characteristic equation of the system get considerably more complicated and detailed modelling becomes difficult. Thus, from the point of view of system modelling, the condition of resonance and unity power factor is desirable.
The most common approach consists in optmizing the equivalent load impedance (i.e. the secondary side AC/DC converter input impedance). It can be performed from secondary side [42][44][57]–[60] by impedance matching. By using a two stage converter setup (AC/DC converter followed by DC/DC converter) and modifying the duty cycle, it is possible to modify the DC link voltage of the secondary side and therefore set the load impedance to the critical value related to maximum efficiency condition. This approach works both for static and dynamic WPT; however, in case of dynamic WPT the coupling coefficient variation generates a change of the circuit characteristics, possibly leading to undesired operation areas (e.g. frequency bifurcation phenomenon due to air gap change) and posing a

challenge in terms of controller design. In this thesis, too, the impedance matching method is adopted in the controller design of chapter 3.
It is worth noting that the maximum efficiency of a WPT system is achieved by using the optimized equivalent load impedance approach. However, there may be cases where the optimized load impedance operation point is different from the converter efficiency operation zone, therefore more losses are generated in the converter and the maximum efficiency condition is lost. It is then of the utmost importance to design the system in such a way that the rated converter's operation point coincides with the maximum transfer efficiency operation point.

2.5.2 Power control theory

Controlling the power flow is important, especially for CVL needing a constant current charge. The control can be executed either on the primary side [41][51] or in the secondary side [58][62]–[64]. Dual side control has also been proposed [46]. Intuitively, the power sent to the load depends on the voltage amplitude of the primary and secondary coil and the coupling coefficient.
The regulation of the primary side is carried out by modifying the primary side coil voltage by smartly operating switching and augmenting the current circulating in coil; in case of intermediate PFC circuit, it is possible to perform a more efficient frequency and duty control. Phase shift control is not used because in high frequency environment as WPT it would increase switching losses; operation in ZVS or ZCS is performed whenever possible. In the case of regulation by secondary side, the concept is similar: depending on the composition of the converter circuit, different methods have been proposed. With only one converter, it is possible to implement an ON/OFF control regulating the average current; on the other hand, if a DC/DC converter is also present, then a current control can be performed.
As power flow regulation includes many different control methods, communication is used. Power control for dynamic WPT needs to be sufficiently quick to adapt to coupling coefficient variation and be able to avoid the steep changes in power generated by the relative movement of the coils. This thesis will deal with secondary side power flow control in chapter 3, by proposing a ON/OFF type control.

2.5.3 Short review on past literature

In Tab. 1, a comparison between past research results is shown. All types of load and all types of control are reported. It is noted that while the first studies only considered the transfer efficiency and resistance load, the more recent ones deal mostly with constant voltage (CV) loads, as the declared application target is EV battery charging. A particular case is reported in [36], where the load is constant power (CP) and the high efficiency is due to optimized design of the resonant network and

Tab. 1: Comparison of power and efficiency controls for WPT in past literature

Type of control	Controlled side	Type of load	Maximum efficiency	Power [W]	Frequency [kHz]	Communication	Scenario
No control (design only) [12]	None	CR (resistance)	0.95 (AC-AC)	3000	20	No	Static
Power [23]	Secondary	CV (battery)	0.80 (DC-DC)	100000	20	No	Dynamic
Power [36]	Both	CP (motor)	0.91 (DC-DC)	3300	85	Yes	Static
Efficiency [42]	Secondary	CR, CV, supercapacitor	up to 0.72 (DC-DC)	40	13560	No	Static
Power and efficiency [44]	Both	CR, CV	0.90 (AC-AC)	3000	85	Yes	Static
Power and efficiency [45]	Both	CV	up to 0.95 (DC-DC)	500–3000	35	Yes	Static
Power and efficiency [46]	Both	CV	up to 0.94 (DC-DC)	5000	20	Yes	Static
Power [51]	Primary	CV (battery and supercapacitor)	up to 0.91 (DC-DC)	2000	25	No	Dynamic
Efficiency [61]	Secondary	CV	up to 0.71 (DC-DC)	10	140 (out of resonance)	No	Static
Power [63]	Primary	CR	up to 0.71 (DC-DC)	5	97	No	Static

the conversion circuits. In that case, the control is a little more complicated because the CP load is unstable in open loop and need therefore closed loop stabilization must be satisfied. In the case of high frequency as in [42], the power is still low because the switching losses would be enormous otherwise; the DC-to-DC efficiency (also called end-to-end efficiency) is low only because the output power itself is low. In fact, for higher power, the efficiency will be generally higher. In case of literature with EV as target application, although now the standard resonant frequency from the Society of Automotive Engineers (SAE) is between 75 and 90 kilohertz, the frequency used was around 20 kilohertz. In case of dual side coordinated control, the results are quite good and extremely competitive against wired chargers; however, it is necessary to adopt communication. The use of communication may not be applicable or available and it is thus advisable developing alternative such as estimation or sensorless parameter detection, but research in this sense is still at its early stages. Control only on the secondary side is widely used to maximize the transmitting efficiency, whilst power control on the primary is equally a popular choice. However, literature rarely considers real time parameter variation such as coil movement or load change: in order to cope with these issues, typical of dynamic WPT, control on the secondary side is necessary as more realistic and practical. In particular, the control of both power and efficiency on the secondary side is a solution that requires no communication and able to perform well in a variety of situation, making it a valid contribution to WPT research and development.

2.6 Conclusion

In this chapter, an overview of EVs and their feature has been given. In order to solve the issues preventing their widespread use, WPT is deemed one of the most feasible solution. The combination of EVs and WPT brings forth two different scenarios: static WPT and dynamic WPT. The main points of these two scenarios have been discussed, presenting also some past research and application results.

CONTROL FOR WPT SYSTEMS	PRIMARY SIDE	SECONDARY SIDE	NUMBER OF CONVERTER	MERIT	DEMERIT	ORIGINALITY
PRIMARY SIDE POWER CONTROL (CVL)	Inverter +DC/DC converter	Diode bridge	2+1	Simple	Low DOF, not good for DWPT	Low
PRIMARY SIDE EFFICIENCY CONTROL (CVL)	Inverter	Diode bridge	1+1	Simple, cheap	Need of communication, low DOF, not good for DWPT	Low
SECONDARY SIDE EFFICIENCY CONTROL (CVL)	Inverter (+DC/DC converter)	Diode bridge +DC/DC converter	1(2)+2	No need of communication, good for DWPT	Space consuming	Medium
SECONDARY SIDE POWER CONTROL (CVL)	Inverter (+DC/DC converter)	Diode bridge +DC/DC converter	1(2)+2	No need of communication, good for DWPT	Space consuming	Medium
SECONDARY SIDE POWER&EFFICIENCY CONTROL (CVL)	Inverter	Full bridge active rectifier or HAR +DC/DC converter	1+2	High DOF, no communication, good for DWPT	Space consuming	High
SECONDARY SIDE POWER CONTROL (CPL)	Inverter	Full bridge active rectifier	1+1	High DOF, no communication, good for DWPT, little space	Advanced control required, limits by primary side	High
COORDINATED TWO-SIDE CONTROL (CVL,CPL)	Inverter +DC/DC converter	Full bridge active rectifier or HAR (+DC/DC converter)	2+1(2)	Highest DOF, best performance	Space consuming, need of communication, bad for DWPT	Medium

Fig. 7: Different types of control for WPT.

Thus, in a brief discussion about the compensation topologies, it is established that SS compensation is the most suited for EV application. Finally, the control theories have been introduced. In WPT, optimal hardware design alone is necessary but not sufficient to achieve competitive results: control plays an important part, too. Efficiency control is based on matching the load impedance in order to minimize to impedance seen from the source; on the other hand, several power control methods have been investigated in the past, therefore it must be chosen according to the scenario conditions.

A summary including advantages and disadvantages of the possible type of control can be found in Fig. 7. In this thesis, the control reported on the fifth and sixth row are discussed and novel schemes are investigated. Hence, secondary-side-only power and efficiency control in case of CVL as well as secondary side power control in case of CPL will be the main theme of this thesis.

Chapter 3

Secondary-side-only power and efficiency control for constant voltage load

In this chapter, a novel control is proposed based on the consideration explained in chapter 2: no communication between sides is used and only secondary side is manipulated. The control is designed for a WPT system with constant voltage load (CVL) and two power converters in the secondary side. In order to have two degree of freedom of control, both converters contain active devices. The regulated parameters are the average power and the transmitting efficiency. After defining the conditions for correct operation, the controller design is described. Experiments show the feasibility of the proposed control method both in static WPT and dynamic WPT.

3.1 Case of study

This study focuses on the secondary side of a WPT system with series-series (SS) compensation, as shown in the equivalent circuits of Fig. 8. It is possible to write the AC circuit equation by using the impedance matrix as follows:

$$\begin{bmatrix} V_1 \\ 0 \end{bmatrix} = \mathbf{Z} \begin{bmatrix} I_1 \\ -I_2 \end{bmatrix} \tag{3-1}$$

$$\mathbf{Z} = \begin{bmatrix} R_1 + \frac{1}{j\omega C_1} + j\omega(L_1 - L_m) & j\omega L_m \\ j\omega L_m & R_2 + \frac{1}{j\omega C_2} + j\omega(L_2 - L_m) + R_L \end{bmatrix} \tag{3-2}$$

where I_1, and I_2 are the RMS values of the primary current and the secondary current, respectively, and R_L is the load impedance. As for V_1, it is the RMS value of the fundamental wave component of the primary inverter square wave output voltage. Similarly, V_2 is the RMS value of the fundamental wave component of the secondary AC/DC converter input voltage. The primary side coil resistance

is represented by R_1, while R_2 is the one of secondary side coil; on the other hand, the equivalent load impedance is R_L. The phase shift of $\frac{\pi}{2}$ between primary and secondary parameters in Eq. (3-2) is expressed through j.

In the case of perfect resonance, it is possible to consider only the fundamental wave component, thus simplfying the analysis of the circuit. The resonant frequency of the system is obtained from the coil parameters, which are independent from the load and the distance between the coils. The resonant frequency f_{res} and therefore the relative angular frequency ω are expressed as:

$$\omega = 2\pi f_{res} = \frac{1}{\sqrt{L_1 C_1}} = \frac{1}{\sqrt{L_2 C_2}} \tag{3-3}$$

with L_1 and C_1 as the primary coil inductance and capacitance, respectively; similarly, L_2 and C_2 are the secondary coil inductance and capacitance. The coils' internal resistances only affect the losses and the dynamic response of the system. The mutual inductance L_m between the primary and secondary coil depends mainly on the coil geometry and the air gap. The mutual inductance is thus related to the coupling coefficient k as follows:

$$k = \frac{L_m}{\sqrt{L_1 L_2}} \tag{3-4}$$

In this case, the impedance matrix in Eq. (3-2) becomes:

$$\mathbf{Z} = \begin{bmatrix} R_1 & j\omega L_m \\ j\omega L_m & R_2 + R_L \end{bmatrix} \tag{3-5}$$

and the equation in Eq. (3-1) can be rewritten as follows as a function of the AC currents:

$$\begin{bmatrix} I_1 \\ -I_2 \end{bmatrix} = \mathbf{Z}^{-1} \begin{bmatrix} V_1 \\ 0 \end{bmatrix} \tag{3-6}$$

From the aforementioned circuit equations, the voltage ratio A_V and the current ratio A_I between the primary side and the secondary side are described as follows:

$$A_V = \frac{V_2}{V_1} = j\frac{\omega L_m R_L}{R_1(R_2 + R_L) + (\omega L_m)^2} \tag{3-7}$$

$$A_I = \frac{I_2}{I_1} = j\frac{\omega L_m}{R_2 + R_L} \tag{3-8}$$

The transmitting efficiency is consequently derived as following:

$$\eta = \frac{(\omega L_m)^2 R_L}{(R_2 + R_L)[R_1(R_2 + R_L) + (\omega L_m)^2]} \tag{3-9}$$

The load power can be instead obtained easily from:

$$\begin{aligned} P_L &= \frac{V_2^2}{R_L} \\ &= \frac{\|A_V\|^2}{R_L} V_1^2 \\ &= \frac{(\omega L_m)^2 R_L}{[R_1(R_2 + R_L) + (\omega L_m)^2]^2} V_1^2 \end{aligned} \tag{3-10}$$

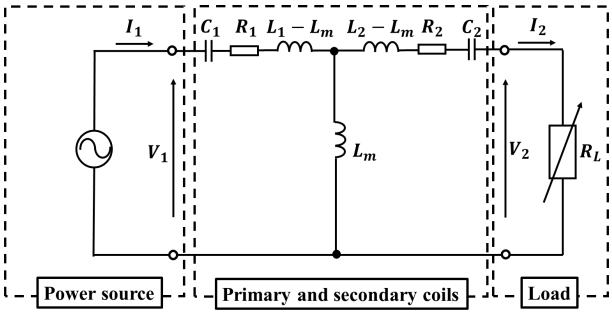

Fig. 8: Equivalent circuit of WPT with magnetic resonant coupling and SS compensation.

The influence of R_L has been the subject of past research [59]–[62]. In particular, the equivalent load impedance associated with maximum transmission efficiency, the one related to maximum deliverable power and the one related to the desired power are different because their operation points are different. When R_L changes, the secondary side voltage V_2 changes accordingly. In case of maximum transmitting efficiency condition, the equivalent load impedance is calculated as:

$$R_{L,\eta max} = \sqrt{\frac{R_2}{R_1}(\omega L_m)^2 + R_2^2} \tag{3-11}$$

Its related secondary side voltage $V_{2,\eta max}$ is given by:

$$V_{2,\eta max} = \sqrt{\frac{R_2}{R_1}} \frac{\omega L_m}{\sqrt{R_1 R_2 + (\omega L_m)^2} + \sqrt{R_1 R_2}} V_1 \tag{3-12}$$

The voltage in Eq. (3-12) is a RMS value. The load power P_L is active power and related to the fundamental wave components of AC parameters. Therefore, in this paper, the focus will be on the fundamental wave components of V_1 and V_2. In addition, the secondary side current I_2 is assumed to be a sinusoidal wave, in phase with V_2.

3.1.1 Topology

3.1.2 Fundamental characteristics of WPT

In Fig. 9 is shown the reference circuit. The coils' inductances and the compensating capacitors are designed according to Eq. (3-3). The primary side includes a DC voltage source and an inverter, where in the secondary side there are a HAR, a DC/DC converter and the battery load. The battery is considered not optimized to receive ripple current, therefore the capacitance C_{DC} and inductor L are chosen in such a way that the current I_{DC0} is smoothened enough before reaching the battery.

The HAR is an AC/DC converter whose topology resembles the bridgeless PFC circuit [37]. In the high side there are two diodes, but in the low side there are two active devices. Its operation is divided into two modes, as shown in Fig. 10:

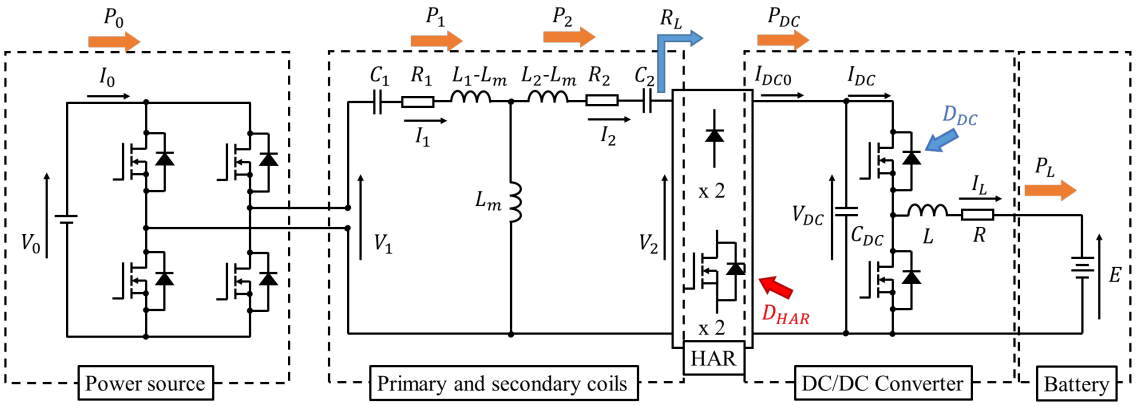

Fig. 9: Reference circuit of WPT system.

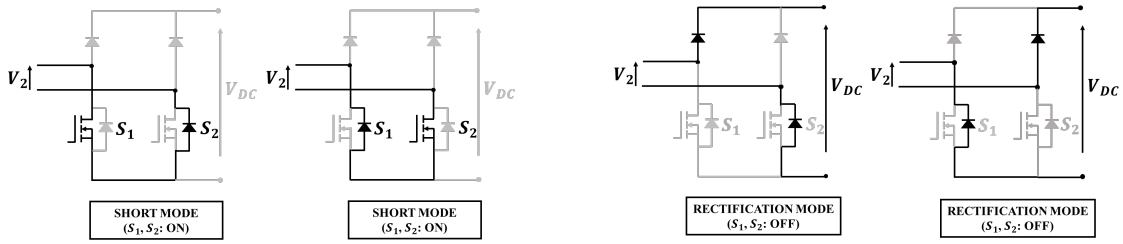

(a) Short mode.

(b) Rectification mode.

Fig. 10: HAR operation modes.

- Short mode: both the low side devices S_1 and S_2 are turned ON. In so doing, the coil terminal are short-circuited and no current flows to the secondary DC bus. The DC link voltage V_{DC} consequently decreases as the smoothing capacitor C_{DC} supplies the load. This is possible because the SS compensation topology makes the secondary side coil act like an equivalent current source, thus allowing the secondary side coil short-circuit. There is meaning in short mode because the impedance seen from the secondary side is very high, thus the primary side current I_1 becomes very low. In fact, the reflected impedance from the secondary side is expressed by:

$$Z_R = \frac{(\omega L_m)^2}{R_2 + R_L} \tag{3-13}$$

As it can be seen, during short mode R_L becomes very little because the secondary coil's terminals are shorted and the only resistance is given by the series of the active devices' and diodes' on-resistances. Therefore, since R_L is on the denominator side, Z_R will become very big. Thus, since the primary side coil input impedance (i.e. the resonant network input impedance) Z_{in} is given by:

$$Z_{in} = R_1 + Z_R \tag{3-14}$$

it is clear that Z_{in} will become very big as well. Consequently, with bigger input impedance, the primary side current I_1 will become very low. It is shown in Fig. 10a.

- Rectification mode: both the low side devices S_1 and S_2 are turned OFF. The HAR behaves like a full bridge diode rectifier and consequently the load is supplied. The DC link voltage V_{DC} increases as C_{DC} is charged. It is shown in Fig. 10b.

By switching between these two modes, the average power can be controlled. The HAR operation limits secondary side heating but increases the electromagnetic interference (EMI)[37]. Finally, the duty cycle expresses the ratio between short mode and switching period, as written in Eq. (3-15):

$$0 < D_{HAR} = \frac{t_{short}}{t_{short} + t_{rect}} = t_{short} f_{HAR} < 1 \tag{3-15}$$

with f_{HAR} as the HAR switching frequency.

3.2 Proposed control concept

In this paper, a novel control combination carried out entirely on the secondary side of a WPT system is proposed. The HAR and the DC/DC converter operate independently from the primary side inverter, whose duty cycle is fixed. The secondary side is not synchronized with the primary side and do not benefit from any kind of communication device (e.g. Bluetooth). The simultaneous regulation comprises the average power control by the HAR and the efficiency control through DC link voltage regulation via DC/DC converter. The proposed control method can be adopted for any power level.
In the conventional maximum efficiency control from secondary side, the operation point is fixed. For a given R_L, there are a unique secondary power P_2 and a unique DC-to-DC efficiency η_{DC}. Hence, when the load impedance seen from the secondary coil is equal to $R_{L,\eta max}$, the efficiency is η_{max} and the power is $P_{L,\eta max}$. This will not change unless the mutual inductance L_m or the primary side voltage V_1 varies. In the proposed control, the operation point is the same; however, the switching between short mode and rectification mode allows manipulating the average power P_{DC}. Hence, it is possible to send a different power value while maintaining nearly the same transmitting efficiency.

The control concept can be visually explained by Fig. 11. In rectification mode, the RMS value of secondary side voltage is unchanged because the DC/DC converter controls V_{DC} to be equal to $V_{DC,\eta max}$ according to Eq. (3-16):

$$V_{DC,\eta max} = \frac{\pi}{2\sqrt{2}} V_{2,\eta max} \tag{3-16}$$

The RMS value of secondary current I_2 during rectification mode can be calculated by rearranging Eq. (3-7) and Eq. (3-8) and is given by [38]:

$$I_2 = \frac{\omega L_m V_1 - R_1 V_2}{R_1 R_2 + (\omega L_m)^2} \tag{3-17}$$

However, given the short mode, the HAR output current I_{DC0} can be rewritten by considering Fourier

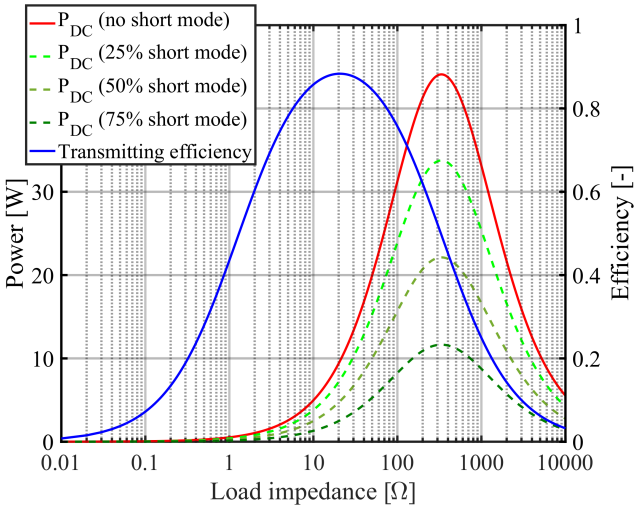

(a) Power and efficiency curves for the parameters in Tab. 2.

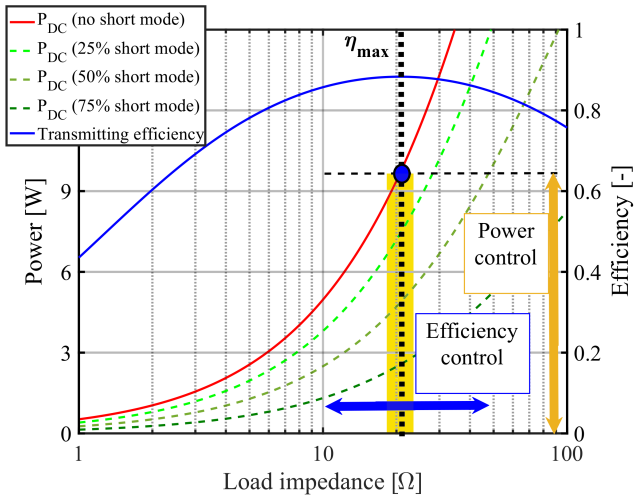

(b) Enlargement of power and efficiency curves with operation ranges.

Fig. 11: Proposed control concept.

series and its value is equal to:

$$I_{DC0} = \begin{cases} \frac{2\sqrt{2}}{\pi} I_2 & \text{(Rectification mode)} \\ 0 & \text{(Short mode)} \end{cases} \tag{3-18}$$

Since I_{DC0}'s value depends on the operation mode of the HAR, the average value of Eq. (3-18) over the HAR switching period can be derived as follows:

$$\bar{I}_{DC0} = \frac{2\sqrt{2}}{\pi} I_2 (1 - D_{HAR}) \tag{3-19}$$

The power $\bar{P}_{DC}$ is the parameter under control and is calculated via multiplication of Eq. (3-19) by Eq. (3-16). Therefore, $\bar{P}_{DC}$ is the averaged value of P_{DC}.

It should be noted that, during short mode, the smoothing capacitor C_{DC} provides the power to the load. Consequently, P_L is not intermittent but a continuous value and the load is always supplied

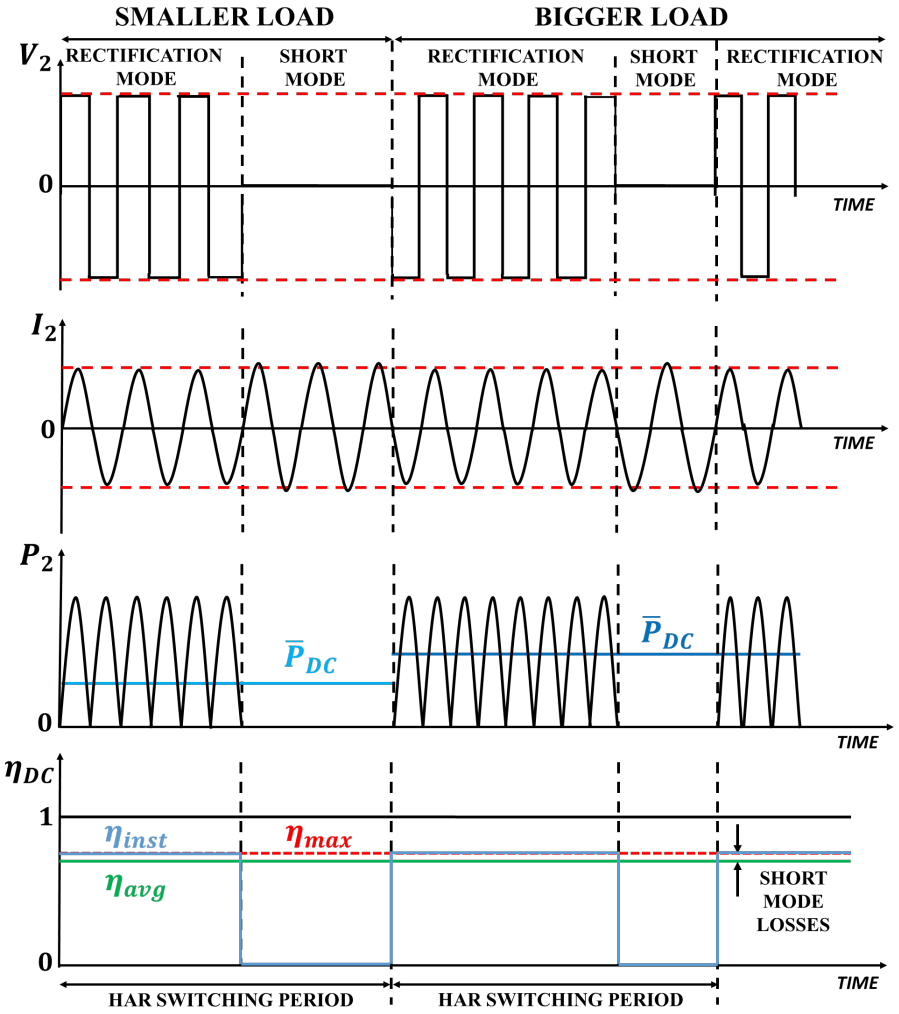

Fig. 12: Parameters waveforms.

with a high transmitting efficiency. The proposed control is highlighted by the transparent area in Fig. 11b. For the experimental evaluation of the DC-to-DC efficiency, the DC powers in both primary and secondary side are taken into account. With reference to Fig. 9, P_0 is the primary side DC power and P_{DC} is the secondary side one. However, since P_{DC} is an averaged value which includes short mode time, the DC-to-DC efficiency will be slightly lower. In fact, during rectification mode the DC-to-DC efficiency is maximum, while during short mode it will drop. In this latter case, there are losses in the secondary side coil and the primary side circuit due to the circulating current. However, the reflected impedance to the primary side becomes very high, causing I_1 to be very low. Hence, considering the HAR switching period, the short mode losses P_{short} consist mainly in conduction loss determined by I_2 and R_2 and the on-resistance of active devices S_1 and S_2. On the contrary, the rectification mode losses P_{rect} include both conduction and switching losses in both sides. In other words, P_{rect} is much bigger than P_{short}. Thus, the DC-to-DC efficiency reduction due to averaging is limited and is proportional to R_2 and the active devices' on resistance. In fact, both P_0 and P_{DC} change along D_{HAR}, so that their ratio is unvaried and the only difference is the addition of short mode losses.

As for the waveforms of the proposed control, they are shown in Fig. 12. The HAR input voltage V_2 becomes close to zero during short mode, while the HAR input current I_2 is slightly higher. The input power P_2 then changes accordingly to the previous waveforms; its average value P_{DC} depends on short mode duration. As for efficiency, the instantaneous value η_{inst} is equal to the maximum value η_{max} in rectification mode, while in short mode it is equal to zero. When calculating the efficiency over the switching period, the averaged value is constant even if the instantaneous value changes according to the operation mode.

3.3 Controller design

In the previous chapter, the proposed control method has been explained. In order to proceed with the controller design, the following two conditions are assumed:

1. The primary side source voltage V_0, the resonant frequency f_{res}, the system operation frequency f and the mutual inductance L_m are given and fixed.

2. The HAR switching frequency is at least one order of magnitude lower than the DC/DC converter switching frequency and their values are fixed.

The first assumption means that the primary side has a fixed operation point that sets the limits for maximum load power and the maximum transmitting efficiency achievable. If the V_0 changes, the proposed control will still operate but with a lower performance.
The second assumption prevents operation conflicts due to the two different time constants. Switching frequency modulation is not considered in this paper.

The block diagram of both HAR and DC/DC controllers are shown in Fig. 13. Each controller is composed by a feedforward part and a feedback part. The feedback part of both the controllers is designed with the pole placement method.

3.3.1 HAR controller

The HAR controller actually controls the current because the DC/DC converter regulates the secondary DC voltage V_{DC}. Considering Eq. (3-18) and Eq. (3-19), the HAR plant can be derived easily and it is given by:

$$P_{DC} = \begin{cases} P_2 & \text{(Rectification mode)} \\ 0 & \text{(Short mode)} \end{cases} \tag{3-20}$$

Then, by the same averaging expression over the switching time used previously, Eq. (3-20) becomes:

$$P_{HAR} = \bar{P}_{DC} = P_2(1 - D_{HAR}) \tag{3-21}$$

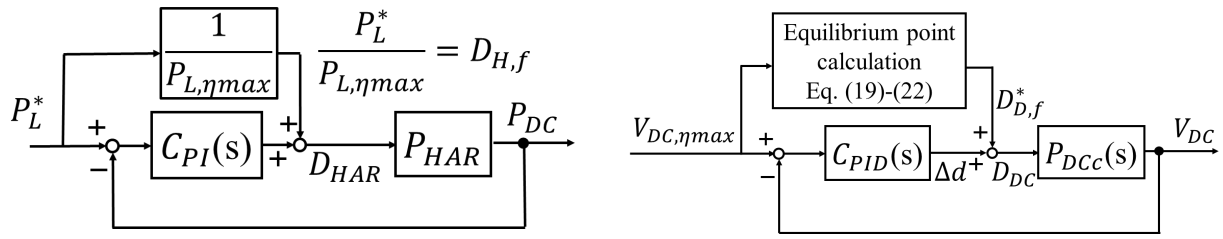

(a) HAR.

(b) DC/DC converter.

Fig. 13: Block diagram of controllers.

The linearized plant model of the HAR is simple, consequently a PI controller $C_{PI}(s)$ is deemed sufficient.

In order to set the equilibrium point, it is necessary to know the value of the transmitted power at maximum efficiency condition. First, by substituting Eq. (3-12) in Eq. (3-17), the secondary current in maximum efficiency condition is obtained as following:

$$I_{2,\eta max} = \frac{\omega L_m V_1 - R_1 V_{2,\eta max}}{R_1 R_2 + (\omega L_m)^2} \tag{3-22}$$

Then, by simply multiplying Eq. (3-12) to Eq. (3-22), the transmitted power at maximum efficiency condition $P_{L,\eta max}$ is calculated and it is given by:

$$P_{L,\eta max} = V_{2,\eta max} I_{2,\eta max} \tag{3-23}$$

The feedforward part of the HAR duty $D_{H,f}$ is then determined as the ratio between the desired power P_L^* and Eq. (3-23):

$$D_{H,f} = \frac{P_L^*}{P_{L,\eta max}} \tag{3-24}$$

Clearly, P_L^* must be smaller than $P_{L,\eta max}$, otherwise the proposed control will not operate as expected. If higher power is needed, the solution simply consists in increasing the primary side voltage V_1 and recalculating the parameters.

3.3.2 DC/DC converter controller

In this case of study, the DC/DC converter is a buck converter. Past research described thoroughly how to model the converter by the state space averaging [60][54]. Thus, in this paper the modeling process will be omitted. Since the DC/DC converter is a non-linear system, it is necessary to linearize the converter plant and obtain Eq. (3-25) for control design. The linearized converter plant P_{DCc} is a transfer function from Δd to the DC link voltage V_{DC}, given by:

$$P_{DCc}(s) = \frac{\Delta V_{DC}}{\Delta d} = \frac{b_1 s + b_0}{s^2 + a_1 s + a_0} \tag{3-25}$$

$$a_1 = \frac{R}{L} + \frac{8}{\pi^2}\frac{R_1(1-D_{HAR})}{C_{DC}[R_1R_2+(\omega L_m)^2]}$$
$$a_0 = \frac{1}{LC_{DC}}\left[D_{D,f} + \frac{8}{\pi^2}\frac{RR_1(1-D_{HAR})}{R_1R_2+(\omega L_m)^2}\right]$$
$$b_1 = -\frac{I_L}{C_{DC}}, \quad b_0 = -\frac{RI_L + D_{D,f}V_{DC}}{LC_{DC}}$$

where R and L are the DC/DC converter resistance and inductance, respectively; $D_{D,f}$ is the feedforward part composing the high side device duty cycle and I_L is the load current. The transfer function is a second order system, therefore it is desirable to use a PID controller $C_{PID}(s)$. In the controller, a low pass filter is cascaded with the derivative term to reduce the high frequency noise. The aim of the control is matching V_{DC} with the maximum efficiency voltage, whose expression is derived by Eq. (3-16). The equilibrium value in Eq. (3-26) and Eq. (3-27) satisfy the state space model of DC/DC converter and are given as follows:

$$V_{DC}^* = \frac{ED_{D,f}^* + RI_{DC}^*}{{D_{D,f}^*}^2} = V_{DC,\eta max} \tag{3-26}$$

$$I_L^* = \frac{I_{DC}^*}{D_{D,f}^*} \tag{3-27}$$

where V_{DC}^*, I_L^*, I_{DC}^* and $D_{D,f}^*$ are the equilibrium point values of V_{DC}, I_L, I_{DC} and $D_{d,f}$, respectively. From here, it is possible to compute the remaining equilibrium points. The DC/DC converter input voltage reference I_{DC}^* can be derived from Eq. (3-16), Eq. (3-18), and Eq. (3-25):

$$I_{DC}^* = \frac{8}{\pi^2}\frac{\omega L_m V_0 - R_1 V_{DC}^*}{R_1R_2+(\omega L_m)^2}(1-D_{HAR}) \tag{3-28}$$

Finally, the feedforward part of the DC/DC converter duty $D_{D,f}^*$ is computed from Eq. (3-26) and Eq. (3-28) as follows:

$$D_{D,f}^* = \frac{E + \sqrt{E^2 - 4RV_{DC}^*I_{DC}^*}}{2V_{DC}^*} \tag{3-29}$$

These formulations are very easy to obtain and can be calculated offline in case of the static scenario. However, in case of dynamic scenario, efficiency control must be performed in real time. This means that the information of mutual inductance must be estimated and used in the controller. Consequently, the DC/DC converter controller uses a PID feedback.

3.4 Static charging scenario experiment

In order to verify the effectiveness of the proposed method, experiments have been performed in a static scenario. In this scenario the coil position is fixed, therefore the mutual inductance L_m is constant.

The experimental setup is shown in Fig. 14. It includes a DC generator (TAKASAGO ZX-400LA),

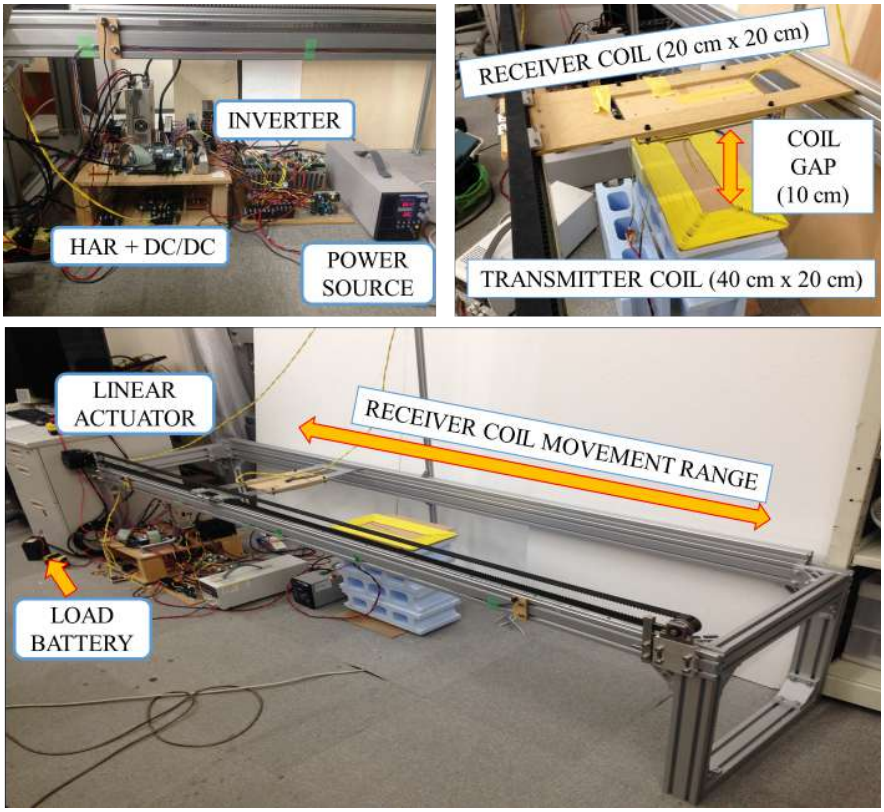

Fig. 14: Experimental setup.

the primary side inverter, the primary and secondary coils, the HAR, the DC/DC converter and the load battery. Both the HAR and the DC/DC converter use silicon MOSFETs (IRFB3607) as active devices. The control is carried out with a DSP board (Myway PE-PRO/F28335A). In each side there are one voltage and one current sensor: in the primary side the inverter input voltage V_0 and current I_0 (and consequently P_0) are measured; the secondary side sensors measure the HAR output current I_{DC0} and voltage V_{DC} (and consequently P_{DC}). The reason for using only DC sensors is to reduce the installation cost. The receiving coil is mounted on a stage and it is possible to move it via a linear actuator. The controller poles frequencies chosen in the experiment are 10Hz for the HAR and 170Hz for the DC/DC converter. The experiment parameters are reported in Tab. 2. The proposed control is compared with the secondary side efficiency control in order to prove that the desired power is delivered with near maximum efficiency. The comparison is carried out by experiments. The experiments are performed on low power, but the concept can be applied to any power level. The experimental results for the secondary side efficiency control and the proposed one are shown in Fig. 15 and Fig. 16, respectively. In the first case, the secondary side control only maximizes η_{DC}. Thus, the power is not manipulated at all and η_{DC} is the maximum achievable efficiency for the system. In the other case, a desired power of 3 W is considered; then, halfway in the experiment, the power reference has a step change up to 6 W. This means that the HAR duty cycle D_{HAR} has a step change. This variation is introduced to prove the proposed control robustness. In both the

Tab. 2: System parameters.

Parameter	**Value**
Primary side DC voltage source V_0	18 V
Primary side coil resistance R_1	1.83 Ω
Secondary side coil resistance R_2	1.683 Ω
Primary side coil inductance L_1	417.8 μH
Secondary side coil inductance L_2	208.3 μH
Primary side coil capacitance C_1	6.03 nF
Secondary side coil capacitance C_2	12.15 nF
Operation frequency f	100 kHz
Mutual inductance L_m (best alignment)	37.9 μH
Coil gap (best alignment)	100 mm
Smoothing capacitor C_{DC}	1000 μF
DC/DC converter resistance R	0.2 Ω
DC/DC converter inductance L	1000 μH
Load battery voltage E	6 V
HAR switching frequency f_{HAR}	0.5 kHz
DC/DC converter switching frequency f_{DC}	10 kHz

conventional state-of-the-art efficiency control and the proposed one, the efficiency maximization is achieved with the equivalent load impedance optimization method, as explained in Section II and Section IV; this method is sound and it has been adopted in previous literature as [36]–[57] and [58]–[54]. In the figures, the instantaneous values are indicated by thin lighter lines while averaged values are represented by thicker dark lines.

In Fig. 15a and Fig. 16a, the DC link voltage V_{DC} is controlled to match the reference value, represented by the black dashed line. In particular, Fig. 16a shows that the voltage control of the proposed method is resistant to power steps.

The DC power P_{DC} is shown in Fig. 15b and Fig. 16b. In Fig. 15b the power is not controlled; on the other hand, Fig. 16b shows that P_{DC} is successfully controlled. In fact, the instantaneous power fluctuates due to the switching between the operation modes. Here, the red line represents P_0, the

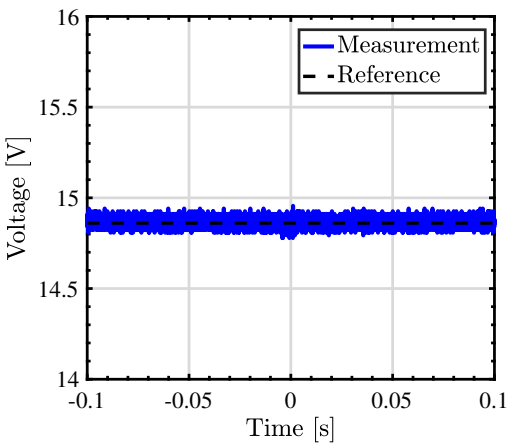

(a) DC link voltage V_{DC}.

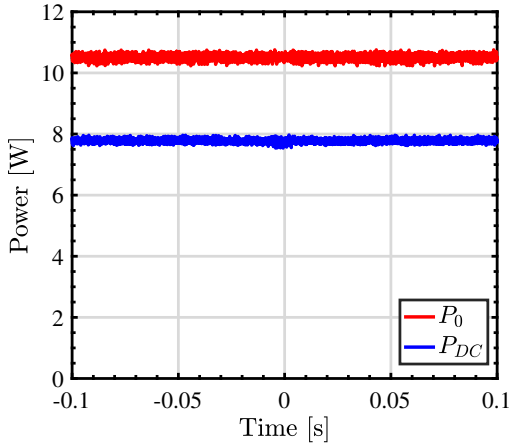

(b) Primary power P_0 and secondary power P_{DC}.

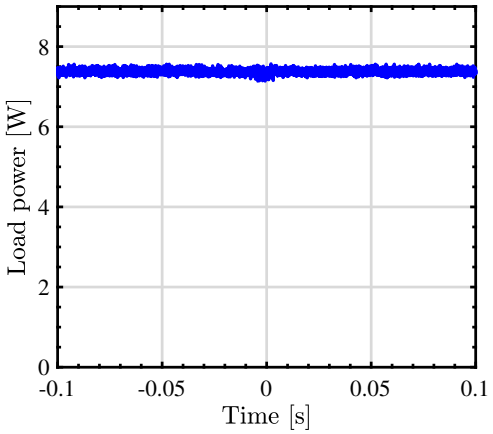

(c) Load power P_L.

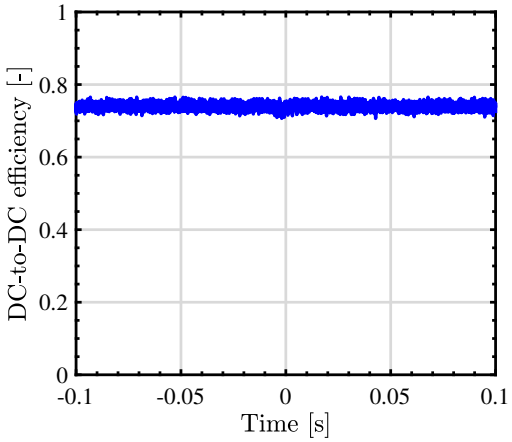

(d) DC-to-DC efficiency η_{DC}.

Fig. 15: Experimental results of secondary side efficiency control (only maximum efficiency).

blue line is P_{DC} and the black dashed line is the secondary side power reference.

The load power P_L is shown in Fig. 15c and Fig. 16c. With the secondary side efficiency control, it is impossible to change the power; however, as shown in Fig. 16c, the proposed control successfully regulates the power to the desired value.

Finally, the DC-to-DC efficiency η_{DC} is shown in Fig. 15d and Fig. 16d. The instantaneous value is obtained from the ratio between P_{DC} and P_0. In Fig. 15d, its value is 0.74 and it is the maximum achievable efficiency for the system; on the other hand, in Fig. 16d η_{DC} follows the same pattern of the power in Fig. 16b. However, the averaged value is 0.7 and is unvaried regardless of the step change of D_{HAR}, apart from the short transient occurring at the moment of the step change. As surmised in the previous section, the short mode losses depend on R_2 and the active devices' on resistance, accounting for a average DC efficiency reduction of about 4%. Furthermore, in Fig. 17, the experimental data on the variation of η_{DC} with the duty of the HAR D_{HAR} is shown. It is clear that with D_{HAR} equal to zero the maximum efficiency can be achieved as short mode does not occur; similarly, when D_{HAR}

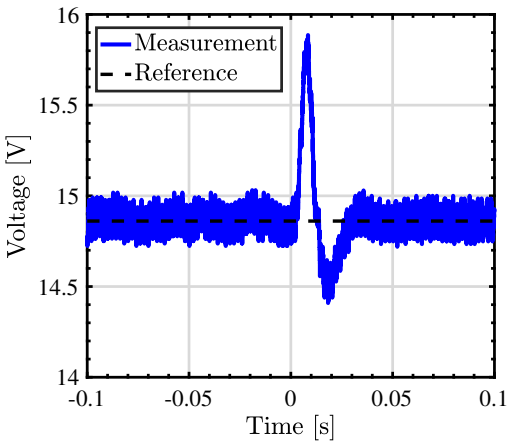

(a) DC link voltage V_{DC}.

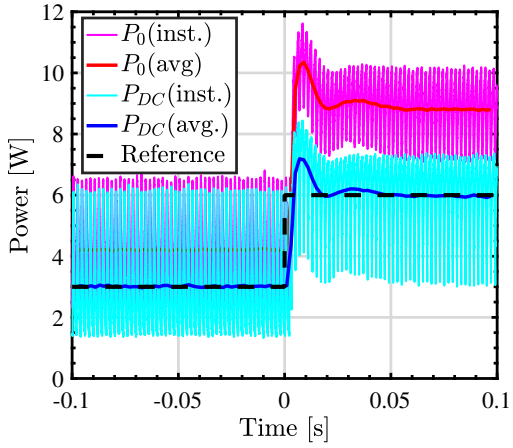

(b) Primary power P_0 and secondary power P_{DC}.

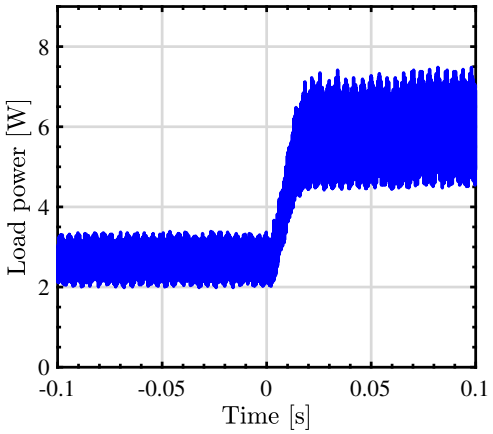

(c) Load power P_L.

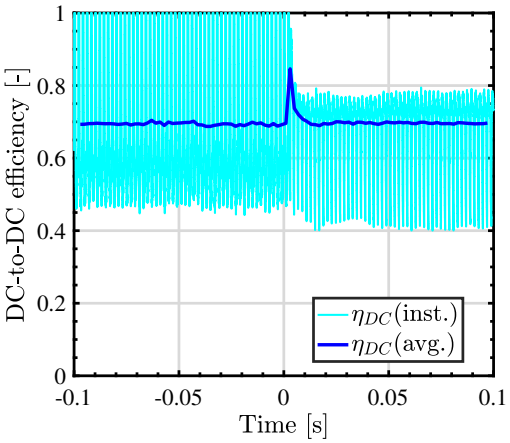

(d) DC-to-DC efficiency η_{DC}.

Fig. 16: Experimental results of proposed control (near-maximum efficiency and desired power).

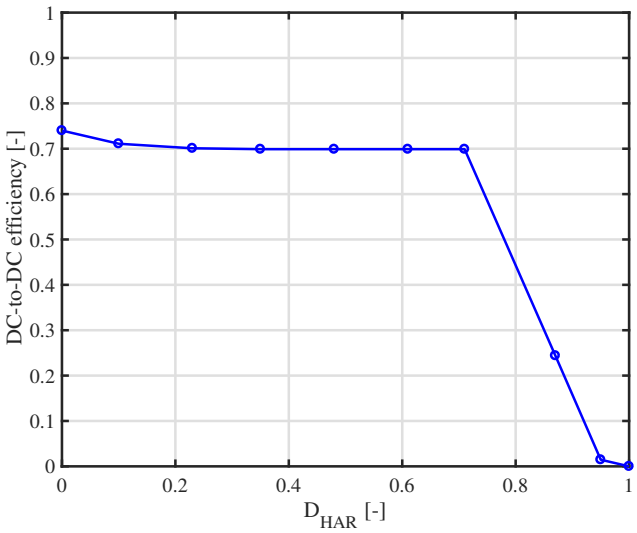

Fig. 17: DC-to-DC efficiency η_{DC} for different HAR duty cycle

(a) Power supply and electronic load pQUBE.

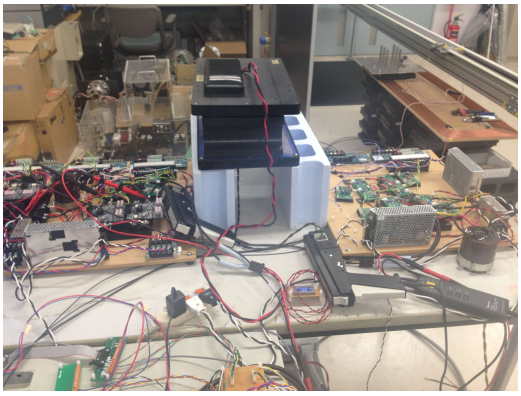

(b) Primary coil (lower) and secondary coil (higher).

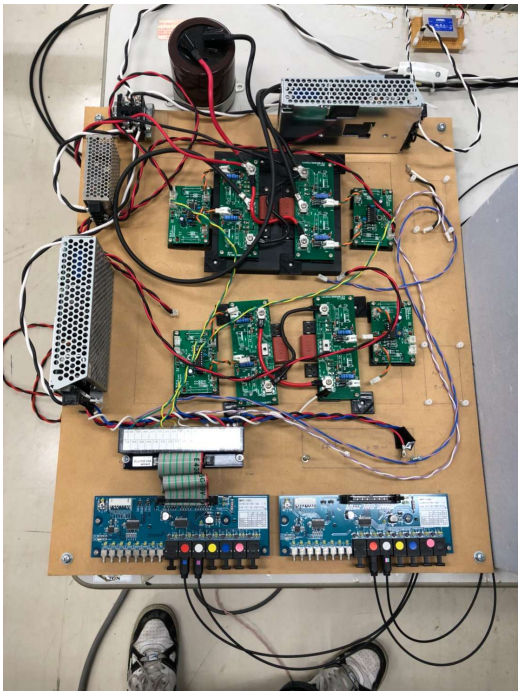

(c) Primary side circuit.

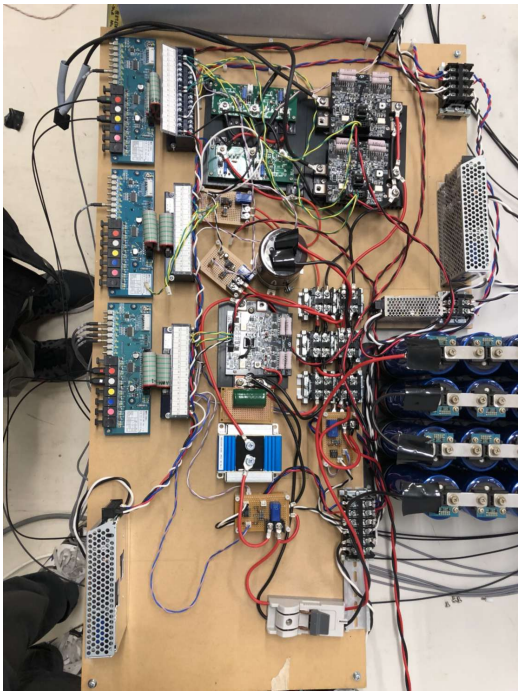

(d) Secondary side circuit.

Fig. 18: Experimental setup for high power experiment.

is equal to one the efficiency is zero because no power sent from the source reaches the load. It is seen that the η_{DC} is practically unchanged for values of D_{HAR} from 0.3 to 0.7, with short mode losses reducing the efficiency of about 4%. For higher values, the short mode losses become of the same magnitude of the desired power and therefore the efficiency is greatly decreased.

3.4.1 Higher power experiment

According to the Japanese law [65][66], the power level must be kept under 50 W in a system using high frequency. For higher power levels, permission must be obtained from the government after demostrating that the experimental equipment does not interfere with the surrounding environment at

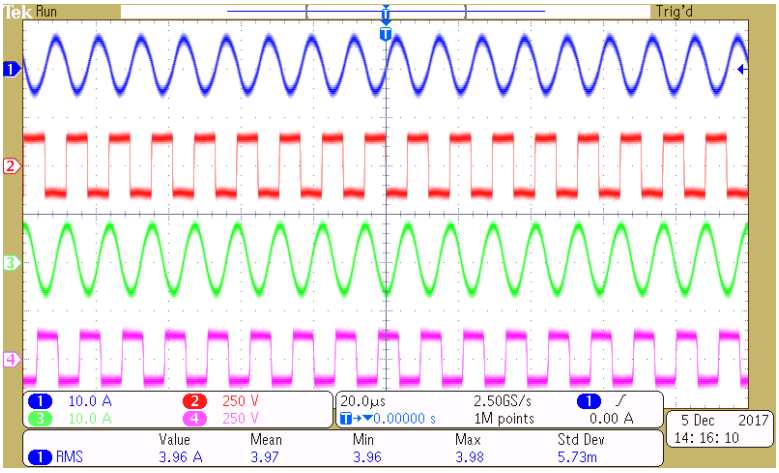

Fig. 19: AC voltages and currents in steady state with conventional efficiency control.

high power. Since the experimental setup has not been given the permission for higher power, another experimental setup, which is approved, is used to prove the effectiveness of the proposed control at higher power. The experimental setup is shown in Fig. 18. Two units of the same DC power supply (pQUBE MWBFP3-1250-J02, Myway), shown in Fig. 18a, have been used: one is used as primary side power supply, another is used as electronic load simulating a 48V battery. A little overview of the conversion circuit as well as the coils is shown in Fig. 18b. The coils are in best alignment condition, at a gap of 10 millimeters. The primary side circuit is shown in Fig. 18c; the converter circuit in the middle is part of the setup but it is bypassed since it is not included in the original reference circuit of Fig. 9. Similarly, the secondary side is pictured in Fig. 18d; here, the upper converter in the green board and the bank of supercapacitor in the right are bypassed, too, since are not part of this experiment. The pole placement procedure in this higher power experiment is the very same as before, with the HAR controller having a pole at a frequency of 10Hz and the DC/DC converter at 170Hz.

The system parameters of this setup are reported in Tab. 3. In this experiment, too, the conventional secondary side impedance matching control for maximum efficiency is compared to the proposed secondary-side-only simultaneous power and efficiency control. Just like in the previous subsection, in the experiments, at the time $t = 0$ the power reference is changed; this applies only to the proposed control, because the conventional efficiency control cannot perform power control. With respect to the previous experiment, the power converted wirelessly in this case is more than 50 times higher, thus providing a better simulation of the real EV application. The experimental results are in Fig. 19, Fig. 20 and Fig. 21.

In Fig. 19, the AC parameters of voltages and current are reported in the case of conventional efficiency control by impedance matching. The square waves are voltages, and the sinusoidal waveforms are currents. In particular, the blue line is I_1, the red line is V_1, the green line is I_2 and the magenta line is V_2. It is possible to see that the secondary side parameters are shifted by 90 degrees, thus confirming the condition of perfect resonance.

Tab. 3: System parameters for higher power experiment.

Parameter	**Value**
Primary side DC voltage source V_0	150 V
Primary side coil resistance R_1	0.558 Ω
Secondary side coil resistance R_2	0.362 Ω
Primary side coil inductance L_1	269.9 μH
Secondary side coil inductance L_2	224.5 μH
Primary side coil capacitance C_1	12.99 nF
Secondary side coil capacitance C_2	15.62 nF
Operation frequency f	85 kHz
Mutual inductance L_m (best alignment)	25.78 μH
Coil gap (best alignment)	100 mm
Smoothing capacitor C_{DC}	2145 μF
DC/DC converter resistance R	0.041 Ω
DC/DC converter inductance L	60.8 μH
Electronic load voltage E	48 V
HAR switching frequency f_{HAR}	0.5 kHz
DC/DC converter switching frequency f_{DC}	10 kHz

In Fig. 20, the experimental results for the conventional efficiency control are shown. In this setup, the DC voltage related to maximum efficiency is around 106V, and the DC/DC converter successfully controls V_{DC} to match the reference, as shown in Fig. 20a. The secondary power P_DC is reported in Fig. 20b; as expected, the value is continuous because no short mode is used. At maximum efficiency condition, P_{DC} is 420W. The load power, on the other hand, is shown in Fig. 20c: in this case its value is continuous as well and is 411W. The time scale is different on purpose to show the minuscule oscillations during the continuous conduction. Finally, in Fig. 20d, the DC-to-DC efficiency (from source to load) η_{DC} for different values of V_{DC} has been measured and plotted in a graphic. The efficiency is derived by the ratio between P_{DC} and P_0. It can be seen that the maximum value of η_{DC} is almost 0.9 and that is practically constant over a V_{DC} range of 30V with a maximum variation of 0.03 points. Since the setup is designed for a nominal V_{DC} of 350V, it means that, at lower power

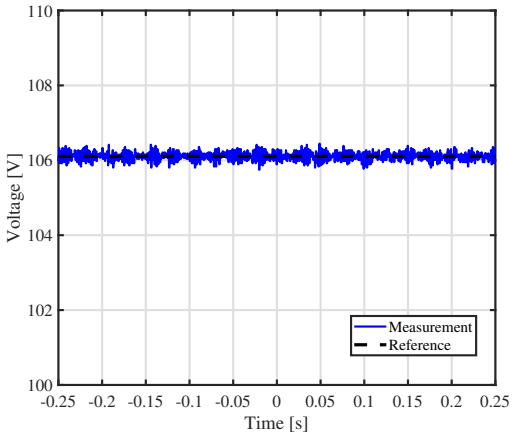

(a) DC link voltage V_{DC}.

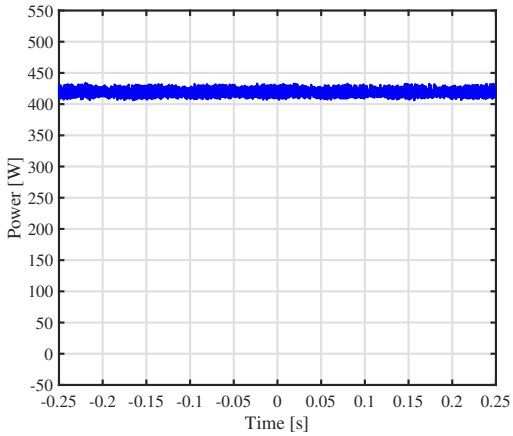

(b) Secondary power P_{DC}.

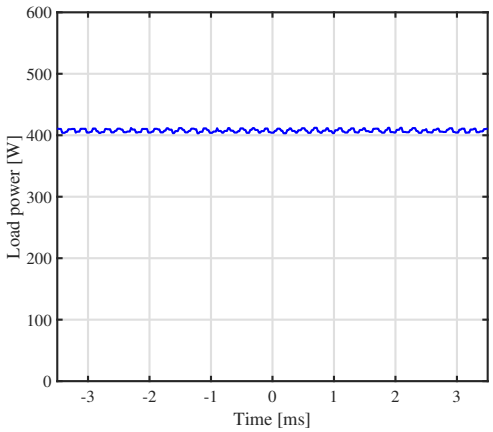

(c) Load power P_L.

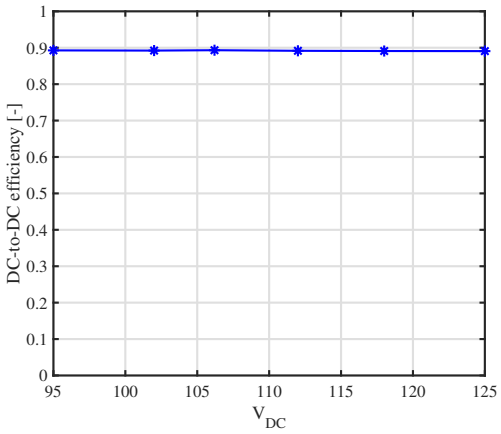

(d) DC-to-DC efficiency η_{DC} for different V_{DC}.

Fig. 20: Experimental results of secondary side efficiency control (only maximum efficiency).

levels, the efficiency does not change much as the variation of load impedance R_L is always within the peak area.

In Fig. 21, the experimental results for the proposed simultaneous efficiency and power control are shown. In this case, at $t = 0$, there is the change of power reference from 250W to 350W; it is noted that in the previous case the load power was 411W with no short mode ($D_{HAR} = 0$). It is expected that the HAR regulates its duty in order for the average secondary power to match the reference. The DC current sensors are placed after the DC capacitor (DC/DC converter input current) and after the converter inductor (load current); on the other hand, the DC voltage sensor is placed at the terminals of the DC capacitor.

In this case, too, the DC voltage related to maximum efficiency is around 106V, and the DC/DC converter successfully controls V_{DC} to match the reference, as shown in Fig. 20a. Although the power reference changes at $t = 0$, the voltage has a little transient but then it returns back to the reference in about 50 milliseconds. The secondary power P_{DC} is reported in Fig. 21b; as expected, the operation

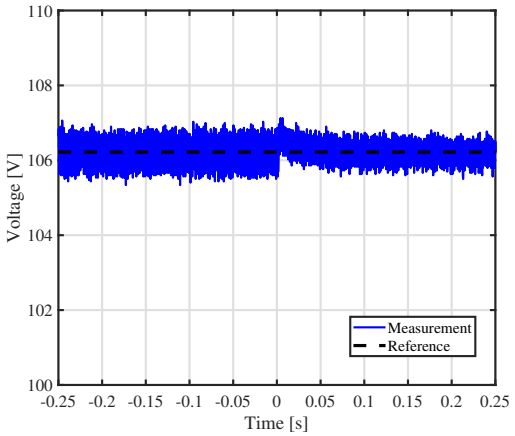

(a) DC link voltage V_{DC}.

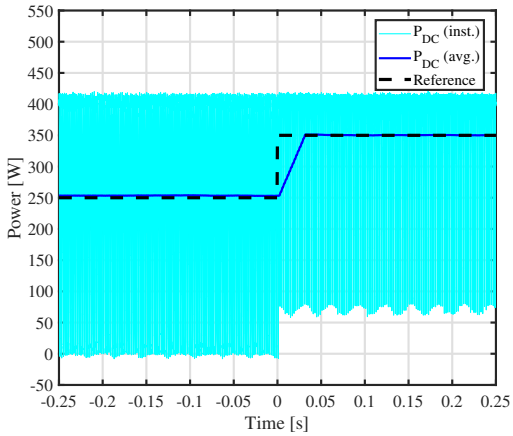

(b) Secondary power P_{DC}.

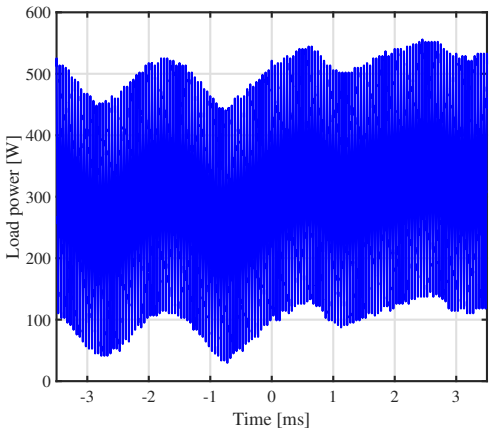

(c) Load power P_L.

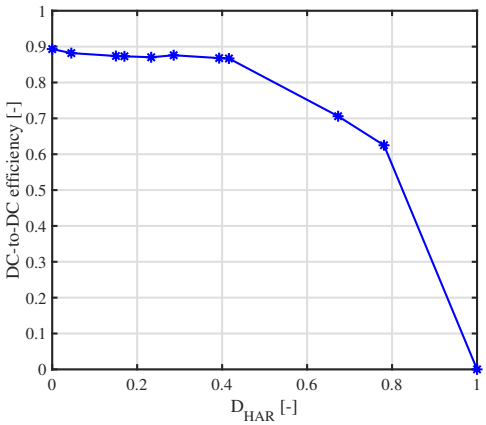

(d) DC-to-DC efficiency η_{DC} for different HAR duty cycle.

Fig. 21: Experimental results of proposed control (near-maximum efficiency and desired power).

of short mode is very visible as P_{DC} is oscillating between zero and the full value. However, it can be seen that the average value of P_{DC} meets the reference in 40 milliseconds. When the power is 350W, the value does not reach zero because of the big capacitor smoothing the DC/DC converter input current. The data of the instantaneous power is obtained with a sampling of 20 μs, and the HAR switching period is 2 ms: it is therefore acceptable to calculate the average from the instantaneous data since the sampling time is more than ten times shorter with respect to the HAR switching. The load power, on the other hand, is shown in Fig. 21c: in this case, the inductor of the DC/DC converter is only $60\eta H$, consequently it effect of short mode is clearly visible. In particular, it is noted the HAR switching periods of 2 milliseconds by looking at the peaks. It is also noticed that, at $t = 0$, the shape of load power P_L (depending on the load current since the load voltage is constant at 48V) changes and becomes more compact and continuous. This is logic since the duty cycle of the HAR D_{HAR} has been reduced due to the change of power reference. However, it is worth noting that in case of lower D_{HAR}, the lower bound of the spike will exceed zero. This means that during short mode, the

battery will start giving back energy to keep V_{DC} to the reference value; furthermore, the DC/DC converter will work in discontinuous conduction mode, whose features are different from continuous conduction mode. Therefore, when designing controllers for WPT systems adopting this ON/OFF control, great care must be taken in selecting an appropriate DC smoothing capacitor and inductor in order to meet the required operation mode. However, it is true that in this experiment the power is continuous and not intermittent. Finally, in Fig. 21d, the averaged DC-to-DC efficiency η_{DC} (from source to load) η_{DC} for different values of D_{HAR} has been measured and plotted in a graphic. It can be seen that the maximum value of η_{DC} is around 0.87 for D_{HAR} up to 0.4; when D_{HAR} gets too high (i.e. short mode operation most of the time), the efficiency drastically drops because the conduction losses become very high due to the high value of the current I_2. However, the pattern of Fig. 17 has been reproduced, even though the high efficiency area is almost halved, passing from $D_{HAR} = 0.7$ to $D_{HAR} = 0.43$. This can be explained by the fact that at low power the current is so low that short mode losses and switching losses become relevant only for high values of D_{HAR}. Nevertheless, in both cases, the efficiency reduction observed in the high efficiency area is slight; in the case of higher power experiment the reduction is around 2%, which is a good trade-off for acquiring the capability of regulating the power flow. It is then demonstrated the effectiveness of the proposed method even in case of high power level.

3.5 Dynamic charging scenario experiment

Achieving highly efficient dynamic WPT will greatly widen the application range for this technology. Previous research has already been carried out with promising results [18][51], but in those cases the authors concentrated on the optimum coil design or the use of additional elements to solve the issues of dynamic charging. In particular, coil detection in the primary side is a major issue but, since it can be performed with a sensorless, communication-less control, it is not discussed in this dissertation, where the focus is the secondary-side-only control method. This does not mean that the primary side is ignored, but simply that the proposed control does not manipulate it. Thus, the proposed secondary-side-only control must be demonstrated in a dynamic scenario.

3.5.1 Mutual inductance estimation

The most notable problem of dynamic WPT is the variation of mutual inductance. As it appears in nearly all expressions, it is a critical parameter for control purposes and knowing its value is necessary. Direct measurement is impossible, therefore the only feasible solution is to estimate it in real time. A real-time estimation of the coils coupling coefficient by means of a buck converter has already been proposed [54]. According to it, the poles of WPT network are much faster than the poles of the mutual inductance L_m change: consequently, estimating the mutual inductance based on the steady

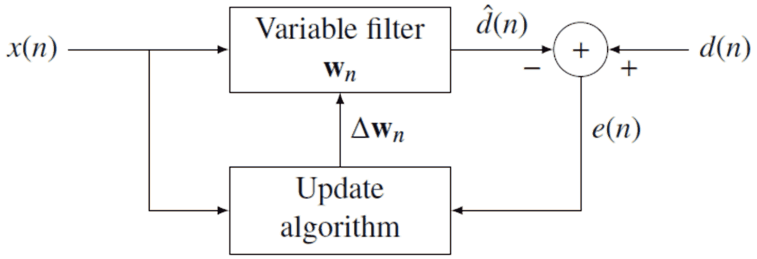

Fig. 22: RLS filter general architecture [55].

state equations of Eq. (3-2) is sufficiently precise. The mutual inductance L_m can then be expressed as follows:

$$\widehat{L}_m = \frac{V_1 + \sqrt{V_1^2 - 4R_1 I_2 (V_2 + R_2 I_2)}}{2 I_2 \omega} \tag{3-30}$$

The secondary side coil voltage V_2 and current I_2 are fundamental waves whose RMS values are extracted respectively from secondary DC link voltage V_{DC} and secondary DC link current I_{DC} by Fourier series expansion. The filter to be used in a condition such as dynamic WPT must be adaptive in order to cope with the varying parameters. In this case the choice is a finite impulse response recursive least square (RLS) filter, because the coefficients are continually updated on a step-by-step basis during the filter operation as shown in Fig. 22. The concept is that a signal input $x(n)$ generated from the desired response $d(n)$ is subject to the noise $v(n)$. It can be expressed as:

$$x(n) = \sum_{k=0}^{q} b_n(k) d(n-k) + v(n) \tag{3-31}$$

with b_n as process coefficient, and $k = 0, 1, 2..., q$ with $q = n - 1$. The input then passes through a filter whose output is $\widehat{d}(n)$. At each timestep the filter coefficients' vector $\mathbf{w}_n$ is updated by means of the error $e(n)$, which is the difference between the desired response $d(n)$, which is usually based on $x(n)$, and the filter output. It can be expressed as follows:

$$\widehat{d}(n) = \sum_{k=0}^{q} w_n(k) x(n-k) = {\mathbf{w}_n}^T \mathbf{x}_n \tag{3-32}$$

with $\mathbf{x}(n)$ as the vector containing the q most recent samples. The complete mathematical derivation of the RLS method can be found in many textbooks, therefore it will be omitted. The important point is that the RLS filter converges fast most of the times and is therefore suitable for use in dynamic WPT systems. However, the operation of HAR is an additional source of noise because of short mode. In fact, during short mode, I_{DC} is zero and thus the filter is not persistently excited. This leads to estimation windup, where the covariance matrix used for filter coefficients updating will inflate and greatly increase the sensitivity. In this condition, the estimation will be very inaccurate. Therefore, the RLS filter with constant trace algorithm is proposed to mitigate estimation mistakes due to enhanced sensitivity. The proposed filter has its output $y[i]$ and input $\psi[i]$ expressed as follows in discrete time

notation:

$$y[i] = V_1 + \sqrt{V_1^2 - 4R_1 I_2[i](V_2[i] + R_2 I_2[i])} \tag{3-33}$$

$$\psi[i] = 2I_2[i]\omega \tag{3-34}$$

with i as the sampling counter. From Eq. (3-33) and Eq. (3-34), the error ζ (including the noise), the covariance matrix T, the forgetting factorλ and the mutual inductance estimation $\widehat{L}_m$ are respectively computed in discrete time as:

$$\zeta[i] = y[i] - \psi[i]\widehat{L}_m[i-1] \tag{3-35}$$

$$T[i] = \frac{1}{\lambda[i]}(T[i-1] - \frac{\psi[i]^2 - T[i-1]^2}{1 + \psi[i]^2 - T[i-1]}) \tag{3-36}$$

$$\lambda[i] = 1 - \frac{1}{trT[0]} \frac{\|\psi[i]T[i-1]\|^2}{1 + \psi[i]^2 - T[i-1]} \tag{3-37}$$

$$\widehat{L}_m[i] = \widehat{L}_m[i-1] + \frac{\psi[i]T[i-1]}{1 + \psi[i]^2 - T[i-1]}\zeta[i] \tag{3-38}$$

where $trT[0]$ as the trace of the covariance matrix. By setting it to a scalar fixed positive number γ, it is possible to establish $T[i] = T[0] = \gamma$ and easily rewrite Eq. (3-38) into Eq. (3-39) as follows:

$$\widehat{L}_m[i] = \widehat{L}_m[i-1] + \frac{\gamma\psi[i]}{1 + \psi[i]^2}\zeta[i] \tag{3-39}$$

with γ as a parameter incorporating the forgetting factor and the trace of the covariance matrix. The control thus becomes simple to write, self-bound due to fixed trace of the covariance matrix. The computational complexity is the same as the RLS filter. The choice of γ is important for the correct estimation. If γ is too big, estimation windup happens; on the other hand, if γ is too small, a strong delay will occur and rapidly changing parameters will not be sensed properly. The effectiveness of this method is shown in the experimental results in Fig. 23, where the mutual inductance estimation for two cases is shown. The control operation in dynamic WPT experiment is performed from 0 to 0.13 seconds. In Fig. 23a, the estimation for the case of conventional efficiency control is reported. The estimation is quite accurate as the excitation of the filter is continuous. On the other hand, this is not the case for Fig. 23b, where the estimation for the proposed simultaneous power and efficiency control: due to the HAR short mode operation, the filter is not permanently excited, therefore as the time passes the estimation error accumulates. However, even though the error is notable, the accuracy is sufficient to successfully regulate V_{DC} and obtain near maximum efficiency. The estimated L_m is then feed to Eq. (3-12), whose value is continuously updated in the controllers and consequently the feedback loop can always have the desired poles.

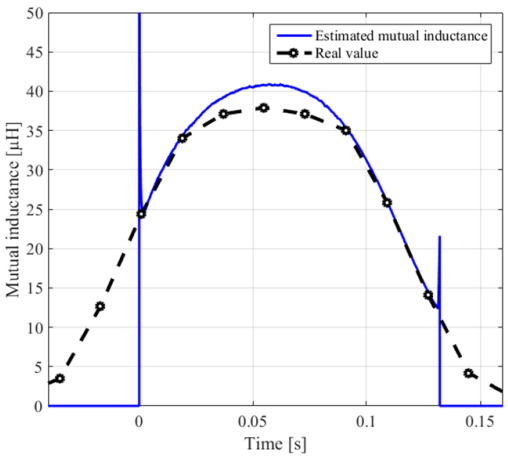

(a) Mutual inductance L_m estimation in case of efficiency only control.

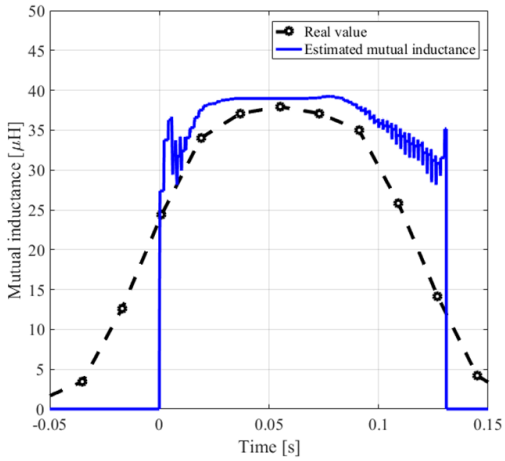

(b) Mutual inductance L_m estimation in case of proposed control.

Fig. 23: Mutual inductance L_m estimation when the coil speed is 10 km/h.

3.5.2 Experimental results

In this section, too, the proposed control is compared with the secondary side efficiency control. The secondary coil is moved thanks to the stage built-in linear actuator. The stage is also equipped with an encoder to control the position and the speed of the secondary coil. In order to avoid big losses, the primary side inverter is operated only when the coils are close enough. The secondary coil speed is set to 10 km/h. The proposed control is performed for two different power references P_L^*: one is 3 W, the other is 6 W. Again, the operation time goes from zero to 0.13 seconds; outside this period, the control of both sides as well as the estimation are not operated. The experimental results are shown in Fig. 24, Fig. 25 and Fig. 26.

The secondary side DC link voltages are shown in Fig. 24a, Fig. 25a and Fig. 26a. The variation of mutual inductance does not have a relevant impact on the maximum efficiency voltage $V_{DC,\eta max}$. Apart from the initial rise time necessary for charging C_{DC} and the final part showing minimal divergence, the controller effectively works as V_{DC} matches the reference in all cases.

The primary side power P_0 and secondary side power P_{DC} are shown in Fig. 24b, Fig. 25b and Fig. 26b; the red line represents P_0, the blue line is P_{DC} and the black dashed line is the secondary side power reference. The power is not regulated in the case of secondary efficiency control, as shown in Fig. 24b. On the contrary, with the proposed control P_{DC} is controlled and matches the reference. This is shown in Fig. 25b and Fig. 26b, where the blue line coincides with the black dashed line.

Clearly, the load power P_L behaves accordingly to P_{DC}, as seen in Fig. 24c, Fig. 25c and Fig. 26c. Without control, P_L changes along with the mutual inductance; on the other hand, when the power is controlled P_L is unvaried, as shown in Fig. 25c and Fig. 26c. A problem is the final power surge, witnessed in all three considered cases. The surge is arguably generated by the discharge of the

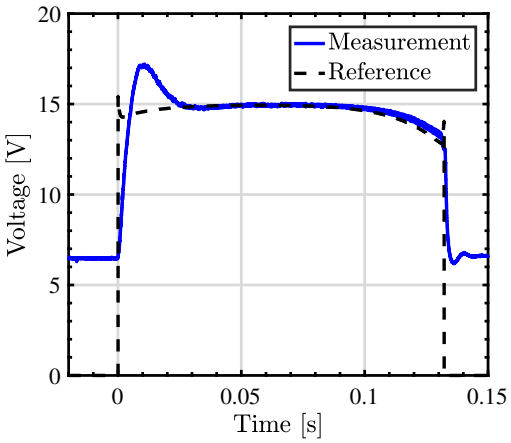

(a) DC link voltage V_{DC}.

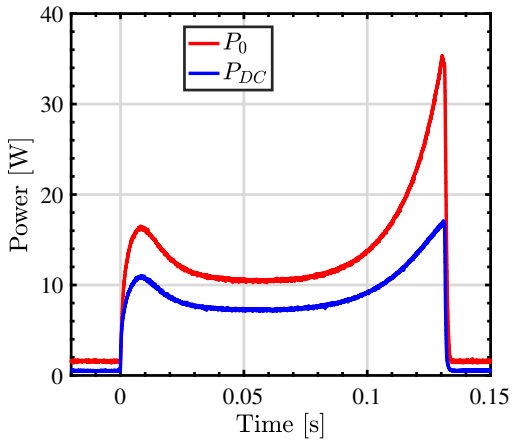

(b) Primary side power P_0 and secondary side power P_{DC}.

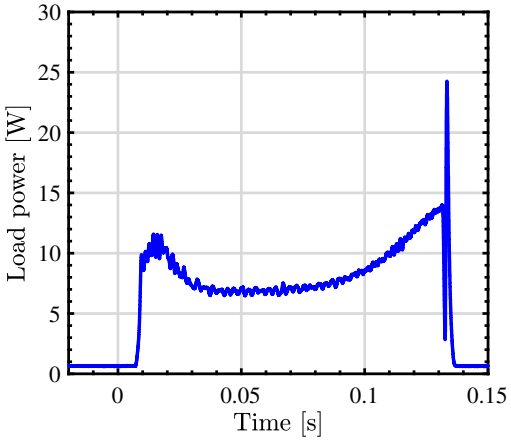

(c) Load power P_L.

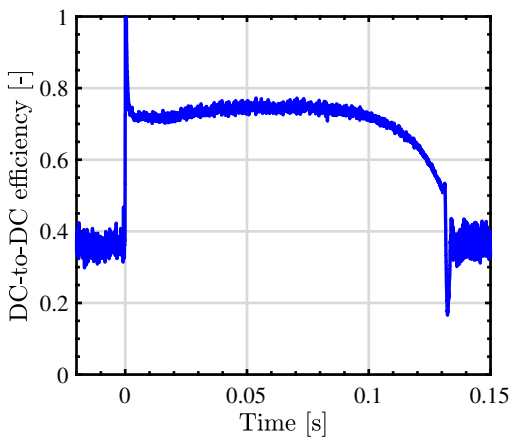

(d) DC-to-DC efficiency η_{DC}.

Fig. 24: Secondary side efficiency control [54] when the coil speed is 10 km/h.

smoothing capacitor C_{DC} into the big DC/DC converter inductance L. In fact, in the experiment there is no coil sensing control on the primary side and the command of start and stop is given according to the readings from the encoder. It is then noticed from Fig. 24b, Fig. 25b and Fig. 26b that the secondary side converters stop working before the primary side inverter, thus having an uncontrolled instant in which the discharging occurs. This shows two things: the importance of a correct sequence for start and stop operation and the effect of many passive elements in the circuits. In this sense, it is desired that, if possible, the secondary side circuit becomes as simple as possible and avoids passive components that may eventually worsen any problem due to incorrect operation.

Finally, the DC-to-DC efficiency η_{DC} is presented in Fig. 24d, Fig. 25d and Fig. 26d. The graphic in Fig. 24d represents the maximum achievable efficiency of the system. In the case of proposed control, η_{DC} behaves accordingly to the power, as seen in Fig. 25d and Fig. 26d. Again, the instantaneous value presents oscillations due to the switching between the operation modes. As expected, the DC-to-DC efficiency in the proposed control is slightly lower than the one in the secondary side

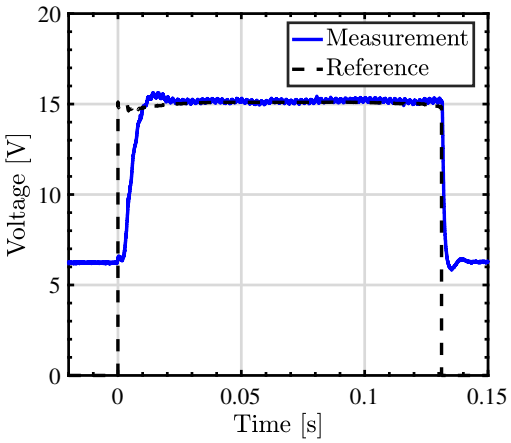

(a) DC link voltage V_{DC}.

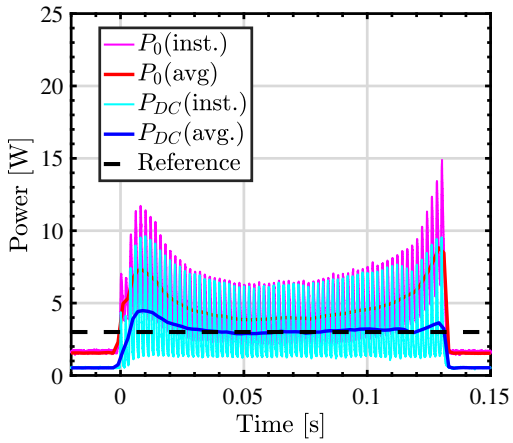

(b) Primary side power P_0 and secondary side power P_{DC}.

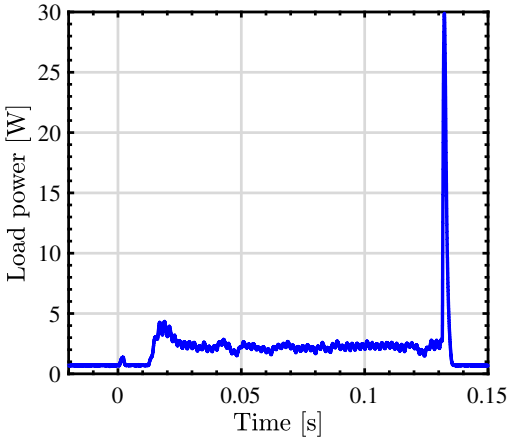

(c) Load power P_L.

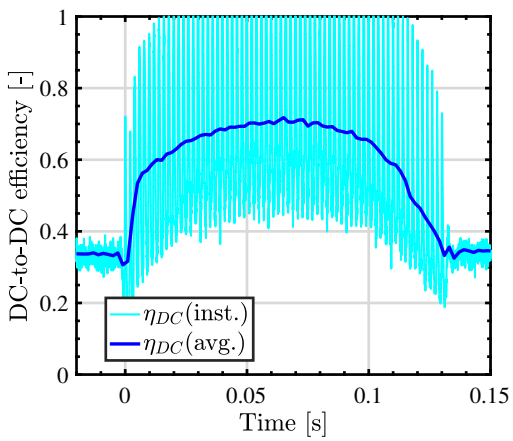

(d) DC-to-DC efficiency η_{DC}.

Fig. 25: Proposed control, power reference 3W when the coil speed is 10 km/h.

efficiency control due to short mode losses. However, Fig. 25d and Fig. 26d show that the control can still achieve high efficiency and simultaneously manipulate the power in a dynamic charging scenario without using any communication between sides. The HAR duty D_{HAR} negatively affects the efficiency in transient low coupling condition; however, once the desired power requirement is met, the average DC efficiency reaches the near-maximum value shown in Fig. 16d.

3.6 Conclusion

In this chapter, a control regulating simultaneously the efficiency and the power flow only by secondary side for WPT systems by magnetic resonant coupling is discussed. When communication between sides is unavailable, the proposed control is adopted to preserve power flow and efficiency. The proposed control is performed with two converters by using two different switching frequencies for the HAR and the DC/DC converter. The power is controlled by a HAR with the two-mode control

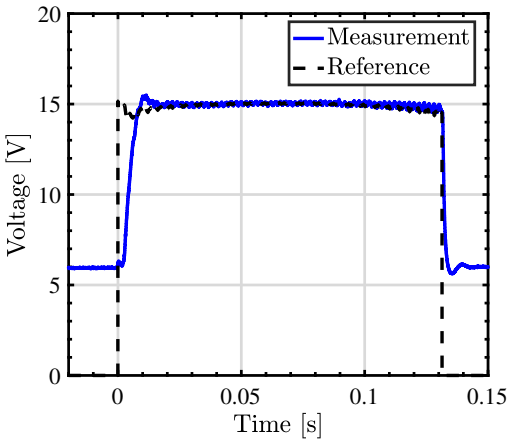

(a) DC link voltage V_{DC}.

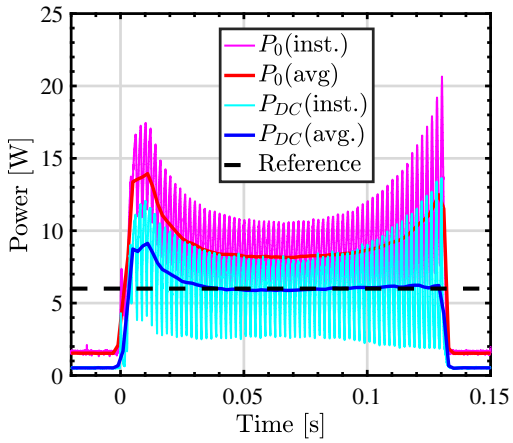

(b) Primary side power P_0 and secondary side power P_{DC}.

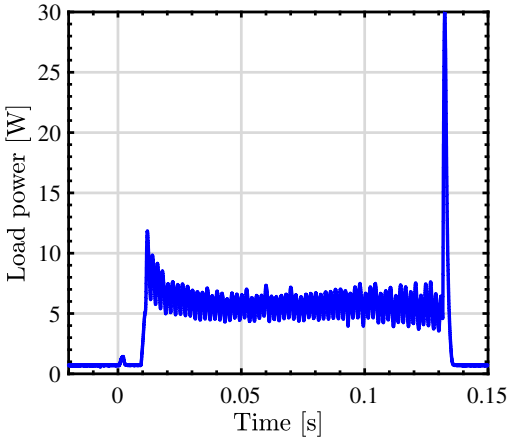

(c) Load power P_L.

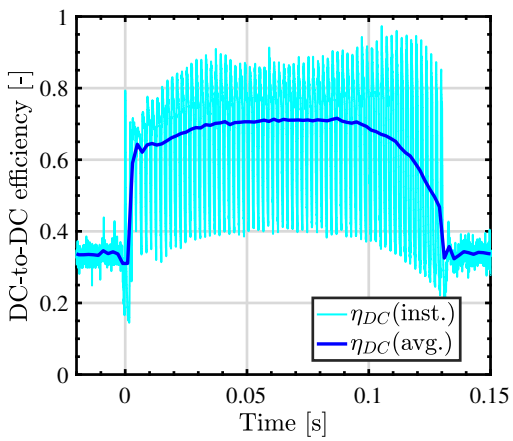

(d) DC-to-DC efficiency η_{DC}.

Fig. 26: Proposed control, power reference 6W when the coil speed is 10 km/h.

and a DC/DC converter regulates the efficiency via the DC link voltage by adopting the equivalent load resistance optimization method. The HAR generates short mode losses but they have limited effect on the system. Combining the efficiency control with mutual inductance estimation, the proposed control can be applied to a dynamic charging scenario as well. Due to non permanent excitation of the filter, the estimation contains some error but its effect on the control is negligible. Experimental results, both in a static and dynamic scenario, confirm the soundness of the proposed method and show that the secondary-side-only control concept is applicable to two converters. On a side note, the importance of correct start and stop operation for the converters is remarked, as well as the possibility to simplify the circuit by eliminating passive components.

Chapter 4

FPGA-based implementation of digital current limiter and secondary DC current controller

4.1 Necessity of a FPGA in controllers for WPT systems

In recent years, control boards technology has steadily improved. In the beginning, control tasks were accomplished by use of gate arrays containing standard discrete logic gates. However, while being a cheap solution, it allowed only for a very limited range of applications depending on its physical specifications such as number of pins. They are a type of fixed logic devices, with the circuits cannot be modified once set. On the other hand, programmable logic devices offer ever different amount of logic capacity, features, speed, and voltage characteristics because they are based on rewritable memory technology that can be reprogrammed at any time. The product development thus becomes faster and cheaper. These devices ranges from simple packages containing few logic gates with simple combinatorial logic (e.g. AND, OR, NOT, etc.) or flip flops to complex packages with thousands of logic gates that can be implemented in an array by combining the inputs (Sum of Products). The user will need to complete the design by computing the interconnections, but predictable timing characteristics, and low power makes them useful in cost-sensitive portable applications (e.g. mobile phones). Nowadays, field programmable gate arrays (FPGAs) are the most advanced type of programmable logic device. They contain large amounts of both logic and memory blocks that are hierarchically wired together with reconfigurable interconnects. One example is shown in Fig. 27. Furthermore, in the most recent products on the market, a microprocessor is embedded within the FPGA fabric thus creating a system-on-chip (SoC) which grants very high clock frequency, parallel operation and higher overall reliability. While the timing management becomes more complex, the

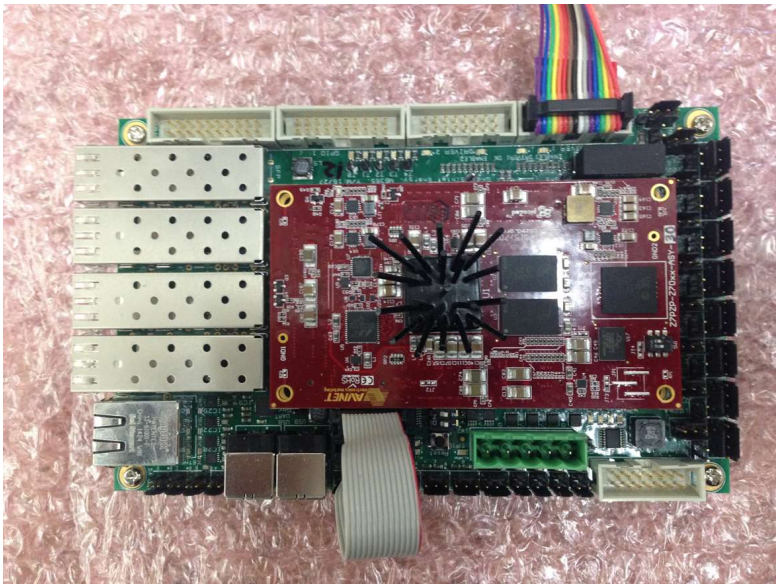

(a) Frontal view of FPGA.

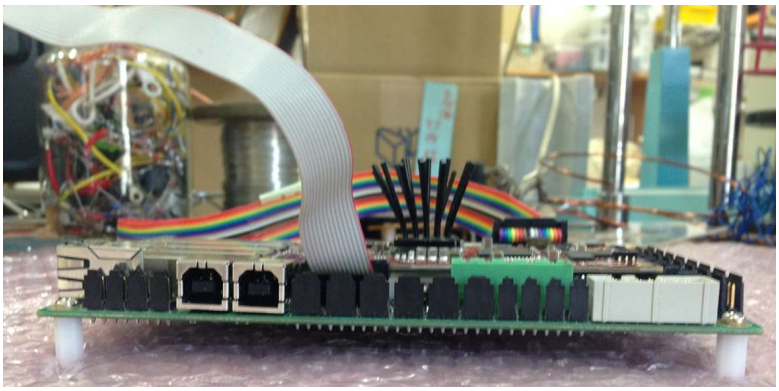

(b) Lateral view of FPGA.

Fig. 27: Example of FPGA.

high degree of customization makes a FPGA a very good platform for solving computable problems and broadens the range of possible applications. Among the possible applications, there is wireless power transfer (WPT) via magnetic resonant coupling. A FPGA is necessary for advanced controls (e.g. synchronous rectification (SR)) when there is a very high frequency environment such as a WPT system. Implementing a phase locked loop (PLL) becomes necessary and it cannot be done on a software level because it is not fast enough for the resonant frequency of the system. This means that the implementation must be executed at hardware logic level by programming accordingly the FPGA. In this sense, the creation of a new logic design is needed and becomes an extension of the converter control design for a WPT system.

The design workflow with a FPGA, shown in Fig. 28, comprises the following steps: design entry, design synthesis, design implementation, and device programming. Design verification, which includes both functional verification and timing verification, takes places at different points during the design flow. In the first step, the project is created and the user loads IP blocks, connects them, adds

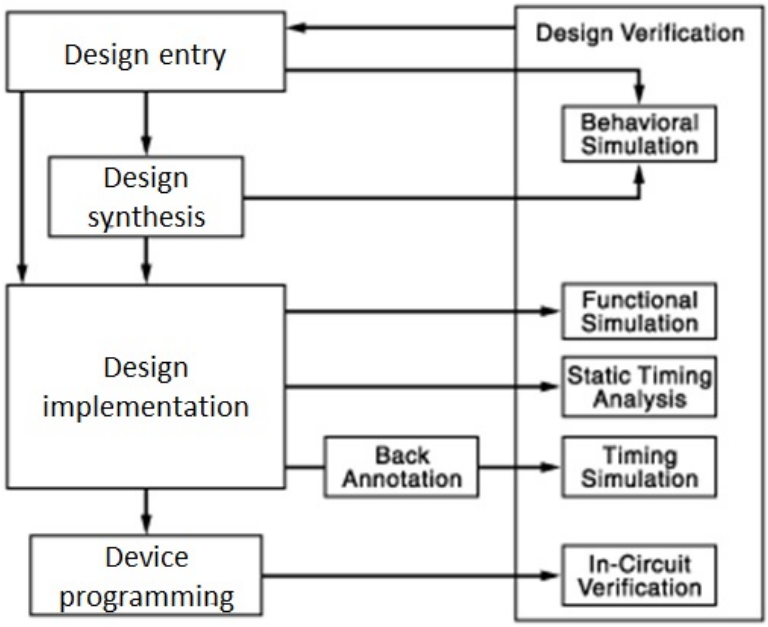

Fig. 28: Design workflow of a FPGA.

buffers, adds eventual timing or pin assignment constraints, and assigns an address to the IPs generating register netlist. The netlist is a feature of programmable boards, because it changes according to the user design method. Another feature of programmable boards is that the user can design customized blocks and by using hardware description language (VHDL or Verilog). The design can then be validated by behavioral (no netlist error) and gate level (no signal mismatches) simulation. The second step is the design synthesis, where the process will check code syntax and analyze the design hierarchy, ensuring that the design is optimized for the selected architecture. The third step is the implementation, which is subdivided into four phases: translate (merges netlist and constraints into one design file), map (fits the design into the available resources on the target device), route (places and routes the design to the timing constraints) and file generation (creates a bitstream file that can be downloaded to the device). The final step consists in downloading the bitstream file into the FPGA and debugging the control code in the software development tool.

In some cases, the signal is not directly transmitted from the FPGA to the device; in between an interface platform is needed. This is especially true with high power equipment in order to protect the FPGA from eventual faults on the power side [67]. An example is reported in Fig. 29. In this case, regulators and modulators are defined to belong to the control circuit side of the interface; on the other hand driver circuits, galvanic isolation, dead time and cross conduction interlock circuits are defined to belong to the gate driver side. As safety is important, a global active Enable signal must be set to allow any switching, while inactive Enable signal blocks all switching. Actually, both switches in a bridge leg can be independently controlled, but interlock logic (at the transistor driver domain) protects against turning both bridgeleg switches on simultaneously. Given the high grade of customization offered by a FPGA, there are countless variants of these interface drivers for con-

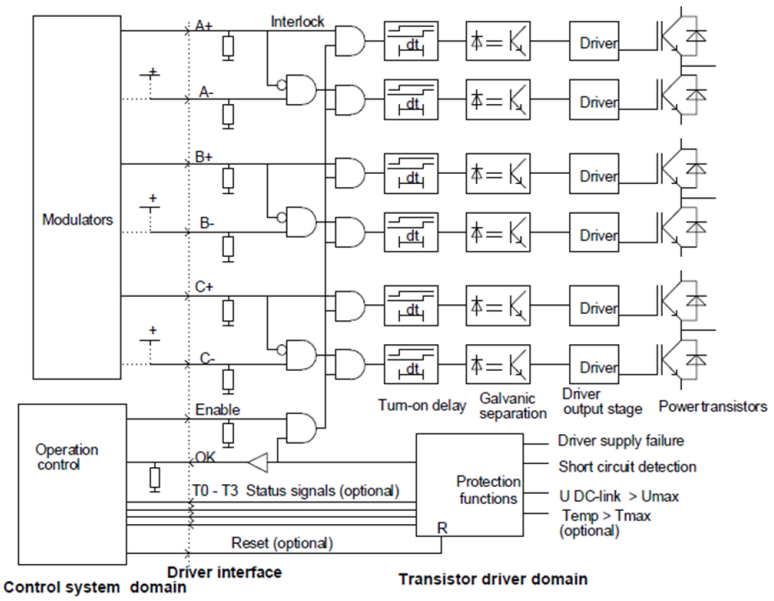

Fig. 29: Driver interface for a FPGA.

Tab. 4: Comparison between FPGA and DSP.

	Programmable DSP	**FPGA**
Performance	$<$ 2MSPS	$<$ 100MSPS
Design flexibility	only software	software and hardware
Design complexity	C language based	HDL or Simulink based
Consumption power per device	low (hundreds of mW)	high (some W)
Consumption power per channel	not scalable	scalable
Cost per device	cheap	somewhat expensive
Cost per channel	not scalable	scalable

verters used in high power environments. Explicit mentions of FPGA in past research about WPT is quite rare [68]. However, FPGA is vital for high level control in high frequency environment and it is expected that it will be used more widely thanks to its many features in control signal management. In Tab. 4, a comparison between FPGAs and conventional digital signal processors (DSPs) is presented. It is clear that, in terms of performance in multichannel environments and adaptability, a FPGA outperforms a DSP. The only negative points are the cost and the power consumption per device of the FPGA, but with the technological process and optimal routing design, these disadvantages will be less marked. As for design complexity, the language used in FPGA design is generally more difficult to learn, but once learned the design will not pose many problems. In short, using a FPGA is

recommended when dealing with WPT systems.

4.2 Example of FPGA digital controller implementation

In this section, the process of logic block creation in order to implement a controller for converters explained in the previous section is performed in a real environment, and tested experimentally in a wireless power transfer system by magnetic resonant coupling. In this case, the used software development tools as well as the FPGA and microprocessor are from Xilinx, but the very same procedure can be repeated with tools from other brands.

4.2.1 Overview and problem setting

Wireless power transfer is a useful techology with many applications. One of the most suitable and therefore researched upon is the contribute to battery charging method of EVs by eliminating wires and enhancing mobility as well as safety both for the user and the vehicle itself. Apart from static charging, dynamic charging is also possibile, with many possibilities concerning charging locations and patterns; however, dynamic charging presents also problems. In fact, the system design must take into account the available charging time, the electric specifications, transient response and activation of wireless charging via protocol signals. In this study, the last case is considered.
Both in static and dynamic charging, it is necessary to study a protocol or some other methods that allow the safe activation of wireless power transfer from the facility to the vehicle. In the case of plug-in EVs, when the pistol of the charging station is inserted into the vehicle outlet, communication occurs between the charging station and the vehicle electronic control unit (ECU). This communication consists in a square wave signal of a determined frequency (for example, 1 kHz in case of SAE J1772 protocol, shown in Fig. 30) from the charging station: the signal tests the protection earth circuit to be closed and functional. The vehicle instead transmits its state through the setting of a resistor circuit: by changing the resistance value, the vehicle notifies whether it is ready or not for the charge. This means that the vehicle must first acknowledge the intercompatibility with the charging station and then communicate whether a charge is needed or not. Furthermore, the charging station uses pulse width modulation (PWM) to notify the EV control unit what is the maximum current available for the charge: for different duty cycles, the maximum available current will be correspondently different. In the charging station as well as in the EV there is further electronics for measurement and protection: often it is composed by simple and robust analog circuits, given the available space. The system is thus reliable and the charging process can be carried out without much problems.
In case of wireless power transfer EV charging, cables are not used and consequently a pilot signal cable is not available. This means that other methods must be implemented to safely begin WPT charging. Vehicle detection systems may adopt sensors placed inside the roadway (pneumatic tubes,

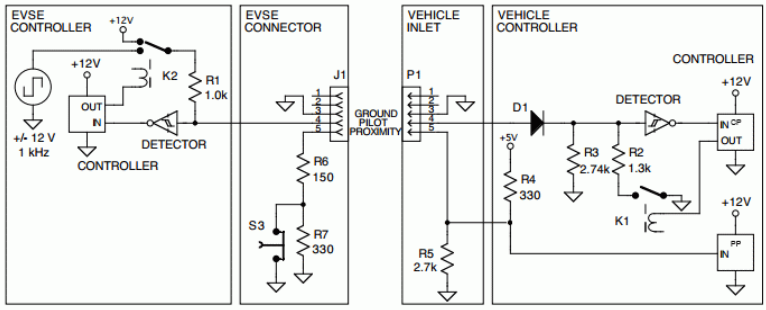

Fig. 30: Pilot circuit of J1772 protocol in case of plug-in charging station [69].

magnetic or piezoelectric sensors) or outside the roadway (infrared sensors, radars or image processors) [70]. Vehicle detection can also be sensorless by measuring the primary side current and controlling its value [71]. This means that in wireless power transfer system the primary side can be used not only for controlling the power flow but also for detecting the movement of the EV. In fact, in the case of WPT by magnetic resonance couplig using SS compensation, the RMS value of the primary side coil current I_1 in perfect resonance condition is expressed by:

$$I_1 = \frac{R_2 + R_L}{R_1(R_2 + R_L) + (\omega L_m)^2} V_1 \tag{4-1}$$

with R_L being the load input impedance and V_1 being the RMS value of primary side coil voltage. It is obvious that R_L, which is a pure resistance, determines the current. The problem lies in the fact that if the vehicle detection system fails and the primary side starts sending power to a non existent load (i.e. open circuit condition where R_L is infinite), the current I_1 will become very high, damaging the circuit. In fact, with reference to Eq. (3-13) and Eq. (3-14), the imput impedance Z_{in} will become equal to the primary coil resistance R_1 which is a few hundreds of milliohms. Therefore, I_1 will become very big. In this case, to avoid a very high current it is necessary to insert some kind of protection. This can very well be an analog protection circuit, but, assuming an already cramped primary side, it is possible to take advantage of the superior performance of the FPGA and implement a digital current limiter. Given the extreme level of customization offered by FPGAs, only the basic tools and logic blocks are preinstalled, and it is often necessary to create a logic block suitable for the situation. Hence, a block able to store the measured value of I_1 and calculate in real time its peak value must be built from scratch in order to implement a current limiter. The digital current limiter becomes then a simple PI controller, using as a reference the current peak value written in the register of the newly created logic block. The high clock frequency and sampling ratio,and the appropriate tuning of the A/D converter filters of the FPGA allows correct reading of high frequency parameters. It is then possible to implement a full digital current limiter preventing big current flowing in the primary side in case of operation when the mutual inductance L_m is too low (i.e. non existent load condition).

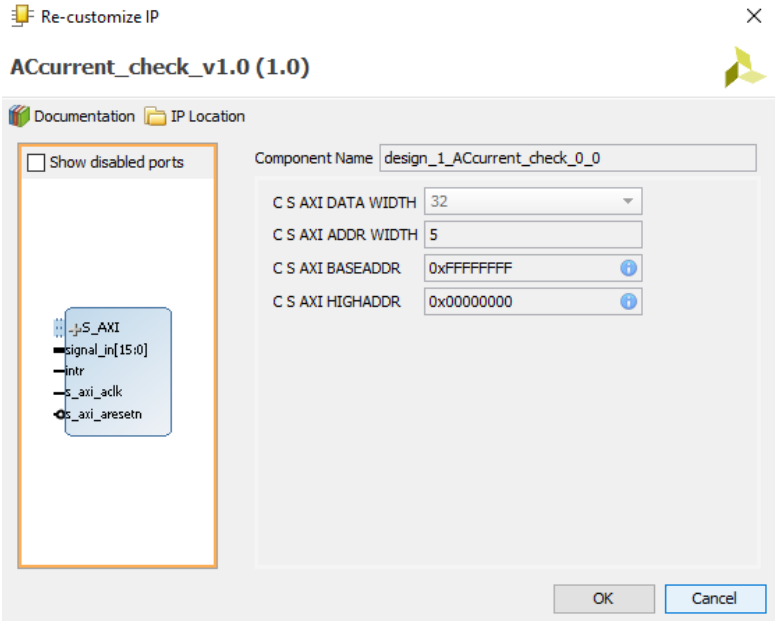

Fig. 31: Overview of new logic block for calculating and storing the peak value of I_1 .

4.2.2 Logic block properties

In the previous section, the process of block creation has been explained. In this case, the objective is to create a logic block receiving the measurement of I_1 from the current sensor, comparing it with the previous sample and updating the register with the higher value between the two. The value written in the logic block register is then accessed by the main user code in C language, which reads the value and implements it as a reference in the PI controller. This is dictated by the user logic file, which is the core of the block. In this case of study, the calculation happens at every sample. For correct operation, the block is synchronized with the global clock and cycle reset of the FPGA and shares the same interrupts of the customized PWM signal generator block connected in the netlist. The logic block is shown in Fig. 31 and Fig. 32.

It is possible to notice that the block has no output, meaning that it is not possible to check the output through one of the board pins. This is an arbitrary decision, and can be easily changed at any time; however, doing so will require to rewrite the core coding of the block in hardware description language and undergo again the process of netlist creation typical of FPGAs. In particular, from Fig. 32 the general characteristic of the block can be seen. The block has five addresses, from 0 to 4, meaning that can handle five different variables at once. The maximum width of each address is 32 bit as a general rule chosen for the netlist, so this applies for the block as well; however, since the signal representing I_1 comes from the D/A converter and is a 16 bit array, the block is made to accept 16 bits input signals from the port called ”signal_in”. The other input signals are composed only by one bit. This last part is the architecture of the block, which is to be paired with the user logic to effectively implement succesfully the logic block.

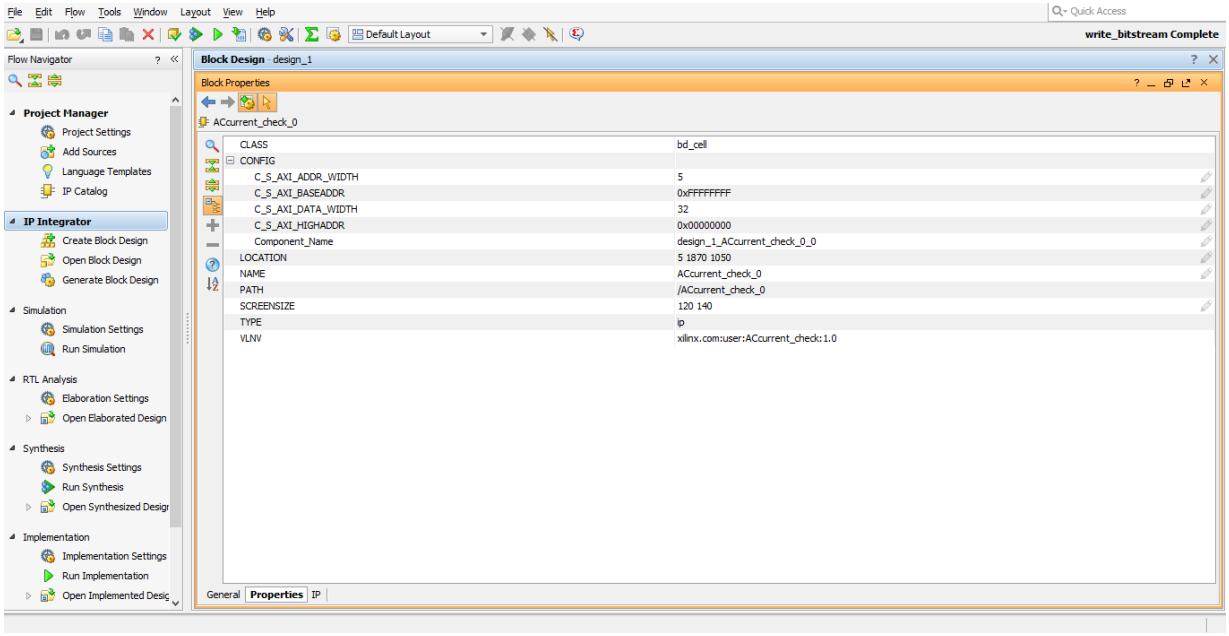

Fig. 32: Features of new logic block for calculating and storing the peak value of I_1.

4.3 Proposed control concept

4.3.1 Symmetric phase shift

Since the primary side is considered fixed, the control must be performed on the secondary side rectifier. In other words, the rectifier has to be equipped with MOSFETs, which are controllable and are more suited to high frequency operation rather than IGBTs. The load is a CPL, which requires voltage stabilization because the its open loop plant is unstable. In particular, having only one rectifier on the secondary side, the control must perform at the same time synchronization to the primary side and load voltage stabilization without recurring to discontinuous operation or primary side regulation. Hence, in this paper the chosen control method is symmetric phase shift as in Fig. 34b.

In order to perform SR, it is necessary to adopt an analog polarity circuit or implement a digital PLL. Given the high frequency environment, an analog circuit is preferrable; however, it is an additional circuitry that occupies space. Therefore, coping with the constraint condition, the only solution is to use a digital phase locked loop (PLL). In this sense, a high performance control board with fast sampling time and calculation time is necessary: in other words, a field programmable gate array (FPGA) is mandatory. The digital PLL control block is shown in Fig. 33a. It comprises of three main elements: a phase detector, a low-pass filter and a voltage controlled oscillator (VCO). The phase detector compares the phase for every sampling period and generates an error signal proportional to the phase difference between input and output. It is generally done by multiplying the two signals, then the output will have twice the input frequency and be proportional to the cosine of the phase difference. The cut-off frequency of the LPF error filter is selected so that all the harmonic compo-

nents at integer multiples of the excitation frequency are properly attenuated, leaving out only the low frequency components associated to the phase shift. The VCO is a linear time-invariant system whose oscillation frequency is determined by the input voltage. The loop gain must be high to reduce phase errors. In WPT systems, the variable fed to PLL is generally AC current; in this case of study, too, the input of the loop is i_2, measured with a high bandwith current sensor. The implementation concept is simple, as shown in Fig. 33b. At every clock enable, decided by the sampling frequency of the board and set by the user, the phase error between the i_2 and the PWM carrier used in firing the devices of the secondary side AC/DC converter is calculated. The error is then fed to a PI feedback controller, whose task is to correct the incremental frequency of the PWM carrier. The reference signal and the feedback signal are periodic and the average value over the common period of their product only depends on the phase shift between the reference and the fundamental harmonic of the feedback. That means that even if the feedback signal contains harmonics and/or the measurement has an offset, performance of the phase-tracking algorithm will not be affected. Also, the PLL will be in equilibrium when the fundamental component of the feedback signal is 90 degrees shifted with respect to the reference signal. Of course, if the error is zero, then the variable and the PWM carrier are in phase and the phase is locked. When this situation happens, it is possible to activate the control for SR without fear of waves with different phase between primary side and secondary side.

With normal SR of Fig. 34a, the output voltage v_{out} of the converter using SR is a square wave and the converter duty cycle is fixed at 0.5 because of the positive and negative halfwave. However, by modifying the parameter t_α, v_2 becomes the three-level waveform represented in Fig. 35 and symmetric phase shift operation is achieved. For square wave operation, t_α is equal to zero. The duty cycle in case of symmetric phase shift is still equal to 0.5, but the converter conversion ratio is different. It can be expressed by:

$$d_{cr} = \frac{t_\alpha}{T} \tag{4-2}$$

where ϕ is the phase angle between v_2 and i_2. In so doing, the amplitude of the fundamental waveform component of the output voltage v_{out}, which depends on V_{in}, changes accordingly to t_α as expressed in the following formula:

$$v_{out} = \frac{2\sqrt{2}}{\pi} V_{in} \cos(2\pi d_{cr}) \tag{4-3}$$

with T as the period of the waveform. This relationship can be applied both to the primary side inverter and the secondary side active rectifier. In the first case it will be:

$$v_1 = \frac{2\sqrt{2}}{\pi} V_0 \cos(2\pi d_{cr}) \tag{4-4}$$

with V_0 as the DC power supply voltage. On the other hand, in the second case, the equation will be as follows:

$$v_2 = \frac{2\sqrt{2}}{\pi} V_{DC} \cos(2\pi d_{cr}) \tag{4-5}$$

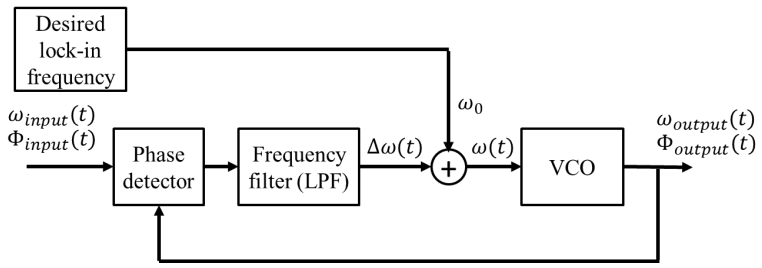

(a) Digital PLL block diagram.

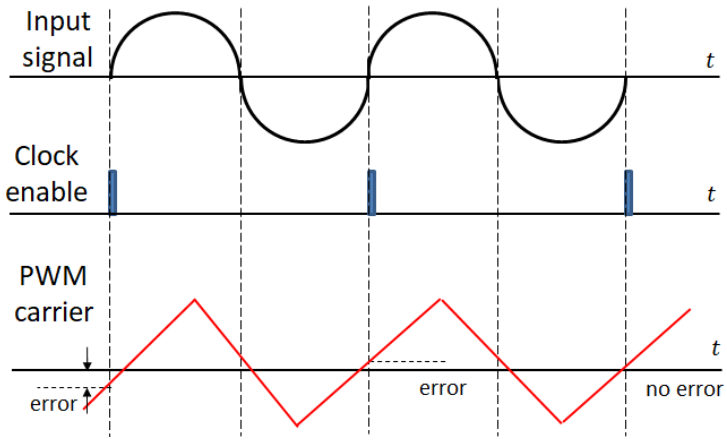

(b) Digital PLL operation.

Fig. 33: Digital PLL.

with V_{DC} as the secondary DC link voltage. By changing the RMS value of v_{out}, the RMS value of the converted DC current I_{conv} varies as well. In fact, during phase shifting, the RMS value of output current $I_{conv,PS}$ will be only a fraction of its square wave correspondent $I_{conv,SW}$. Their relationship is given by:

$$I_{conv,PS} = I_{conv,SW}\cos(2\pi d_{cr}) \tag{4-6}$$

It is then possible to identify the conversion ratio α, given by:

$$\alpha = \cos(2\pi d_{cr}) \tag{4-7}$$

As a case of application, the case of study of the secondary side active rectifier and its output current is considered. In normal square wave operation I_2 is given by (neglecting the internal diodes' forward voltage drop):

$$I_2 \simeq \frac{\omega L_m V_1 - R_1 V_2}{R_1 R_2 + (\omega L_m)^2} \tag{4-8}$$

However, with symmetric phase shift, Eq. (4-8) becomes:

$$I_2(\alpha) = \frac{\omega L_m v_1 - R_1 V_2 \alpha_2}{R_1 R_2 + (\omega L_m)^2} \tag{4-9}$$

and consequently the DC link current I_{DC} can be approximated as following:

$$I_{DC}(\alpha) = \frac{2\sqrt{2}}{\pi} I_2(\alpha)\alpha_2 \tag{4-10}$$

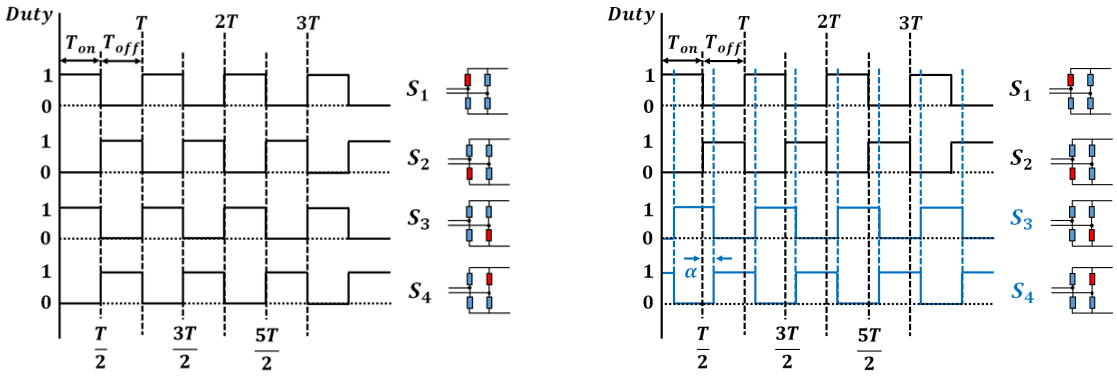

(a) Synchronous rectification (SR).

(b) Symmetric phase shift.

Fig. 34: Duty pattern of SR and symmetric phase shift.

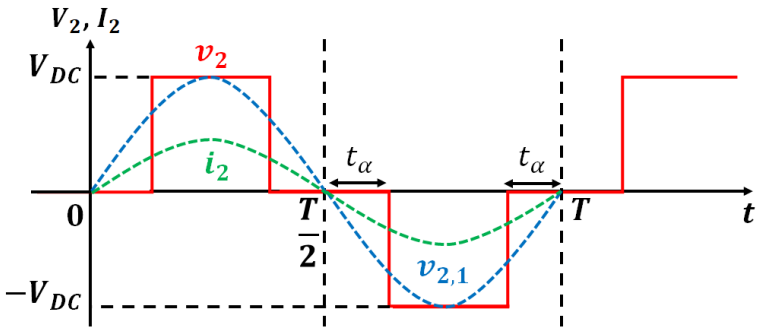

Fig. 35: Three-level voltage waveform of v_2.

with α_2 as the secondary side conversion ratio. A similar reasoning can be used to determine the input current of the primary side inverter $I_0(\alpha)$ as a function of the primary side AC current $I_1(\alpha)$ and the primary side conversion ratio α_1 during phase shift operation. The formula is given by:

$$I_0(\alpha) = \frac{\pi}{2\sqrt{2}} I_1(\alpha)\alpha_1 \tag{4-11}$$

4.3.2 Experimental setup

After succesfully creating the block and completing synthesis, implementation and bitstream file generation, the project can be exported in the software development tool in order to implement the desired program by use of C language. In the case of study, the block operation is tested in a WPT system. As previously stated, the application under investigation is dynamic WPT for EVs: therefore, the control must be performed on both the primary and the secondary side. In particular, the primary side inverter must be equipped with the current limiter controller; on the other hand, the secondary side AC/DC converter must perform power control by manipulating the output current. The reference circuit of the experimental setup is shown in Fig. 36. It is worth noting that, in a real application for dynamic WPT, it is not possible to control both the primary side and the secondary side with a single board. This is why each side is controlled by its own board. No communication is adopted between

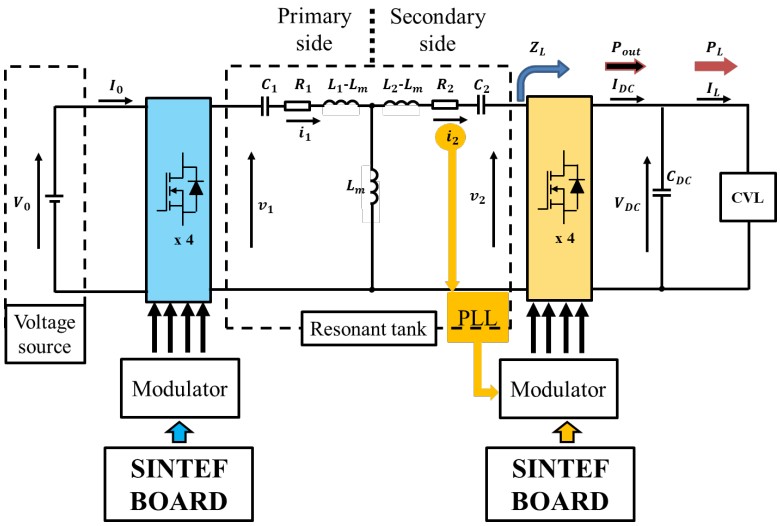

Fig. 36: Reference circuit.

the two sides, in order to show the viability of this simple yet effective control.

The system is shown in Fig. 37. In Fig. 37a, the DC source on the left is used as a constant current source in order to easily test the logic block operation. On the other hand, on the right an electronic load is used to simulate a constant voltage load, that is a battery. In Fig. 37b is shown the primary side coil, which is made with 8 turns of Litz wire; it is 450 millimiters long and 130 millimiters wide. Similarly, in Fig. 37c is shown the secondary side coil; it is made of 8 turns of Litz wire, too, and it is 130 millimiters long and 130 millimiters wide. In both cases it is noted that the coils' self-inductance is not big, but this has no effect in the coupling coefficient k. The circuit parameters are shown in Tab. 5. These parameters refer to the rated parameters for the system, which is meant to be a mini-model of dynamic WPT charger for EVs.

4.3.3 Experimental results

The experiments of this case of study are divided into two parts. Firstly, determine the operation of the current limiter controller of the primary side; then, determine the operation of the current control on the secondary side. Given the circuit of Fig. 36, only two converters are present: this means that the converter control will be using symmetric phase shift, the same concept described in chapter 4. Consequently, the secondary side AC/DC converter must be composed by active devices only. In that case, it is necessary the synchronization to the phase of the primary side, since that can not be performed passively as it is the case of a diode bridge. Hence, in this case, too, PLL is adopted to track the resonance frequency. PLL is implemented digitally, by using the FPGA, under the assumption that in an EV the space is limited and it is better to save space by not using analog circuits whenever possible. The controllers are simple PI feedback controllers and the gains have been chosen with Ziegler-Nichols method.

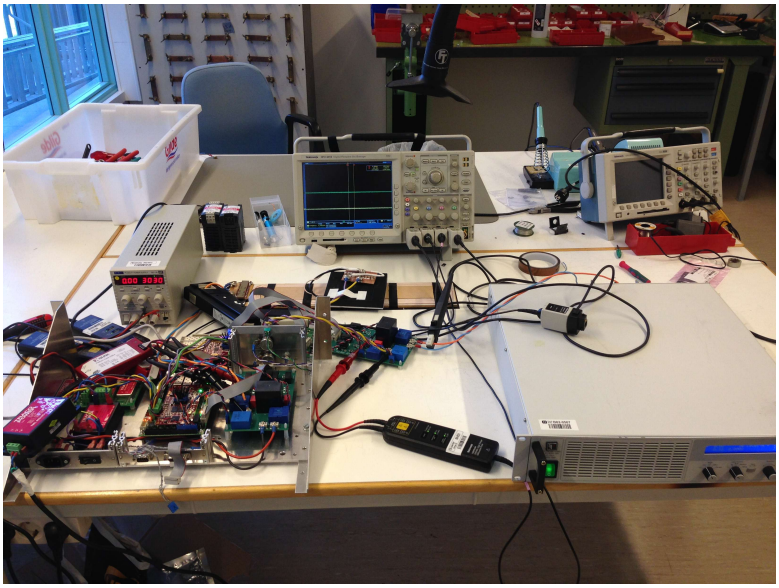

(a) Full view.

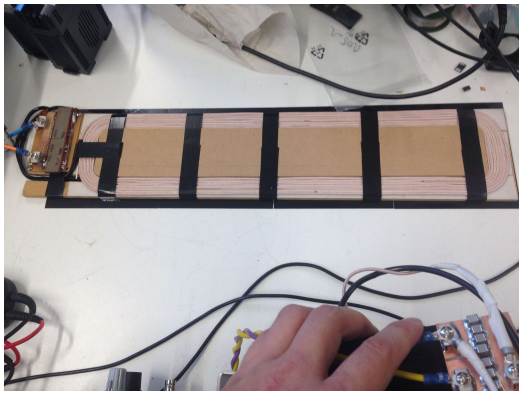

(b) Primary side coil.

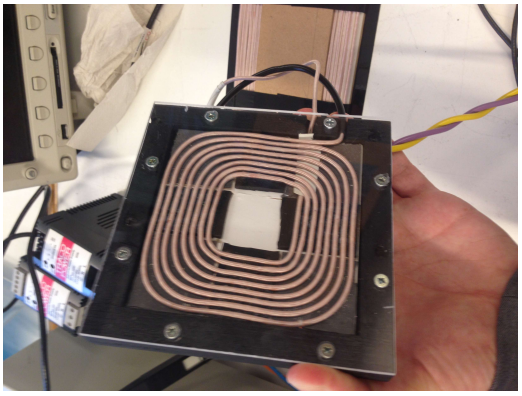

(c) Secondary side coil.

Fig. 37: Experimental setup of WPT system.

The experimental results of the primary side current limiter are shown in Fig. 38. The AC parameters of the circuit are shown in both Fig. 38a and Fig. 38b. The time scale is 10 microseconds per division. In both figures, the square wave lines represent the AC voltages, while the sinusoidal waves are the AC currents. In particular, the magenta line is the primary AC voltage v_1 and the cyan line is the secondary AC voltage v_2. The blue line, which is the gate signal of the secondary side AC/DC converter low arm: it is included in the plot in order to show that the PLL is operating correctly. In fact, the blue waveform is synchronized with the cyan line; the reason behind the opposite direction is the fact that the gate signal is measured on the lower side arm instead of the upper side arm. The minimal delay between the two waveforms is due to the dead times, which can be changed within the FPGA. Finally, the green line is the primary side current i_1. The current is sinusoidal because there is perfect resonance between primary and secondary side. The scale of the AC voltages is 5 volts per division, while the scale of the gate signal is 10 volts per division; the scale of the AC current is 1 ampere per division.

Tab. 5: System parameters for FPGA based current controller.

Parameter	**Value**
Primary side DC source voltage V_0	up to 10 V
Primary side coil resistance R_1	0.49 Ω
Secondary side coil resistance R_2	0.283 Ω
Primary side coil inductance L_1	28.845 μH
Secondary side coil inductance L_2	14.97 μH
Primary side coil capacitance C_1	156 nF
Secondary side coil capacitance C_2	301 nF
Operation frequency f	75.5 kHz
Mutual inductance L_m (best alignment)	13.6 μH
Smoothing capacitor C_{DC}	20 μF
Load voltage E	up to 6.5 V

In Fig. 38, the operation of the logic block designed in the previous section is checked. In practice, the operation in two conditions is shown. In the first one, the current is within the limit. In this case, the limit is set at 3A and the maximum value of $I_1(\alpha)$ is around 2.4A, as pictured in Fig. 38a. In this condition α_1 is equal to one. Consequently, no phase shift is seen in v_1 snd full square wave operation is performed. In the second condition, the current is exceeding the limits. In fact, in Fig. 38b, the limit for the current has been lowered to 1.8A: therefore, the current controller implements phase shift to lower the value of $I_0(\alpha)$ and α_1 is lowered. The logic block designed and included in the netlist project of the FPGA is working properly.

In Fig. 39, the operation of the secondary side current controller is checked. In this case, the square waves represent the same variables as before, and all the settings are as before, but the green line is the secondary side current i_2. It is possible to see that the magenta line has three levels, meaning that the current $I_{DC}(\alpha)$ is being controlled to meet the required value. It is worth noting that, differently than the previous case of Fig. 38b, the secondary current i_2 changes very slightly its peak value accordding to the variation of α_2. This is very clear by comparing Fig. 39a with Fig. 39b. Furthermore, the movement of the current i_2 and the voltage v_2 are only caused by the movement of the full square wave operation window. No offset whatsoever is introduced: this can be confirmed by looking at the blue line, indicating the gate signal during synchronous rectification with the primary side. The blue line is fixed and will not change unless the operating frequency of the primary side is not changed.

Actually, since symmetric phase shift is a derivation of synchronous rectification, in condition of perfect resonance the power factor is unity. With phase shift the power factor is lowered because the active power to the load is reduced, but the reactive power is unchanged. In fact, phase shifting only adds resistive losses under the form of conduction losses and switching losses.

Finally, the dynamic behaviour of controlled parameters is shown in Fig. 40 and Fig. 41. In these two figures, the time scale is 2 milliseconds per division.

In Fig. 40, the dynamic behaviour of the primary side current limiter in case of open circuit is reported. In the figure, the blue line is the primary side current i_1 and the cyan line is the primary side voltage v_1. The current is shown at 2.5A per division while the voltage has resolution of 5V per division. In this condition, the secondary coil is not coupled with the primary side, therefore the reflected impedance is very low and a very high current flows in the primary side. As an arbitrary value, the limit for the peak value of i_1 is chosen to be 2A. Then, the experiment shows the passage from state of inactivity to state of trasmission of the primary side. During the state of inactivity, the current and the voltage of the primary side have very low values. When the transmission starts, the current rises until the limit is exceeded. Afterwards, the limiter is activated and brings back the current to its maximum allowed value. Given the large time scale, it is impossible to see the development of the three level voltage waveform but it can be seen that the voltage is still very low. It is then demonstrated that such a current limiter prevents damaging high currents to flow in the primary side during faults.

In Fig. 41, the dynamic behaviour at the change of secondary current $I_{DC}(\alpha)$ reference is pictured. In this case, the green line is the DC current $I_{DC}(\alpha)$ and the magenta line is the secondary side voltage v_2. The current is shown at 1A per division while the voltage has resolution of 5V per division. In this case, the reference is changed from 2A to 2.8A. The figure aims to represent the extremely quick transient of $I_{DC}(\alpha)$: a reference change of about the 30% is completed is completed in one millisecond. The voltage has a noticeable transient as well due to the stepwise change. In this sense, the transient is not very smooth even if it finishes quickly; this is a point that must be taken into consideration, especially at greater power.

Finally, the DC-to-DC efficiency η_{DC} is calculated from the ratio between primary power P_0 and load power P_L. At the maximum power mode, a power of 21W has been received by the load while the DC source had a power of 27W; in other words, the efficiency η_{DC} is equal to 0.77. This is lower than expected because using symmetric phase shift for great variations of conversion voltage generates too many switching losses. However, the advantage is that the operation is continuous and the transients are more manageable with respect to discontinuous conduction control such as the ON/OFF control presented in the previous chapter. In fact, symmetric phase shift is more suited for application with low voltage regulation and low power factor. Therefore, depending on the application and the requirements, the symmetric phase shift may be preferred over two mode control as a method to control the current.

4.4 Conclusion

This chapter proposes the FPGA as a standard hardware tool for the converter control of WPT systems. After clearly describing the advantages of FPGAs over conventional DSPs, a description of the design flow of the logic project to be uploaded in the hardware has been provided. A case of generation of a logic block needed for comparing the value of the primary side current and storing the highest one into a register has been presented. After describing the features of the block, a realistic case of study involving the block about dynamic WPT is introduced. A circuit using only one converter per side and controlled by one FPGA per side is investigated. In this case, only symmetric phase shift allows for control because it can be performed alongside synchronous rectification. Both the primary side current limiter and the secondary side current controller are simple PI feedback controllers. Experimental results confirm the validity of the controllers: the current limiter can limit the primary side current when the load is not coupled and the secondary current matches perfectly the reference. The transients are very fast, the conduction is continuous but the DC-to-DC efficiency η_{DC} is not very good because the voltage regulation is not small and the power factor is very high, resulting in higher switching losses.

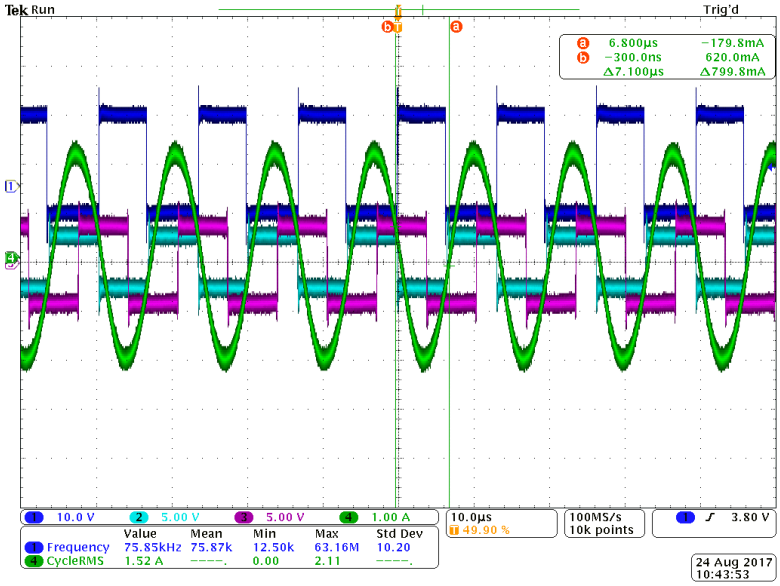

(a) Full wave operation (current limiter is not working, i.e. $I_1(\alpha)$ within the limit).

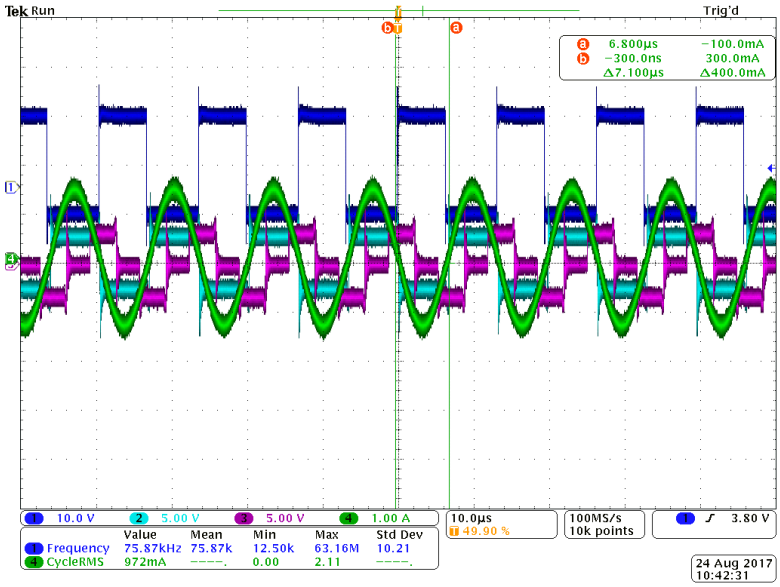

(b) Phase shifting operation (current limiter is working, i.e. $I_1(\alpha)$ over the limit).

Fig. 38: Experiment on primary side current limiter operation.

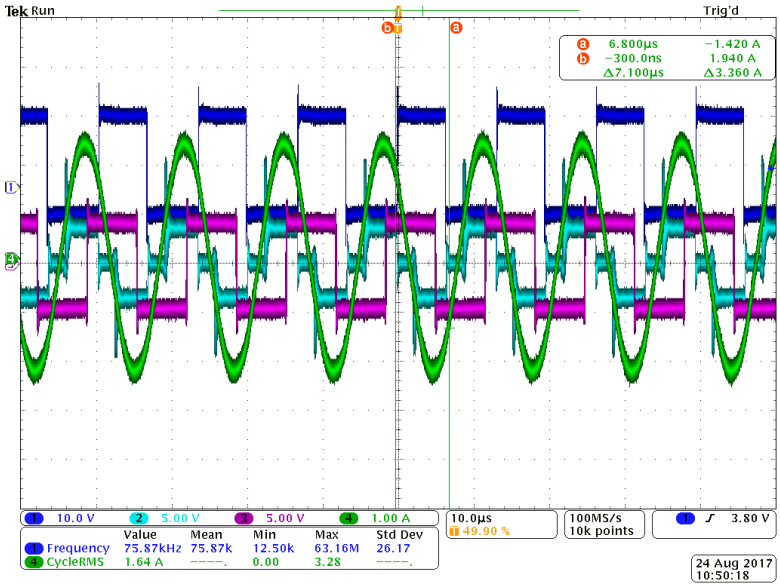

(a) Phase shifting operation ($\alpha_2 = 0.6$).

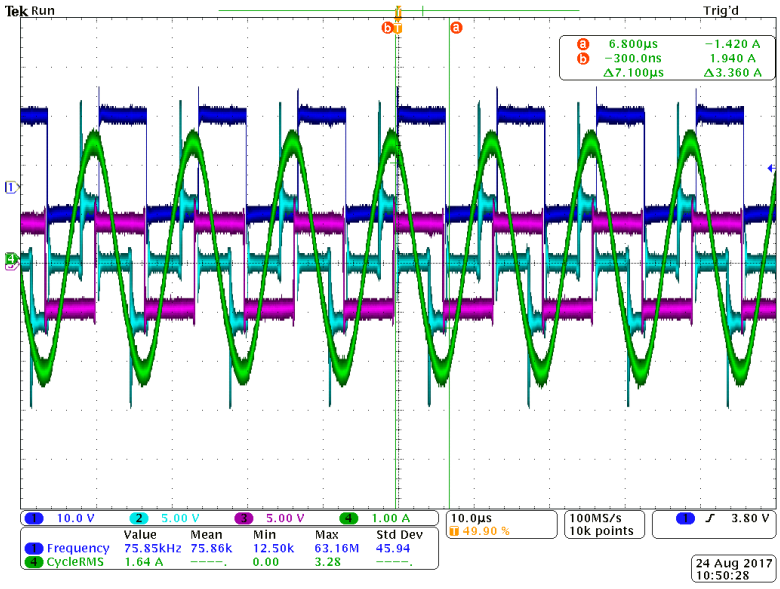

(b) Phase shifting operation ($\alpha_2 = 0.25$).

Fig. 39: Experiment on secondary side current controller operation.

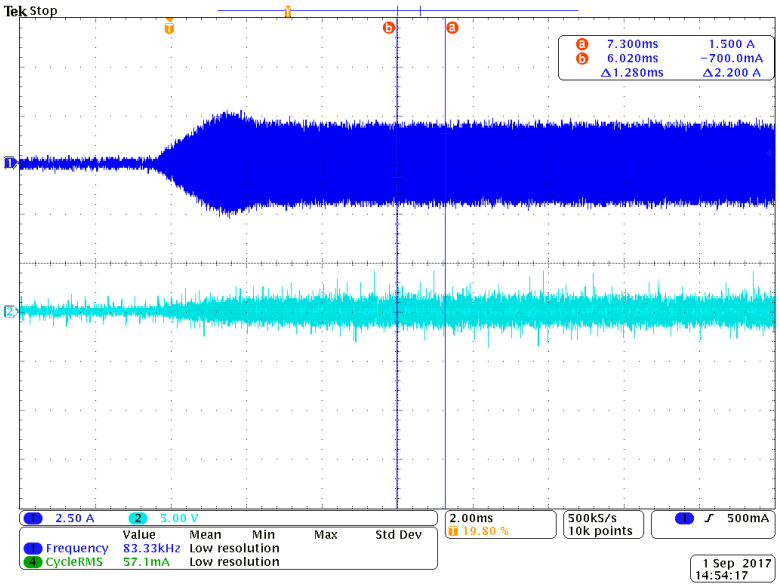

Fig. 40: Dynamic behaviour of primary side current limiter in case of open circuit (no secondary coil).

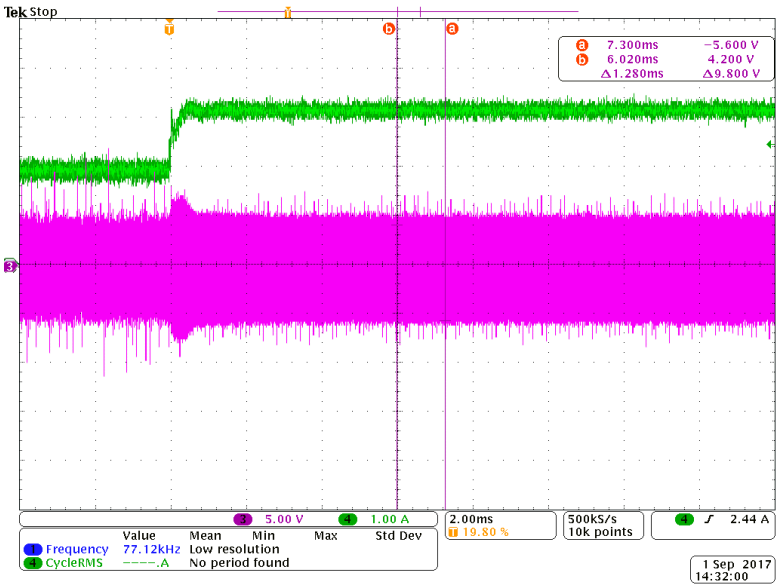

Fig. 41: Dynamic behaviour at the change of secondary current $I_{DC}(\alpha)$ reference.

Chapter 5

Secondary-side-only voltage stabilization control for constant power load

Chapter 5 cannot be disclosed because part of it is scheduled to be presented in a conference (IPEC 2018). Moreover, the chapter in its entirety is scheduled to be published in a journal (IEEJ Journal of Industrial Applications).

Chapter 6

Vision of future WPT society

In this chapter, a brief prediction about the future society in case of widespread use of wireless power transfer (WPT) is introduced. Based on literature up to now, some scenarios will be briefly discussed in relation to the fields who will benefit the most from WPT. The contribute of secondary-side-only control and the use of FPGA will be stated for each application field.

6.1 Paradigm shift

By looking at history, it is possible to characterize an era by the most important industrial and intellectual achievements. There is certainly a direct connection between the ideas that spring out and the industrial application based on these ideas. This is a natural feature of human evolution because, after materializing the concept, humans exploit the newly obtained technological tool to improve their quality of life. Consequently, by this way of reasoning, when mankind is in need of something, it starts studying the problem, eviscerating the central concept, and proposes solutions based on the core concept it sought. Here are some examples:

1. In prehistory, humans had little to nothing and their main concern was to sur-

vive. When they noticed that a fire can keep at bay eventual predators, can be used to cook the food and to warm up cold places, they immediately adopted it and began to develop agriculture and new tools. It was the basis of civilization.

2. In the nineteenth century, the industrial revolution was in full course. With many factories being built, many products were produced and had to be transported to the consumers. In the wake of historical materialism, industries wanted to produce more and spend less: in short, they wanted to be more efficient. Therefore they began study new forms of energy that can be cheaper or more performant to produce their goods with.

3. In the current century, for better control and delivery of services to the users, data can not be anymore transmitted by conventional means but must be collected and gathered in an enormous network, in which each single device sending and receiving data is unique but is also able to interconnect with other devices. This structure is commonly called Internet of Things (IoT). Similarly, since nowadays mankind is inhabitating most parts of the world, communication must be performed from every part of the world: this means that data must be transmitted without relying on wires anymore otherwise the cost would be too high. All these technologies are changing mankind's perception of the world and are creating a new sociey.

In the last example, it is stated that the need of data transmission and sharing, possibly in real time, is changing our society. All the research and technology currently in progress is developing now concepts and needs of society that will be satisfied in the next century.

In the particular case of WPT, the very fact that there is much research about it means

that mankind needs it and is ready to accept it. After all, energy (or power) is the last remaining resource to rely almost exclusively on cables. In fact, nowadays communications are commonly performed without the need of an electrical conductor. Without cables, the environment will be less cramped and more pleasant, personal as well as public facilities will enjoy greater flexibility and safety thanks to interconnection and interoperability of all the services provided to the user. Making wireless also the power will definitely usher society in a new era.

6.2 Impact of WPT on society

If researchers will continue to develop WPT, especially in coordination with techologies increasing the efficiency of renewable energy gathering, the impact on the future society will be remarkable.

In this sense, the concept of secondary-side-only control associated with the use of FPGAs greatly increases the flexibility and allows the development of new products while not changing the core of the power production and distribution. Implementing a change in the already existing power plants and distribution network is too expensive and requires the coordinated work of many different institutions, both from government and private industries. On the other hand, adopting the secondary-side-only control means adapting to pre-existing conditions, which can be performed immediately. Hence, secondary-side-only control is a very good candidate for gradually introducing wireless power transfer to the everyday life of people and letting them accept definitely the WPT technology.

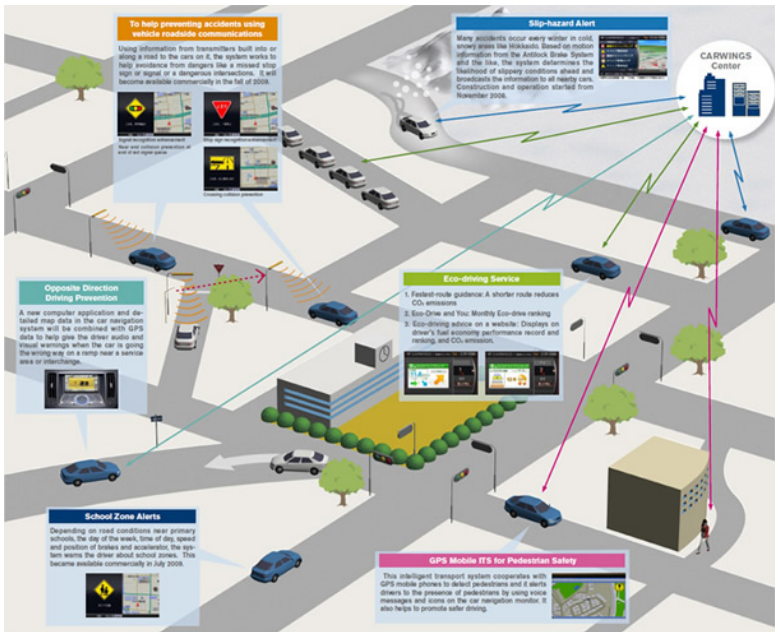

Fig. 42: Example of ITS data exchange [47].

6.2.1 WPT for transportations

In this thesis, the advantages of the combination between EVs and WPT have been made clear. EVs will charge while running, and static charging will be performed in the same manner as current plug/in charging station. The real innovation will be the inclusion of the vehicles in the IoT, thus becoming the intelligent transportation system (ITS). Now, this is a very big area of research and is widely studied in the world not only from car makers [47][49], but also from institutions and research centers affliated with the government of several coutries [72]–[75] as the next generation approach to solve traffic problems, prevent accidents and injuries. Interconnection between the vehicles, will optimize velocity and charging and parking patterns; the concept is in Fig. 42. Each vehicle will send data along with power, and wireless energy harvesting can feed sensors further saving space inside the vehicles. An image is provided in Fig. 48b. This is particularly important as self-driven vehicles relying on wireless exchange of data are already making their debut on the market.

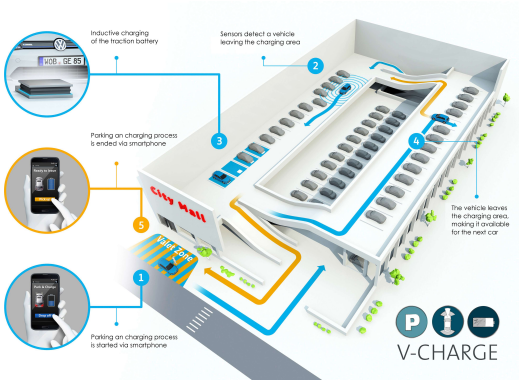

(a) Automated parking [76].

(b) Dynamic WPT in highways [77].

Fig. 43: Image of future transport with WPT.

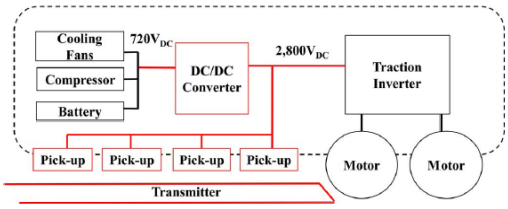

(a) General system of wireless powered train.

(b) Image of a wireless powered train.

Fig. 44: Example of wireless power transfer applied on trains [79].

This exchange of data may also be used from car makers to improve both the ITS and eventually also the vehicle themselves. However, strong cybersecurity must be implemented, otherwise it is possible to create enormous damage in terms of money and fatalities in case of successful cyber-attack.

EVs may even run on solar powered roadways to help the grid sustain the burden represented by the intermittent peaks of dynamic WPT [78]. As a result vehicles will be lighter, further increasing the source-to-wheel efficiency and eventually allowing the installation of ulterior energy storage systems such as supercapacitors. The supercapacitor can absorb the power peaks during dynamic DWPT [51], thus providing further benefits to the EV. The battery inside the vehicle is necessary in any case but it will be much smaller, storing the energy necessary to reach the nearest charging station. Smaller batteries will help cutting the emissions of CO_2 generated by their

(a) WPT coils for ships.

(b) Conceptual image of electric ship supplied with WPT.

Fig. 45: Example of wireless power transfer applied on ships [80].

manufacture and disposal.

The concept of WPT for trains is actually very similar to the one for EVs. The main difference is that the train can be supplied uninterruptedly because its trajectory is fixed [79]. Rather than accumulating energy in a energy storage system regardless of driving time and stopping time, it is feasible and also convenient to have a real time power supply. Instead of a pantograph and a transformer, only the receiving coils and their respective AC/DC converter will be included, as shown in Fig. 44a. Moreover, the same DC link is shared between the auxiliary power system and the powertrain supplying the motors. In this case, since the DC link voltage is very high, a DC/DC converter is used for chopping the voltage controlling the cooling system and feeding the auxiliary battery as well as other circuits. As stated before, a different point between EVs and trains is the trajectory, which is fixed in case of trains. This is a favorable condition for communication between sides and the possibility of a dual side control: in fact, since trajectory, timetables and speed profiles are already known, it is easier to devise a communication system between sides that takes into account communication delay and zone of unavailability. An image of the whole system is given in Fig. 44b.

Another novel application for WPT is for electric ships battery charging. This is still a niche field, and is being actively explored only by countries with many water channels such as Norway [80]. The motivation is the same as WPT for EVs. Using batteries instead of resorting to diesel engines allows significant savings due to the higher efficiency, not to mention the preservation of the natural environment near the harbours. Therefore, for short distance water transportation, WPT is the ideal solution, able to eliminate the laborious process of cable connection and disconnection for battery charging with a fully automated process. Hence, with more time dedicated to charging while docking, for the same energy the required power as well as the impact on voltage quality is lowered. The issue of WPT for ships consists in designing the coils (an image of a pilot application is shown in Fig. 45a) and the control for megawatt range power and considering the tolerance necessary to account for the movement caused by environmental factors such as wind and waves. In so doing, the impact on the frame and electric system of the already existing vessels would be minumum, as shown in the conceptual image of Fig. 45b. On the other hand, the elimination of cables will bring exactly the same benefits as in the case of EVs.

As for conversion circuits, wide band gap devices will be the new standard, thus allowing an eventual increase of the resonant frequencies. This means that the reactive elements, which occupy remarkable space, will have reduced dimensions and weight, saving up even more space for additional sensors. With the ITS, communication is available to implement dual side control and achieve very high efficiency from source to end; however, the vehicle side must always be able to fulfill the task of moving the passengers to the destination, indipendently of ITS. Thus, sensorless estimation of primary side or secondary side parameters should be implemented as a redundant alternative to ensure controllability is not lost in any circumstance. There-

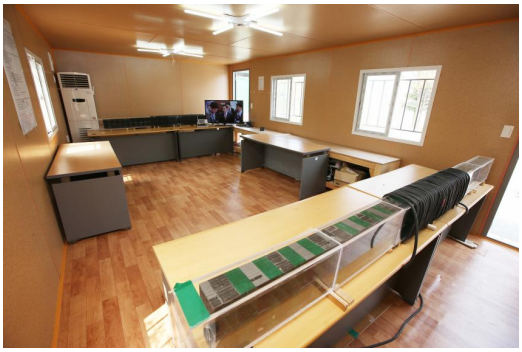

(a) Example of domestic appliances powered by WPT [81].

(b) Example of home adopting WPT [82].

Fig. 46: Example of domestic use of WPT.

fore, the secondary-side-only control concept is necessary for granting the core operation of transportation without burdening the primary side, which is used not only for transportation but for other applications as well and therefore must be kept as much simple as possible.

6.2.2 WPT and buildings

WPT used in buildings will clear the space from cables, too, allowing new interior designs and automated appliances. Power sockets will disappear with increased safety for children. Charging multiple domestic utilities at the same moment becomes fast and easy. In particular, while in a zone covered by WPT, mobile loads such as cellphones and vacuum cleaner will not be impeded by the cords. New research showed that a large LED TV as well as three 40 W fans can be powered from a 5 meter distance thanks to an optimally designed coil structure that has two magnetic dipole coils with compact ferrite core rods with windings at their centers [81]. Recently, many companies and start-ups are promoting cable-free solutions for home and offices [83][84].

Actually, in the domestic environment, both the static charging scenario and dy-

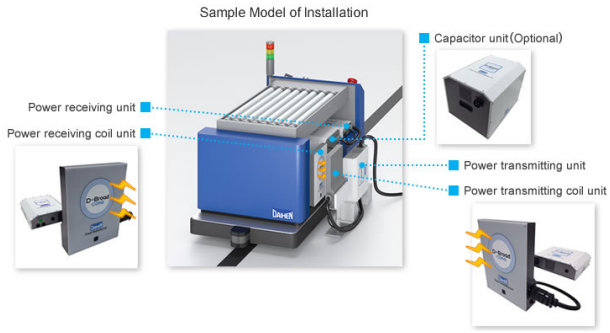

(a) Example of AGV charged by WPT [86].

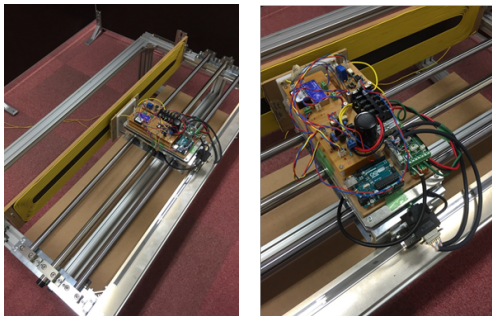

(b) Example of stage powered by WPT [8].

Fig. 47: Examples of industrial machines using WPT.

namic charging scenario occur, just like the case of transportations. For the same reasoning explained before, the secondary-side-only control concept is important to manage the single domestic appliance under use. A FPGA will allow also localized coordination by simultaneous secondary-side-only control and data elaboration, in accord to the concept of smart house.

6.2.3 WPT for industrial machines

Few years ago, industry already started looking about methods for charging tools not encompassing the substitution of batteries [85]. Use of WPT in the industry will eliminate the risk of dirtying or breaking the tools during the operations of charge. Automated guided vehicles (AGVs) are a very popular machine found in factories and is a perfect candidate for WPT, as shown in Fig. 47a. Given the fixed route, it is has a charging pattern similar to the one of a bus. With WPT, the storage system of AGV will be reduced, allowing for lighter vehicles and simplifying their composition. As for other advantages, WPT will significantly mitigate the cable disturbance affecting the velocity and the position control [8] of servo stages, similarly to Fig. 47b. The elimination of cables will make the setup lighter, too, and reduce the risk of incidents to human workers tripping on cables. Moreover, since other machineries

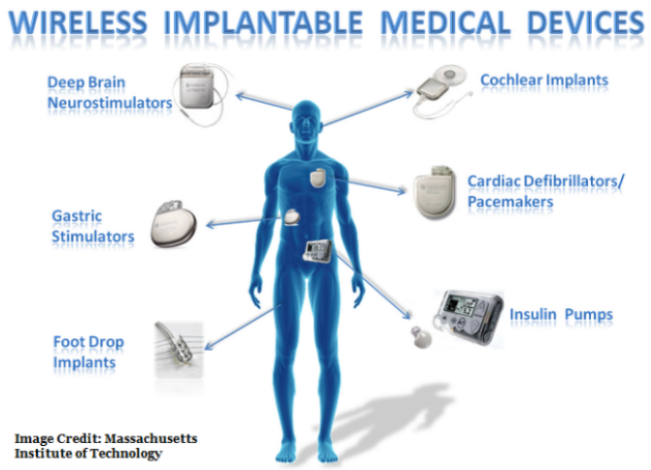

(a) Implantable wireless powered devices in the human body [87].

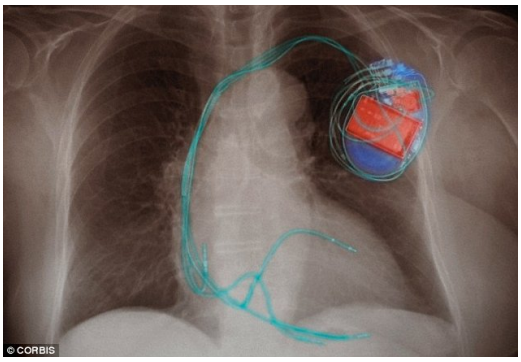

(b) X-rays showing a device powered by WPT implanted in human body [88].

Fig. 48: Examples of WPT used in biomedical application.

are present in the neighbouring areas, it is necessary to ascertain not only the safety of human beings near the tools, but also the compatibility with other machineries as well.

In the industrial case as well there are no many differences from the transportation case. Secondary-side-only control is very well paired with automation. The use of FPGAs is then very much welcome since it can be programmed to behave automatically, which is something that most microcontrollers can not achieve. In this sense, the start/stop operation of tools and machineries becomes much quicker and smooth. Therefore, the combination of secondary-side-only control concept and FPGA will provide a huge benefit to the industry.

6.2.4 WPT for medical applications

Being a non invasive method to perform diagnosis after surgery, WPT is even used in surgery and treatment, powering internal medical implants (pacemaker) and auxiliary equipment, as shown in Fig. 48. In particular, microrobots powered wirelessly will allow doctors to deliver accurate treatments. In this sense, wireless power trans-

fer has the potential to be a stepping stone to medicine as well as robotics, with the use of miniaturized tools. When humans are involved, saftey standards must be met: in this sense, the standards of ICNIRP [89] may be revised with the progress of research. It is not unlikely that localized application of very strong electromagnetic field is found to be an effective treatment against illnesses. Eliminating wires reduces the risk of infection and improve noticeably the quality of the therapy and recovery of a patient.

Interestingly, these wireless devices must be equipped with strong types of data encryption: in fact, it is entirely possible that a cyber-attack paralyzes or implements a wrong operation mode in this devices, potentially causing the death of the patient. Therefore cybersecurity, just like in the case of EVs, must be researched actively. In this sense, cybersecurity is linked to data elaboration, which is something that a FPGA can perform in parallel with converter control without additional delays. Past research never quite encompassed simultaneous data and converter control, and it will surely be an important research theme in the future. Secondary-side-only control is fundamental because it directly affects the patient (e.g. controlling the power on the secondary side will limit the coil heating). Moreover, the operating frequencies are in the ISM band, therefore using a FPGA to perform advanced control becomes mandatory.

6.2.5 Conclusion

With the more and more widespread use of WPT, the quality of life of society will be increased. By adopting WPT many problems in multiple fields of society will be mitigated or solved. Transmission of data and power without wires will become the future standard as research progresses and will allow humanity to evolve. Right now,

the field benefitting the most from WPT is transportation systems, but other fields are quickly catching up. By using WPT, hopefully more and more renewable energy sources will be employed, and intelligent automated systems will be encouraged. Currently, the most practical contribution of WPT to the society is the reduction of batteries in storage systems, meaning that less batteries will be necessary and therefore less CO_2 will be generated for their production. Secondary-side-only control and FPGA will be fundamental in the acceptance by the public of WPT and will ease the transition process from a society using only cables to a society using only wireless power and data transfer.

Chapter 7

Conclusions

This research focused on circuit modelling and converter control for wireless power transfer (WPT) systems by magnetic resonant coupling. The objective of this research revolves around the composition of the conversion circuit, the method of control and the type of load in secondary side. In real WPT applications for electric vehicles (EVs), there are several constraints that complicate the control: the main point of this thesis's framework is the ability to maintain controllability notwithstanding those constraints and propose a control concept applicable to a wide range of different scenarios. The two most demanding constraints are the lack of communication between sides and the reduced number of power converters: this dissertation proposes some novel controls achieving good results even under such disadvantageous conditions. For WPT systems, it is important to work at highest efficiency possible while supplying the load. After analyzing the WPT model and the desired operation point, a simultaneous control of efficiency and power for a constant voltage load (CVL) has been proposed by making use active devices in the AC/DC converter. In case of constant power load (CPL), the analysis of the WPT system function and a controller for stabilizing the load voltage has been proposed. By adopting active devices in the converters, it is possible to icrease the degree of freedom, thus allowing

a reduction and simplification of conversion circuit while maintaining at the same time the necessary controllability.

In chapter 2, the features of EVs as well as static and dynamic WPT applied to EVs have been introduced. Moreover, the suitability of WPT systems by magnetic resonant coupling with series-series (SS) compensation applied to EVs has been stated.

In chapter 3, a control performed only in the secondary side and covering at the same time time transmitting efficiency and desired power is proposed for a WPT system with CVL. As stated before, constraints are taken into account: communication and primary side manipulation are not available. A common point with past research is the use of two power converters in the secondary side: an AC/DC converter followed by a DC/DC converter. However, past research rarely used active devices in the AC/DC converter stage. After analyzing the WPT system and stating the important parameters, the use of half active rectifier (HAR) is introduced. With the HAR, a two-mode control can be performed by exploiting the features of SS compensation and the average power can be controlled. On the other hand, the DC/DC converter is used to regulate the DC voltage by adopting equivalent input impedance optimization method and therefore operate on the maximum efficiency point. The control period of the two converters must be different in order to avoid conflicts. The controller design of the HAR and the DC/DC converter is provided after analyzing each power converter plant, with the setting method of the feedforward part of the PI is explained. The feedback part is designed by pole placement. Experimental results are provided and discussed firstly for a static scenario. The proposed control is compared with conventional efficiency control. The two-mode HAR control switches between ON state and OFF state, thus introducing transient and noise especially during the passage between OFF state and ON state. However, this issue does not affect the

operation of the controller; the reference values for both average power and DC link voltage are matched. The power supplied to the CVL is continuous and not intermittent. The efficiency is slightly lower than maximum due to introduction of short mode losses, but this is a trade-off for acquiring power controllability. Evaluation for dynamic scenario is also provided. Since mutual inductance information is required in the controller, an estimation method based on constant trace RLS algorythm is devised. The accuracy of the estimation is not high due to non persistent excitation of updating coefficient, but the algorithm is self bounded and the error propagation is mitigated. This issue also has little effect on the controller performance. Then experimental results for dynamic scenarios are provided, comparing the proposed control with the conventional efficiency control. In this case, too, the average power and DC link voltage match with the reference; in particular, the load power in the proposed control is not affected by the change of coil position. The proposed control concept is simple and shows an advantageous trade-off between slight reduction of transmitting efficiency and power controllability. An experiment with high power level has been performed and confirmed the effectiveness and the behaviour of the proposed control at low power.

In chapter 4, a discussion about the advantages of FPGA in controlling the converters for wireless power transfer systems will be presented. In fact, FPGA is a necessary tool because of its superiority when compared to conventional DSP control board in terms of calculation time, diagnostics and flexibility in system integration. Consequently, it is possible to implement digitally controllers (e.g. peak current limiter) that can effectively substitute analog protection circuits. Furthermore, it allows easily the implementation of advanced control such as phase shift in a high frequency environments. After explaining the netlist project design flow and logic block cre-

ation process inside of the FPGA, a case of study is presented. In order to provide an effective current limiter for use in case of vehicle detection failure in dynamic WPT environment, a customized logic block automatically acquiring the AC peak value of the current from the sensor and updating it to the highest value is created. The block stores the value in a register, which can be accessed by the code and exploited in a phase shifting control to limit the current in case the designated limit is exceeded. At the same time, a simple current controller based on combined phase locked loop (PLL) algorithm and phase shifting is proposed for the secondary side. This is necessary for the secondary-side-only control concept. The logic block performance has been verified by experiments, and therefore the importance of FPGA for control in WPT system has been established.

In chapter 5, a control performed only in the secondary side for stabilizing the load voltage is proposed for WPT system with CPL. Almost all literature focuses on resistance load or CVL, but constant power load is rarely if ever considered. The CPL voltage is unstable, thus stabilization is required. Again, communication and primary side manipulation are not available. A common point with past research is the use of only one power converter in the secondary side (an AC/DC converter). However, the stabilization method must be substantially different from those proposed in past research. The objective of the control is set to achieve voltage stabilization with smooth voltage transient and simple controller design. As only one power converter can be used for control, the only control available is the combination of synchronous rectification (SR) and symmetric phase shift. The method for achieving SR and symmetric phase shift is then described while introducing the conversion ratio. By symmetric phase shift, the secondary side AC voltage is controlled and assumes a three-level waveform: by changing the width of the three-level waveform the load

voltage is stabilized. The controller is chosen to be a high bandwith PI feedback. The PI controller design of the AC/DC converter is provided along with the setting method of the gains of the feedback. The poles are chosen with pole placement method. The closed loop plant is then analyzed to set the stability conditions around the arbitrary equilibrium point. The voltage equilibrium value can be chosen as the voltage related to maximum transfer efficiency, thus allowing simultaneous power and efficiency control. The proposed control then is fast enough to cope with the slow pole dynamics of the open loop function, it is able to avoid big transients and it is easy to design. The robustness against the variation of load condition and mutual inductance, as well as the efficiency evaluation for different operating points has been given.

In chapter 6, the vision and the benefits for the society obtained by wireless power transfer are described. It is shown that the society wellness can be significantly improved with WPT, with more flexibility in both public and private life. In the field of EVs, the integration to the IoT thanks to the ITS will allow great reduction of traffic and accidents and the widespread use of autonomous driving, along with providing feedback data to improve the system. The importance of FPGA and the secondary-side-only approach in the future of WPT are remarked.

From the aforementioned description, this research aimed at maintain controllability and reduce system costs of WPT systems for EVs when there are several constraints. Past research mostly proposed control methods applied to ideal conditions, without considering the constraints typical of practical applications, such as unavailable communication between sides and unavailable regulation of the primary side. This research focused on secondary-only-control, which is important for the future development of dynamic WPT. In this sense, this research considered CVL and CPL.

In particular, papers dealing with CPL are very rare in literature, making this an original point. Furthermore, past research placed considerable weight on the coupler design; on the other hand, this thesis tried to see the WPT from a control viewpoint, without relying too much on hardware particuarities. The techniques of feedforward and feedback and PI control are well known, yet not much discussion about their application to WPT system is present in literature. The proposed control for CVL in this thesis can be utilized for both static WPT and dynamic WPT and is simple to design and implement. Similarly, the proposed voltage stabilization control for CPL is easy to design and achieves smooth transient, which is beneficial to converter operation. Many applications use CPL such as motor, therefore including them in WPT system is necessary in order to advance the technology. The proposed controls presented in this dissertation are valuable from practical point of view as a way to ascertain how much controllability is possible to achieve with constraints, especially in conditions of low degree of freedoms and lack of communication; therefore, while they may not achieve the extreme results of state-of-the-art WPT systems in which optimization of a single parameter is considered, their versatility allows them to achieve good overall results and to be employed in a wide range of applications. As a consequence, it is expected that the combination of secondary-side-only control and FPGA will promote the acceptance of WPT by the public, finally leading to a society not using cables anymore.

Acknowledgments

This doctoral dissertation is the product of three years of hard work, excitements and delusions. In writing this thesis, both my natural determination and the support of those wonderful people near to me realized the hopes and dreams I always maintained inside my heart. In Japanese, my whole time at the laboratory can be expressed by the proverb “七転八起”. Many times I fell, but I refused to give up. Then I fell again, and I refused again. And again and again. My determination alone, however, is not strong enough for such demanding effort: it has been boosted by everyone who cheered and cared for me. It is now these wonderful people who I want to thank from the bottom of my heart.

First is professor Yoichi Hori, my supervisor. I am extremely grateful to professor Hori for accepting me into Hori-Fujimoto laboratory and give me a chance to prove my skills as a researcher. I consider professor Hori like my Japanese foster father, as half of the time the advices he gave (and is stil giving me) are not related to research. I always treasured his words, even if sometimes it took me a long time before understanding them. Professor Hori always managed to find the good point of my work and also gave me a big helping hand in finding a job in Japan after my graduation, so I do not think there is a word expressing thanks big enough for him.

Second is professor Hiroshi Fujimoto. I would like to express my deepest gratitude to professor Fujimoto for the countless times he discussed with me about my

research, giving me precious advices and often pointing me at the right direction. I also appreciate very much professor Fujimoto's precison, rigour and dedication in research, a quality that always pushes his students, including me, to improve themselves and produce the best results possible. Moreover, it is merit of professor Fujimoto if I have been able to go to Norway and study about FPGA technology for two years in a row. And I thank him very much for that. I will do my best to transmit the knowledge I acquired to other lab members and continue the study of FPGA technology at laboratory level.

Third is professor Takehiro Imura. Professor Imura is the leader of the team researching wireless power transfer and, as such, always helps the team members in identifying the core concepts and setting up the research at the beginning of the course. It is always the first filter in the very noisy input that is raw research data for the team members, including me. I had countless discussion with prof.Imura about my research, and he helped me very much in shaping it up by tireless minute work and suggestions. Incidentally, I am also professor Imura's unofficial English cross-checker, a job which stimulated me to think very much about the correct expression to use to communicate a concept. This is a useful skill and I will make good use of it.

I would like to thank one more time professor Hori, professor Fujimoto and professor Imura for the great amount of time and effort they dedicate to their students, giving them impeccable guidance and top-class education. This kind of relationship is very special to Japan, and I am still amazed to see that students who graduated a few years ago often come to greet everyone and have a nice time together. This is yet another proof of the strong bond between the professors of Hori-Fujimoto lab and their students.

Furthermore, talking about professors, I would like to thank the professors who have been members of my examination committee: Other than professor Hori and professor Fujimoto, professor Hiroyuki Ohsaki, professor Takafumi Koseki, professor Junpei Baba and professor Yoshihiro Kawahara. I greatly appreciate your time and your comments to my work, allowing me to improve the quality and revise the errors of my thesis.

Then, I would like to thank all my fellow students at Hori-Fujimoto laboratory. We have spent so much time together in many different places and had always had a laugh and a word for each other. In particular, I would like to thank all the members of the wireless power transfer team for the constructive discussions and for studying together. We are a good team.

On a more personal terms, I would like to say my sincerest appreciation to Toshiyuki Hiramatsu, Gaku Yamamoto, Daita Kobayashi, Motoki Sato, Wataru Ohnishi, Yoshi Ri, Toshiki Niinomi and Akiyuki Hasegawa. Thank you very much for keeping up with me, helping me out and having fun with me. In particular, thank you very much to Toshiki Niinomi and Wataru Ohnishi for giving me a hand with Japanese language and Japanese customs I did not know before.

A very special thanks and my greatest appreciations go to Giuseppe Guidi and Marta Molinas, who accepted me in Norway and allowed me to have a superb experience both in terms of research and travel. I had learned a lot both from Giuseppe Guidi and Marta Molinas and I had the honour of spending a lot of time with their family. I greatly enjoyed my time in Norway and I would love to come back again. If I will ever work again with them, I hope I will be able to help him more than what I did until now.

Yet another special thanks to my former supervisor back in Italy, professor Giuseppe

Buja, and also to professor Manuele Bertoluzzo, who helped me quite a lot during the writing of the master's thesis. It is only thanks to prof. Buja that I have been able to come into contact with professor Hori, paving the way for my coming in Japan. I can very well say that his help changed the very course of my life. He is a very good professor and I am proud to have been one of his students. I have been able to meet again professors Buja and Bertoluzzo at international conferences and it was wonderful to exchange news on each other's research activity. I hope I have kept high their honour while being in Japan.

A super thanks to my friends back in Italy who have not yet forgot me. It is clear that I made the right choice when I decided to became friends with you. Some I hear from often, others only sometimes, but when I come back home for Christmas I always meet you all with the greatest pleasure. Even though I changed after coming to Japan, the core is still the same and the same can be said for you.

I would like to express my feelings of gratitude and love to Miyuki Omori, who has always been present at my side since my arrive in Japan and will be present at my side even more from now on. Even though she is momentarily far because of her work, everyday we would call each other, making my day and my mood better. I consider myself lucky to have met her, because that was yet another life-changing experience for me.

And finally, last but not least, I would like to express my deepest gratitude and affection to my whole family: my cousins, my uncles and aunts, my remaining grandmother and my beloved parents. A relentless stream of encouragement has been coming from them every day. They are the core of my determination and this thesis is dedicated to them. In particular, my parents have proven to me once more how much they care to keep supporting me with eternal patience and unending love, even

in the direst of circumstances. I would not be where I am without them.

These acknowlegments conclude this thesis and this chapter of my life. I hope that you, the reader, enjoyed my thesis and found it useful for your purposes.

References

[1] A. Kurs, A. Karalis, R. Moffatt, J.D. Joannopoulos, P. Fisher and M. Soljacic, "Wireless power transfer via strongly coupled magnetic resonance", Science Express, vol. 317, no. 5834, pp. 83-86 (June 2007).

[2] J. Moon, H. Hwang, B. Jo, C. Kwon, T. Kim, S. Kim "Design and implementation of a high-efficiency 6.78MHz resonant wireless power transfer system with a 5W fully integrated power receiver", IET Power Electronics, vol. 10, no. 5, pp. 577-587 (June 2017).

[3] W. Ahn et. al, "Design of coupled resonators for wireless power transfer to mobile devices using magnetic field shaping," IEEE Int. Symp. on Electromag. Comp. (EMC), DOI: 10.1109/ISEMC.2012.6351667, pp. 772-776 (2012).

[4] P. Si, A.P. Hu, S. Malpas, D. Budgett " A Frequency Control Method for Regulating Wireless Power to Implantable Devices", IEEE Trans. on Biom. Circ. and Sys., vol. 2, no. 1, pp. 22-29 (2008).

[5] X. Luo, S. Niu, S.L. Ho, W.N. Fu, "A design method of magnetically resonating wireless power delivery systems for bio-implantable devices", IEEE Trans. Magn., vol. 47, no. 10, pp. 3833-3836 (2011).

[6] J. Kim, C. Sun, I. Suh, "A proposal on wireless power transfer for medical implantable applications based on reviews", IEEE Wireless Power Transfer Con-

ference, pp. 166-169 (2014).

[7] J. Kim, C. Sun, I. Suh, “A 13.56 MHz Wireless Power Transfer System With Reconfigurable Resonant Regulating Rectifier and Wireless Power Control for Implantable Medical Devices”, IEEE Jour. Sol. St. Phys., vol. 50, no. 4, pp. 978-989 (2015).

[8] T. Nishimura, K. Hata, T. Imura, Y. Hori, “Velocity Estimation and Control of DC Motor Driven by Wireless Power Transfer” 2016 Asian Wireless Power Transfer Workshop (2016).

[9] T. Imura, H. Okabe and Y. Hori, “Basic experimental study on helical antennas of wireless power transfer for Electric Vehicles by using magnetic resonant coupling”, in IEEE Veh. Pow. and Prop. Conf., pp. 936-940 (2009).

[10] M. Kato, T. Imura and Y. Hori, “New characteristics analysis considering transmission distance and load variation in wireless power transfer via magnetic resonant coupling”, in IEEE 34th Int. Telecom. En. Conf. (INTELEC), pp. 1-5 (2012).

[11] S. Li and C.C. Mi, “Wireless power transfer for electric vehicle applications”, IEEE Journ. of Em. and Select. Top. in Pow. El., vol. 3, issue 1, pp. 4-17 (2015).

[12] Y. Nagatsuka, N. Ehara, Y. Kaneko, S. Abe and T. Yasuda, “Compact contactless power transfer system for electric vehicles”, in Int. Pow. El. Conf. (IPEC), pp. 807-813 (2010).

[13] C.S. Wang, O.H. Stielau, and G.A. Covic, “Design consideration for a contactless electric vehicle battery charger”, IEEE Trans. on Ind. El., vol. 52, no. 5 pp. 1308-1314 (2005).

[14] M. Budhia, J.T. Boys, G.A. Covic, and C. Huang, “Development of a Single-Sided Flux Magnetic Coupler for Electric Vehicle IPT Charging Systems”, IEEE Trans. on Ind. El., vol. 60, no. 1 pp. 318-328 (2013).

[15] G.A. Covic and J.T. Boys, “Modern Trends in Inductive Power Transfer for Transportation Applications”, IEEE Journ. of Em. and Select. Top. in Pow. El., vol. 1, issue 1, pp. 28-41 (2013).

[16] K. Throngnumchai, A. Hanamura, Y. Naruse, and K. Takeda, “Design and evaluation of a wireless power transfer system with road embedded transmitter coils for dynamic charging of electric vehicles”, in El. Veh. Symp. and Exhib. (EVS27), pp. 1-10 (2013).

[17] S.W. Lee, J. Huh, C.B. Park, N.S. Choi, G.H. Cho, and C.T. Rim, “On-line electric vehicle using inductive power transfer system”, in IEEE En. Conv. Cong. and Expo. (ECCE), pp. 1598-1601 (2010).

[18] J. Huh, S.W. Lee, W.Y. Lee, G.H. Cho, and C.T. Rim, “Narrow-width inductive power transfer system for on-line electrical vehicles”, IEEE Trans. on Pow. El., vol. 26, no. 12, pp. 3666-3679 (2011).

[19] C.H. Choi, H.J. Jang, S.G. Lim, H.C. Lim, S.H. Cho, I. Gaponov, “Automatic wireless drone charging station creating essential environment for continuous drone operation”, 2016 International Conference on Control, Automation and Information Sciences (ICCAIS), pp. 132-136 (2016).

[20] S.H. He, Y.S. Kim, H.S. Lyou, M.S. Kim, J. Lyou, “The applications of wireless technology for operating Nuclear Power Plants”, 2014 14th International

Conference on Control, Automation and Systems (ICCAS 2014), pp. 1475-1478 (2014).

[21] C.S. Wang, O.H. Stielau, G.A. Covic, “Design considerations for a contactless electric vehicle battery charger,” IEEE Trans. Ind. Elect., vol. 52, no. 5, pp. 1308-1314 (2005).

[22] S.Y.R. Hui, W. Zhong, C.K. Lee, “A Critical Review of Recent Progress in Mid-Range Wireless Power Transfer”, IEEE Trans. Pow. Elect., vol. 29, no. 9, pp. 4500-4511 (2014).

[23] J. Shin et al., “Design and implementation of shaped magnetic resonance based wireless power transfer system for roadway-powered moving electric vehicles”, IEEE Trans. Ind. Electron. (2013).

[24] K. Furusato, T. Imura, Y. Hori “Design of Multi-frequency Coil for Capacitor-less Wireless Power Transfer using High Order Self-resonance of Open End Coil”, The IEEE MTT-S Wireless Power Transfer Conference 2016 (2016).

[25] W. Zhong, C.K. Lee and S.Y. Hui, “General analysis on the use of Tesla ’ s resonators in domino forms for wireless power transfer”, IEEE Trans. Power Electron., vol. 60, no. 1, pp. 261-270 (2013).

[26] B.L. Cannon, J.F. Hoburg, D.D. Stancil, S.C. Goldstein, “Magnetic resonant coupling as a potential means for wireless power transfer to multiple small receivers”, IEEE Trans. Power Electron., vol. 24, no. 7, pp. 1819-1825 (2009).

[27] H. Fujimoto, S. Harada, “Model-Based Range Extension Control System for Electric Vehicles With Front and Rear DrivingBraking Force Distributions”, IEEE Trans. Ind. Electron., vol. 62, no. 5, pp. 3245-3254 (2015).

[28] T. Hofman, C.H. Dai, “Energy Efficiency Analysis of Powertrain with Toroidal Continuously Variable Transmission for Electric Vehicle”, Proc. 2010 IEEE Vehicle Power and Propulsion Conference, pp. 1-6 (2010).

[29] Y. Ikezawa, H. Fujimoto, Y. Hori, D. Kawano, Y. Goto, M. Tsuchimoto, K. Sato, “Range Extension Autonomous Driving for Electric Vehicles Based on Optimal Vehicle Velocity Trajectory Generation and Front-Rear Driving-Braking Force Distribution with Time Constraint”, IEEJ Journal of Industry Applications, Vol. 5, No. 3, pp. 228-235 (2016).

[30] H. Yoshida, H. Fujimoto, D. Kawano, Y. Goto, M. Tsuchimoto, K. Sato, “Range Extension Autonomous Driving for Electric Vehicles Based on Optimal Velocity Trajectory and Driving Braking Force Distribution Considering Road Gradient Information”, 41st Annual Conference of the IEEE Industrial Electronics Society (IECON), pp. 4754-4759 (2015).

[31] SAE International (2013, Nov. 14th). “SAE International Task Force Announces Agreement on Frequency of Operation and Power Classes for Wireless Power Transfer for its Electric and Plug-In Electric Vehicle Guideline” [online]. Available: http://www.sae.org/

[32] G.A. Covic, “A past present and future perspective on wireless power transfer for electric vehicles”, 2013 IEEE Energy Conversion Congress and Exposition (ECCE), invited talk, Denver, Colorado (2013).

[33] W. Zhang, S.C. Wong, C.K. Tse, Q. Chen, “A study of sectional tracks in roadway inductive power transfer system”, in Proc. IEEE Energy Convers. Congr. Expo. (ECCE), pp. 822826 (2011).

[34] G.A.J. Elliott, J.T. Boys, A.W. Green, “Magnetically coupled systems for power transfer to electric vehicles”, in Proc. Int. Conf. Power Electron. Drive Syst., pp. 797801 (1995).

[35] H. Kohara, “Research trend for EV ’ s in National Institute for Land and Infrastructure Management, ” Transactions of the Society of Automative Engineers of Japan, vol.130, no. 1, pp. 84-92, (2010) (in Japanese).

[36] M. Sato, G. Yamamoto, D. Gunji, T. Imura and H. Fujimoto, “Development of Wireless In-Wheel Motor Using Magnetic Resonance Coupling”, IEEE Trans. on Pow. El., vol. 31, no. 7, pp. 5270-5278 (2016).

[37] F. Musavi, W. Eberle and W.G. Dunford, “A High-Performance Single-Phase Bridgeless Interleaved PFC Converter for Plug-in Hybrid Electric Vehicle Battery Chargers”, IEEE Trans. on Ind. Appl., vol. 47, no. 4, pp. 1833-1843 (2011).

[38] D. Gunji, T. Imura and H. Fujimoto, “Stability analysis of constant power load and load voltage control method for Wireless In-Wheel Motor”, in Proc. 9th Int. Conf. on Pow. El. and ECCE Asia (ICPE-ECCE Asia), pp. 1944-1949 (2015).

[39] M. Miyazaki, S. Abe, Y. Suzuki, N. Sakai, T. Ohira, M. Sugino, “Sandwiched parallel plate capacitive coupler for wireless power transfer tolerant of electrode displacement”, in 2017 IEEE MTT-S International Conference on Microwaves for Intelligent Mobility (ICMIM), pp. 29-32 (2017).

[40] H.L. Li, A.P. Hu, G.A. Covic, and C. Tang, “A new primary power regulation method for contactless power transfer”, in IEEE Int. Conf. on Ind. Tech. (ICIT), pp. 1-5 (2009).

[41] J.M. Miller, C.P. White, O.C. Onar, and P.M. Ryan, “Grid side regulation of wireless power charging of plug-in electric vehicles”, in IEEE En. Conv. Cong. and Expo. (ECCE), pp. 261-268 (2012).

[42] M. Fu, C. Ma and X. Zhu, “A cascaded boost-buck converter for high efficiency wireless power transfer systems”, IEEE Trans. on Ind. Informat., vol. 10, no. 3, pp. 1972-1980 (2014).

[43] K. Kusaka and J. Itoh, “Reduction of Reflected Power Loss in an AC-DC Converter for Wireless Power Transfer Systems”, IEEJ Journ. of Ind. Appl., vol. 2, no. 4, pp. 195-203 (2013).

[44] H. Ishihara, F. Moritsuka, H. Kudo, S. Obayashi, T. Itakura, A. Matsushita, H. Mochikawa and S. Otaka, “A voltage ratio-based efficiency control method for 3 kW wireless power transmission”, in IEEE Appl. Pow. El. Conf. and Expo. (APEC), pp. 1312-1316 (2014).

[45] T. Diekhans and R.W. De Donker, “A Dual-Side Controlled Inductive Power Transfer System Optimized for Large Coupling Factor Variations and Partial Load”, IEEE Trans. on Pow. El., vol. 30, no. 11, pp. 6320-6328 (2015).

[46] H.H. Wu, A. Gilchrist, K.D. Sealy and D. Bronson, “A high efficiency 5 kW inductive charger for EVs using dual side control”, IEEE Trans. on Ind. Informat., vol. 8, no. 3, pp. 585-595 (2012).

[47] www.nissan.co.jp/ [online] (2017).

[48] https://www.mercedes-benz.com/ [online] (2017).

[49] http://www.toyota.co.jp/ [online] (2017).

[50] N. Kuyvenhoven, C. Dean, J. Melton, J. Schwannecke, A.E. Umenei, “Development of a foreign object detection and analysis method for wireless power systems”, 2011 IEEE Symposium on Product Compliance Engineering Proceedings, pp. 1-6 (2011).

[51] J.M. Miller, O.C. Onar, C. White, S. Campbell, C. Coomer, L. Seiber, R. Sepe and A. Steyerl, “Demonstrating Dynamic Wireless Charging of an Electric Vehicle: The Benefit of Electrochemical Capacitor Smoothing”, IEEE Pow. El. Mag., vol. 1, no. 1, pp. 12-24 (2014).

[52] K.E. Koh, K. Song, P. Sukprasert, T. Imura, Y. Hori, “Two-Transmitter Wireless Power Transfer with LCL Circuit for Continuous Power in Dynamic Charging”, IEEE PELS Workshop on Emerging Technologies; Wireless Power, pp. 1-6 (2015).

[53] K. Song, C. Zhu, K.E. Koh, T. Imura, Y. Hori, “Wireless Power Transfer for Running EV Powering Using Multi-Parallel Segmented Rails”, IEEE PELS Workshop on Emerging Technologies; Wireless Power, pp. 1-6 (2015).

[54] D. Kobayashi, T. Imura and Y. Hori, “Real-time coupling coefficient estimation and maximum efficiency control on dynamic wireless power transfer for electric vehicles”, in IEEE PELS Workshop on Emerg. Tech.: Wireless Pow. (WoW), pp. 1-6 (2015).

[55] https://commons.wikimedia.org/wiki/File:AdaptiveFilter_C.png, [online] (2017).

[56] G.R. Nagendra, L. Chen, G.A. Covic, J.T. Boys, “Detection of EVs on IPT

Highways", in Proc. 2014 IEEE Applied Power Electronics Conference and Exposition , pp. 1604-1611 (2014).

[57] W.X. Zhong and S.Y.R. Hui, "Maximum energy efficiency tracking for wireless power transfer systems", IEEE Trans. on Pow. El., vol. 30, no. 7, pp. 4025-4034 (2015).

[58] G. Lovison, M. Sato, T. Imura and Y. Hori, "Secondary-side-only simultaneous power and efficiency control for two converters in wireless power transfer system", Proc. 41st Ann. Conf. of the IEEE Ind. El. Soc. (IECON), pp. 4824-4829 (2015).

[59] M. Kato, T. Imura and Y. Hori, "Study on maximize efficiency by secondary side control using DC-DC converter in wireless power transfer via magnetic resonant coupling", in El. Veh. Symp. and Exhib. (EVS27), pp. 1-5 (2013).

[60] K. Hata, T. Imura and Y. Hori, "Maximum Efficiency Control of Wireless Power Transfer Considering Dynamics of DC-DC Converter for Moving Electric Vehicles", in IEEE Appl. Pow. El. Conf. and Expo. (APEC), pp. 3301-3306 (2015).

[61] A. Berger, M. Agostinelli, S. Vesti, J.A. Oliver, J.A. Cobos and M. Huemer, "Wireless Charging System Applying Phase-Shift Amplitude Control to Maximize Efficiency and Extractable Power", IEEE Trans. on Pow. El., vol. 30, no. 11, pp. 6338-6348 (2015).

[62] T. Hiramatsu, X. Huang, T. Imura and Y. Hori, "Wireless Charging Power Control for HESS Through Receiver Side Voltage Control", in IEEE Appl. Pow. El. Conf. and Expo. (APEC), pp. 1614-1619 (2015).

[63] W.X. Zhong and S.Y.R. Hui, “Charging Time Control of Wireless Power Transfer System Without Using Mutual Coupling Information and Wireless Communication System”, IEEE Trans. on Ind. El., vol. 64, no. 1, pp. 228-235 (2017).

[64] K. Hata, T. Imura, Y. Hori, “Dynamic Wireless Power Transfer System for Electric Vehicle to Simplify Ground Facilities - Power Control Based on Vehicle-side Information -”, 28th Int. El. Veh. Symp. and Ex. (EVS28), pp. 1 - 12, (2015).

[65] General rules for equipment using high frequency waves, Japanese Electromagnetic Wave Standard, “高周波利用設備の通則”, last adjourned in August 2016 (in Japanese).

[66] Miscellaneous rules for equipment using high frequency waves, Japanese Electromagnetic Wave Standard, “高周波利用設備の雑則”, last adjourned in August 2016 (in Japanese).

[67] K.Lyokelsoy, “Driver interface v2.3”, Application Note, last adjourned in November 2014.

[68] A.J. Moradewicz, M.P. Kazmierkowski, “Contactless Energy Transfer System With FPGA-Controlled Resonant Converter”, IEEE Trans. Ind. El., vol. 57, no. 9, pp. 3181-3190 (2010).

[69] DavideAndrea at English Wikipedia, CC BY-SA 3.0, https://commons.wikimedia.org/w/index.php?curid=19090771, [online] (2017).

[70] L.E.Y. Mimbela and L.A. Klein, “A Summary of Vehicle Detection and Surveillance Technologies used in Intelligent Transportation Systems”, August 2007, [online] (2017).

[71] D. Kobayashi, K. Hata, T. Imura, H. Fujimoto and Y. Hori, “Sensorless Vehicle Detection Using Voltage Pulses in Dynamic Wireless Power Transfer system”, Electric Vehicle Symposium & Exhibition 29 (2016).

[72] https://ec.europa.eu/transport/themes/its_en, [online] (2017).

[73] https://www.its.dot.gov/, [online] (2017).

[74] http://www.jari.or.jp/tabid/224/Default.aspx, [online] (2017).

[75] http://www.tmt.or.jp/research/pdf/its-e.pdf, [online] (2017).

[76] https://cvg.ethz.ch/research/v-charge/, [online] (2017).

[77] https://rac.com.au/car-motoring/info/future_charging-roads, [online] (2017).

[78] http://www.solarroadways.com/, [online] (2017).

[79] J.H. Kim, B.S. Lee, J.H. Lee, S.H. Lee, C.B. Park, S.M Jung, S.G. Lee, K.P. Yi and J. Baek, “Development of 1-MW Inductive Power Transfer System for a High-Speed Train”, IEEE Trans. on Ind. El., vol. 62, no. 10, pp. 6242-6250 (2015).

[80] G. Guidi, J.A. Suul, F. Jenset and I. Sorfonn, “Wireless Charging for Ships: High-Power Inductive Charging for Battery Electric and Plug-In Hybrid Vessels”, IEEE Electrification Magazine, vol. 5, no. 3, pp. 22-32 (2017).

[81] https://phys.org/news/2014-04-wireless-power-five-meter-distance.html, [online] (2017).

[82] https://edition.cnn.com/2014/03/14/tech/innovation/wireless-electricity/index.html, [online] (2017).

[83] http://wirelesspowertechno.com/application/, [online] (2017).

[84] http://www.ikea.com/us/en/catalog/categories/departments/wireless_charging/, [online] (2017).

[85] https://www.toolstop.co.uk/bosch-wireless-charging-power-up-on-the-go-and-on-the-site-a1539, [online] (2017).

[86] http://www.daihen.co.jp/en/products/wireless/agv/, [online] (2017).

[87] https://groups.csail.mit.edu/netmit/IMDShield/, [online] (2017).

[88] https://physics.aps.org/articles/v6/57, [online] (2017).

[89] Guideline for Limiting Exposure to Time-Varying Electric and Magnetic Fields (1 Hz to 100 kHz), International Commission on Non-Ionization Protection (ICNIRP), Health Physics Society (2010).

Publications

International journal papers with review

[1] Authors: Giorgio Lovison, Daita Kobayashi, Motoki Sato,
Takehiro Imura, Yoichi Hori
Title: "Secondary-side-only Control for High Efficiency and Desired Power with Two Converters in Wireless Power Transfer Systems"
Journal: IEEJ Journal of Industry Applications, Vol.6, No. 6, pp.473-481 (2017)

[2] Authors: Giorgio Lovison,Takehiro Imura, Hiroshi Fujimoto, Yoichi Hori
Title: "Secondary-side-only Phase-shifting Voltage Stabilization Control by One Converter for WPT Systems with Constant Power Load"
Journal: IEEJ Journal of Industry Applications, (submitted)

International conferences with review

[1] Authors: Giorgio Lovison, Motoki Sato, Takehiro Imura, Yoichi Hori

Title: "Secondary-side-only Control Simultaneous Power and Efficiency Control for Two Converters in Wireless Power Transfer Systems"

Conference: 41st Annual Conference of the IEEE Industrial Electronics Society (IECON), pp. 4825-4829

Presented: November 2015

[2] Authors: Giorgio Lovison, Daita Kobayashi, Takehiro Imura, Yoichi Hori

Title: "Secondary-side-only Simultaneous Power and Efficiency Control in Dynamic Wireless Power Transfer System"

Conference: International Electric Vehicle Technology Conference and Automotive Power Electronics Japan 2016

Presented: May 2016

[3] Authors: Giorgio Lovison, Takehiro Imura, Yoichi Hori

Title: "Secondary-side-only Control Simultaneous Power and Efficiency Contr by Online Mutual Inductance Estimation for Dynamic Wireless Power T

Conference: 42nd Annual Conference of the IEEE Industrial Electronics Society (IECON), pp. 4553-4558

Presented: October 2016

[4] Authors: Giorgio Lovison,Takehiro Imura, Hiroshi Fujimoto, Yoichi Hori

Title: "Secondary-side-only Control for Smooth Voltage Stabilization in Wireless Power Transfer Systems with Constant Power Load"

Conference: International Power Electronics Conference (IPEC) 2018, (accepted)

Awards

[1] Winner: Giorgio Lovison

Award: Outstanding presentation award (EVTeC and APE Japan 2016)

Achieved: May, 2016

[2] Winner: Giorgio Lovison

Award: Best session presentation award (IECON 2016)

Achieved: October, 2016